

UNIVERSIDADE FEDERAL DO PARANÁ

BRUNA ARCIE POLLI

MODELING OF HEAT TRANSPORT IN LAKES: SPATIAL AND TEMPORAL
CHARACTERIZATION

CURITIBA

2018

BRUNA ARCIE POLLI

MODELING OF HEAT TRANSPORT IN LAKES: SPATIAL AND TEMPORAL
CHARACTERIZATION

Tese apresentada como requisito à obtenção
do título de Doutora, do Programa de
Pós-Graduação em Engenharia de Recursos
Hídricos e Ambiental, Setor de Tecnologia,
Universidade Federal do Paraná.

Orientador: Prof. Dr.-Ing. Tobias Bleninger

CURITIBA

2018

Catálogo na Fonte: Sistema de Bibliotecas, UFPR
Biblioteca de Ciência e Tecnologia

P774m

Polli, Bruna Arcie

Modeling of heat transport in lakes: spatial and temporal characterization /
Bruna Arcie Polli. – Curitiba, 2018.

Tese - Universidade Federal do Paraná, Setor de Tecnologia, Programa
de Pós-Graduação em Engenharia de Recursos Hídricos e Ambiental, 2018.

Orientador: Tobias Bernward Bleninger .

1. Lagos. 2. Reservatórios. 3. Calor – Transmissão. 4. Modelagem. I.
Universidade Federal do Paraná. II. Bleninger, Tobias Bernward. III. Título.

CDD: 551.48

Bibliotecário: Elias Barbosa da Silva CRB-9/1894

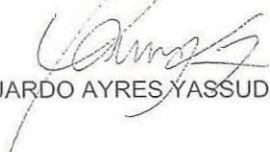
TERMO DE APROVAÇÃO

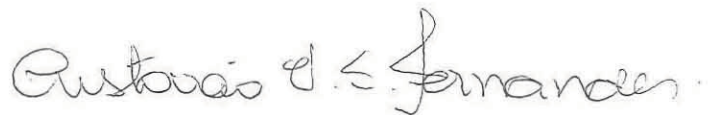
Os membros da Banca Examinadora designada pelo Colegiado do Programa de Pós-Graduação em ENGENHARIA DE RECURSOS HÍDRICOS E AMBIENTAL da Universidade Federal do Paraná foram convocados para realizar a arguição da Tese de Doutorado de **BRUNA ARCIE POLLI**, intitulada: **MODELING OF HEAT TRANSPORT IN LAKES: SPATIAL AND TEMPORAL CHARACTERIZATION**, após terem inquirido a aluna e realizado a avaliação do trabalho, são de parecer pela sua aprovação no rito de defesa. A outorga do título de Doutor está sujeita à homologação pelo colegiado, ao atendimento de todas as indicações e correções solicitadas pela banca e ao pleno atendimento das demandas regimentais do Programa de Pós-Graduação.

Curitiba, 09 de Agosto de 2018.

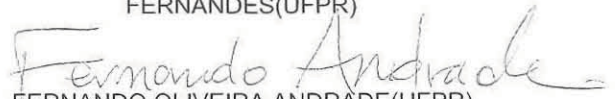

TOBIAS BERNWARD BLENINGER(UFPR)
(Presidente da Banca Examinadora)


JOSÉ RODOLFO SCARATI MARTINS(USP)


EDUARDO AYRES YASSUDA(TT)



CRISTOVÃO VICENTE SCAPULATEMPO
FERNANDES(UFPR)


FERNANDO OLIVEIRA ANDRADE(UFPR)


HELOISE GARCIA KNAPIK(UFPR)

Aos meus pais, Irene e José (in memoriam)
To my parents, Irene and José (in memoriam)

ACKNOWLEDGEMENTS

First, I would like to thank my parents, José (*in memoriam*) and Irene. You always supported my decisions, even when you didn't think was the best choice. Thank you for let me follow the path I wanted and always do the best for me. The person I'm now is because of you. You always taught me and my sisters to be honest, to go after what we wanted, and do not forget what really matters, that is family. Thanks for everything, I love you!

I would like to thank my supervisor, Professor Tobias Bleninger, who supervised me during my under-graduation, master's thesis and then my PhD. This is around seven years of work and I can say that I am a better professional now, after all the encouragement to be better. You are a great supervisor and person. Thank you!

A special thanks to my dear friend Caroline Kozak. We became really good friends during my PhD and you will always be in my heart. You helped in good and really bad times, and showed me what a friend is for. Love you!

To my dear friends, Dani, Luciane, Ana, Ellen, Victória and Carol (again!). Thanks for your friendship, for the support and for all the confusions that we had together! Love you all girls!

To my sisters, Valéria, Marilise and Josirene. We are always together, no matter what happen. We can fight sometimes, but this never last... you are the best sisters I could have. I don't need to say that, but I love you!

To my nephew, Rafael, and my niece, Laura, that make my life happier and easy :D

To my friends and colleagues, Marcelo, Lediane, Liége and Julio. Thanks Heloise for the talks and coffees!

To Cristovão Fernandes, thanks for all the talks, advices for my career and my life, and the support during my PhD.

To all the professors I had during my academic life. You are part of this. Thanks.

To the Federal University of Paraná and its employees. I belong to this University since my under-graduation. It has been 10 years of study and work, and I'm proud to be part of UFPR.

To the Graduate Program in Water Resources and Environmental Engineering, professors and employees.

To the members of my examining board, Professors Cristovão Fernandes, Fernando Andrade, Heloise Knapik, José Rodolfo Scarati and Eduardo Yassuda.

To CAPES, for the funding of my scholarship in Brazil and in Germany (through NoPa Project).

To the Karlsruhe Institute of Technology, Stephan Fuchs and Stephan Hilgert for receiving me for my Sandwich PhD. For all my colleagues at that University... in special

Klajdi, Adrian and Lisa.

To the GEE APINE project: "Monitoramento das Emissões de Gases de Efeito Estufa em Reservatório de Usinas Hidrelétricas", funded by the Agência Nacional de Energia Elétrica - ANEEL.

To Michael Männich, for the support in the field measurements during the development of this thesis.

To COPEL and Sanepar, companies from Paraná State, for providing data from Vosoroça and Passaúna reservoirs.

To all the Brazilian people that I met during my Sandwich PhD in Germany.

To everybody that, at some point, contributed to this thesis.

Thanks!

RESUMO

Lagos e reservatórios apresentam um comportamento sazonal relacionado à sua estrutura térmica, de mistura e estratificação ao longo do ano, devido às condições meteorológicas, entradas e saídas, profundidade e localização do reservatório. Desta maneira, medições em reservatórios aliadas à modelagem numérica são ferramentas importantes para o entendimento dos processos físicos que ocorrem no corpo d'água e identificação de períodos característicos. Neste contexto, esta tese visa aliar medições com a modelagem dos processos físicos em reservatórios, de maneira que os gradientes verticais e horizontais de temperatura sejam resolvidos. As medições em campo tem como objetivo a análise da variação espacial da temperatura, tanto na vertical quanto horizontal, com medições de temperatura com alta resolução espacial e temporal, o controle das entradas e saídas e medições de dados meteorológicos, forçantes do sistema. A modelagem proposta neste projeto consiste de um modelo em setores no reservatório, tendo como base um modelo unidimensional de transporte de calor, que possibilita a análise de gradientes verticais e horizontais de temperatura, com custo computacional reduzido. Além da modelagem em setores, é realizada a modelagem tridimensional do transporte de calor com o modelo Delft3D. O objetivo da modelagem é comparar o modelo setorial proposto e análise das possíveis vantagens/desvantagens de se aplicar um modelo em setores em contraposição a um modelo mais complexo, apoiando as entradas e resultados dos modelos nas medições de campo. Os resultados mostram que um modelo unidimensional ou setorial pode ser utilizado para classificação do reservatório (períodos de mistura e estratificação), tendo como vantagem o baixo tempo de processamento. No caso do transporte de massa, por outro lado, as análises realizadas mostram que um modelo tridimensional deve ser aplicado, devido a tridimensionalidade dos processos no corpo d'água, e que a temperatura tem um efeito significativo no transporte advectivo e dispersivo no corpo d'água.

Palavras-chave: Lagos; Reservatórios; Transporte de Calor; Medições; Modelagem em Setores; Modelagem Tridimensional.

ABSTRACT

Lakes and reservoirs show a seasonal behavior related to its thermal structure – they may stratify/mix in some periods of the year, due to meteorological conditions, inflows/outflows effects, depth and reservoir location. Thus, measurements coupled with numerical modeling are important tools for understanding physical processes in the water body and identification of specific periods of stratification. In this context, this thesis focusses on measurements and modeling of physical processes in reservoirs, solving both vertical and horizontal temperature gradients. Field measurements have the objective of analysing spatial variations of temperature, in horizontal and vertical directions, with high spatial and temporal resolution, inflows and outflows control and meteorological data, forcing of the system. The modeling proposed in this thesis consist in a sector reservoir model, based in a one-dimensional heat transport model, which allows the analysis of vertical and horizontal temperature gradients, with reduced computational cost. In addition, three-dimensional modeling (with the model Delft3D) is performed for comparisons of the sector model proposed and analysis of advantages/disadvantages of applying a sector model in contrast to a more complex model, being supported by field measurements. The results show that the one-dimensional and the sector model can be used for reservoir classification (identification of mixing and stratification periods), with the advantages of low processing time. For mass transport, on the other hand, the analysis performed show that a three-dimensional model should be applied, due the three-dimensionality of the processes, and that temperature has a significant impact on advective and dispersive transport in the water body.

Key-words: Lakes; Reservoirs; Heat Transport; Measurements; Sector Modeling; Three-dimensional Modeling.

LIST OF FIGURES

Figure 1	Thesis organization	22
Figure 2	Temperature and dissolved oxygen (DO) profiles measured in the deepest point of Vossoroça reservoir. Source: Mannich (2013)	25
Figure 3	Temperature measurements in a section of Wellington reservoir (Australia) (Monismith et al., 1990) a) Longitudinal transects at 16:15 hours, 23 February b) 24:00 hours, 23 February c) Water surface temperatures (stations are identified in a and b)	28
Figure 4	Temperature and tracer distribution in a section of Eau Galle reservoir (USA) measured by James and Barko (1991)	29
Figure 5	Representation of the main heat transport parameters in lakes. a) Low inflows and outflows, b) High inflows and outflows, c) Sector approach.	31
Figure 6	CE-QUAL-W2 waterbody division for simulations – Waterbody, Branches and Segments. Adapted from Cole and Wells (2015) – examples from CE-QUAL-W2	43
Figure 7	Location of Vossoroça, Passaúna and Capivari reservoirs in Brazil	52
Figure 8	Available data of Vossoroça, Passaúna and Capivari reservoirs	53
Figure 9	Vossoroça reservoir bathymetry and monitoring sites	53
Figure 10	Vossoroça reservoir monitoring sites a) floating platform and b) meteorological weather station in Vossoroça reservoir and c) Limnometric station in São João river	55
Figure 11	Temperature measured in Vossoroça reservoir in the floating platform	55
Figure 12	Meteorological data near to Vossoroça reservoir. a) Wind speed, b) Air temperature, c) Relative Humidity and d) Shortwave radiation	56
Figure 13	Wind speed and direction measured in the meteorological weather station in Vossoroça reservoir	57
Figure 14	a) Inflow/Outflow and b) Water level from Vossoroça reservoir	57
Figure 15	Water level and temperature in São João river	57
Figure 16	Passaúna reservoir	58
Figure 17	Meteorological data near to Passaúna reservoir. a) Wind speed, b) Air temperature, c) Relative Humidity and d) Shortwave radiation	59
Figure 18	Flow and water level in Passaúna reservoir	60
Figure 19	Water intake volume in Passaúna reservoir	60
Figure 20	Surface temperature in Capivari reservoir	60
Figure 21	Meteorological data from Capivari reservoir a) Wind speed, b) Air temperature, c) Relative Humidity and d) Shortwave radiation	61
Figure 22	Location of CTD measurements in Vossoroça reservoir	62

Figure 23	Temperature profiles in different regions of Vossoroça reservoir at 11/12/2015. a) Profiles in the floating platform and São Joãozinho river. b) Section from shallow to deeper region. c) All measured profiles	63
Figure 24	Temperature profiles in different regions of Vossoroça reservoir at 12/03/2015. a) Profiles in the floating platform, São João river and a point in the reservoir P2. b) Section from shallow to deeper region. c) All measured profiles	64
Figure 25	Wedderburn number and Lake number in Vossoroça reservoir	65
Figure 26	Points of temperature measurements in February 2017 in Passaúna reservoir	66
Figure 27	Temperature measurements in the longitudinal direction in Passaúna reservoir	67
Figure 28	Side arms temperature sections in Passaúna reservoir (see Figure 26) . . .	67
Figure 29	Temperature in Passaúna reservoir. a) 02/28/2016, b) 04/18/2016 and c) 05/23/2016.	68
Figure 30	Energy fluxes calculated for Capivari reservoir	70
Figure 31	Scheme of the sector model. a) Top view and b) Side view and boundary conditions	71
Figure 32	Vossoroça reservoir 1D heat transport modeling (Polli, 2014)	73
Figure 33	Wedderburn number and Lake number in Vossoroça reservoir with data of the 1D modeling	74
Figure 34	Scheme showing regions of Vossoroça reservoir with different depths	74
Figure 35	Scheme showing the approach to the Vossoroça reservoir sector model. a) Side view of the sectors and b) flows and exchange in each sector	75
Figure 36	Sector model of Vossoroça reservoir without exchange between sectors a) Sector 1, b) Sector 2 and c) Sector 3	76
Figure 37	Sector model of Vossoroça reservoir with exchange according the mean difference in temperature of each sector a) Sector 1, b) Sector 2 and c) Sector 3	77
Figure 38	Surface temperature with and without exchange between sectors in a) sector 1, b) sector 2 and c) sector 3	78
Figure 39	Scheme on MTCR-1 model of inflow entering the reservoir. a) Current approach distributing equally inflows in the water column b) New approach distributing inflows in relation to the volume of layers	79
Figure 40	Vossoroça reservoir 1D heat transport modeling – inflow distributed according the volume of the layers	80
Figure 41	Sector model of Vossoroça reservoir without exchange between sectors – inflow distributed according the volume of the layers a) Sector 1, b) Sector 2 and c) Sector 3	81
Figure 42	Sector model of Vossoroça reservoir with exchange according the mean difference in temperature of each sector – inflow distributed according the volume of the layers a) Sector 1, b) Sector 2 and c) Sector 3	82

Figure 43	Scheme of exchange using a system of reactors in the sector model	82
Figure 45	Surface temperature of Vossorooca reservoir using a system of reactors to calculate heat exchange between the sectors	83
Figure 44	Sector model of Vossorooca reservoir using a system of reactors to calculate heat exchange between the sectors. a) Sector 1, b) Sector 2 and c) Sector 3	84
Figure 46	Temperature results using a) Murakami and b) Ocean heat flux models in Delft3D	87
Figure 47	Heat flux with Murakami and Ocean models	88
Figure 48	Components of heat flux in Murakami and Ocean models	89
Figure 49	Temperature in Vossorooca reservoir. Three-dimensional model with a) 10 b) 14 and c) 20 layers.	90
Figure 50	Temperature results. a) Measurements at the floating platform, b) 3D modeling results	92
Figure 51	Comparison between measurements and modeling. Points of comparison, from surface a) 1 m, b) 3 m, c) 5 m, d) 7 m, e) 9 m, f) 11 m and g) bottom	93
Figure 52	Temperature gradients (between surface and bottom) in Vossorooca reservoir between September 5th at 00h and September 6th at 04h modelled with Delft3D	94
Figure 53	Period of time (in %) that a certain temperature gradient is expected in Vossorooca reservoir during the period of simulation (94 days)	96
Figure 54	Wedderburn number and Lake number in Vossorooca reservoir with data of the 3D modeling	97
Figure 55	Sector model configuration in Delft3D	98
Figure 56	Delft3D results of temperature as a sector model in Vossorooca reservoir. a) Sector 1 (4 m), b) Sector 2 (8 m), Sector 3 (14 m), Sector 4 (14 m)	99
Figure 57	Temperature in Vossorooca reservoir a) measurements, b) MTCR-1 model, c) MTCR-1 modified and d) Delft3D model	100
Figure 58	Temperature gradients of measured data, 1D and 3D modeling	101
Figure 59	Wedderburn and Lake Number calculated with a) measured data, b) MTCR-1 results, c) MTCR-1 modified results and d) Delft3D results at the floating platform location	102
Figure 60	Water temperature in a point with 4 m depth a) full 3D simulation, b) 3D model as a sector model, c) Sector model without exchange, d) Sector model with exchange, e) Sector model without exchange modified and f) Sector model with exchange modified	103
Figure 61	Water temperature in a point with 8 m depth a) full 3D simulation, b) 3D model as a sector model, c) Sector model without exchange, d) Sector model with exchange, e) Sector model without exchange modified and f) Sector model with exchange modified	105

Figure 62	Monitoring path for tracer modeling	107
Figure 63	Cross-sections for river and side arm tracer modeling	108
Figure 64	Water temperature and tracer concentration in a longitudinal section in Vossoroca reservoir	110
Figure 65	River tracer modeling. Cumulative a) advective transport of temperature, b) dispersive transport of temperature, c) advective transport of tracer and d) dispersive transport of tracer	111
Figure 66	Tracer concentration in a longitudinal section of Vossoroca reservoir (in this simulation, temperature is not modelled)	112
Figure 67	Velocity profiles in points R1, R2 and R3 (see Figure 64) in the river tracer modeling in Vossoroca reservoir	114
Figure 68	Velocity in a section of a side arm in Vossoroca reservoir a) No tracer, b) With tracer and c) Difference in velocity in the simulation considering and not considering tracer	115
Figure 69	Water temperature and tracer concentration in a side arm in 09/23/2012 between 00h and 06h	117
Figure 70	Water temperature and tracer concentration in a side arm in 09/23/2012 between 08h and 14h	118
Figure 71	Side arm simulation. Cumulative a) advective transport of temperature, b) dispersive transport of temperature, c) advective transport of tracer and d) dispersive transport of tracer	119
Figure 72	Tracer concentration in a side arm in 09/23/2012 between 00h and 14h (in this simulation, temperature is not modelled)	120
Figure 73	Velocity profiles in points P1 and P2 (see Figure 69) in the side arm tracer modeling in Vossoroca reservoir	121
Figure 74	Normalised tracer concentration in points P1 and P2 (see Figure 69) in the 2D and 3D side arm tracer modeling in Vossoroca reservoir	122
Figure A.1	Temperature measured in Vossoroca reservoir in the floating platform (measured from surface)	136
Figure A.2	Meteorological data near to Vossoroca reservoir (2013). a) Wind speed, b) Air temperature, c) Relative Humidity and d) Shortwave radiation	136
Figure A.3	Meteorological data near to Vossoroca reservoir (2014). a) Wind speed, b) Air temperature, c) Relative Humidity and d) Shortwave radiation	137
Figure A.4	Meteorological data near to Vossoroca reservoir (2015). a) Wind speed, b) Air temperature, c) Relative Humidity and d) Shortwave radiation	137

LIST OF TABLES

Table 1	Water supply in Curitiba	23
Table 2	Reservoirs monitoring comparison	32
Table 3	Comparison between one, two and three-dimensional models	38
Table 4	Set of equations solved by one and three-dimensional models MTCR-1 and Delft3D	39
Table 5	Delft3D assumptions	44
Table 6	Meteorological sensors installed at Vossoroca reservoir	56
Table 7	Flow and drainage area in Passaúna reservoir (Veiga and Dziedzic, 2010) .	58
Table 8	Coordinates of measurement points and Secchi depth	64
Table 9	Number of days that $\Delta T > 1, 2$ and $3\text{ }^\circ\text{C}$, $W > 1$ and $L_N > 1$ to measured data from Vossoroca reservoir (from 94 days)	65
Table 10	Coordinates of measurement points and Secchi depth in Passaúna reservoir	68
Table 11	Differences between meteorological data measured in the onshore and float- ing platform stations in Capivari reservoir	69
Table 12	MTCR-1 model set-up and calibration parameters for Vossoroca reservoir modeling	72
Table 13	MTCR-1 model required data for Vossoroca reservoir modeling	72
Table 14	Mean absolute and relative error in the 1D modeling	73
Table 15	Number of days that $\Delta T > 1, 2$ and $3\text{ }^\circ\text{C}$, $W > 1$ and $L_N > 1$ of Vossoroca reservoir 1D modeling (from 94 days)	73
Table 16	Mean absolute and relative error in the sector modeling of Vossoroca reservoir	76
Table 17	Mean surface temperature in the sectors of Vossoroca reservoir	78
Table 18	Number of days that $\Delta T > 1, 2$ and $3\text{ }^\circ\text{C}$, $W > 1$ and $L_N > 1$ of Vossoroca reservoir 1D modeling (from 94 days) with inflow distributed according the volume of the layers	80
Table 19	Mean absolute and relative error in the sector modeling of Vossoroca reser- voir with inflow distributed according the volume of the layers	80
Table 20	Absolute and relative error in the 3D modeling using Murakami and Ocean heat flux models	86
Table 21	Absolute and relative error in the 3D modeling of Vossoroca reservoir for the grid testing	88
Table 22	Delft3D model set-up and calibration parameters for Vossoroca reservoir modeling related to turbulence and surface heat flux	91
Table 23	Delft3D model required data for Vossoroca reservoir modeling	92
Table 24	Mean absolute and relative error in the 3D modeling	92
Table 25	Mean absolute error (MAE) and standard deviation (SD) in the 1D and 3D modeling at the measured points in Vossoroca reservoir	93

Table 26	Number of days that $\Delta T > 1, 2$ and 3 °C, $W > 1$ and $L_N > 1$ of Vossorooca reservoir 3D modeling (from 94 days)	95
Table 27	Mean absolute and relative error in the 3D model as a sector model	97
Table 28	Mean absolute and relative error in the 1D and 3D modeling of Vossorooca reservoir	98
Table 29	Temperature gradients comparison between measured data, 1D and 3D modeling (from 94 days of simulation)	101
Table 30	Mean surface temperature calculated for sector of 4 m and difference in % between full 3D modeling and the sector approach	104
Table 31	Mean surface temperature calculated for sector of 8 m and difference in % between full 3D modeling and the sector approach	104
Table 32	Difference in percentage between advective and dispersive transport considering temperature and not considering temperature in the river tracer modeling	113
Table 33	Difference in percentage between advective and dispersive transport considering temperature and not considering temperature in the side arm tracer modeling	121
Table C.1	Discretization of the one-dimensional heat transport equation and boundary conditions.	141

LIST OF SYMBOLS

A	km^2	Area
B	m	Average cross-sectional width
c_p	$\text{Jkg}^{-1}\text{K}^{-1}$	Water specific heat
d	m	Depth below some horizontal plane of reference (datum)
D_H, D_x	m^2s^{-1}	Horizontal diffusivity coefficient
D_s	m^2s^{-1}	Longitudinal diffusivity coefficient
D_V, D_z	m^2s^{-1}	Vertical diffusivity coefficient
E	m^2s^{-1}	Eddy diffusivity coefficient
E_0	m^2s^{-1}	Neutral eddy diffusivity coefficient
f	s^{-1}	Coriolis parameter (inertial frequency)
$f(Ri)$	–	Richardson number function
g	ms^{-2}	Acceleration due to gravity
h	m	Water level
H	m	Total water depth
k^*	–	Function for different latitudes
K	$\text{WK}^{-1}\text{m}^{-2}$	Heat transfer coefficient
L_N	–	Lake Number
M_x	kg ms^{-1}	Depth-averaged mass flux due to Stokes drift in x -direction
M_y	kg ms^{-1}	Depth-averaged mass flux due to Stokes drift in y -direction
P	$\text{kg m}^{-1}\text{s}^{-2}$	Hydrostatic water pressure
P_0	–	Neutral Prandtl number
q	ms^{-1}	Contributions per unit of area/ net lateral inflow per unit of volume in CE-QUAL-W2
q_n	Wm^{-2}	Net heat flux
q_s	Wm^{-2}	Shortwave solar radiation
$q_{s_{max}}$	Wm^{-2}	Maximum shortwave solar radiation
$q_{s_{min}}$	Wm^{-2}	Minimum shortwave solar radiation
$q_{s_{mean}}$	Wm^{-2}	Mean shortwave solar radiation
q_T	s^{-1}	Lateral inflow or outflow mass flow rate per unit volume
$q(z)$	Wm^{-2}	Heat source term
Q	ms^{-1}	Global source or sink per unit of area
Q_{an}	Wm^{-2}	Net incident atmospheric radiation (long wave)
Q_{br}	Wm^{-2}	Back radiation (long wave)
Q_{co}	Wm^{-2}	Convective heat flux (sensible heat)
Q_{eb}	Wm^{-2}	Effective back radiation
Q_{ev}	Wm^{-2}	Evaporative heat flux (latent heat)
Q_{in}	m^3s^{-1}	Inflow

Q_{out}	m^3s^{-1}	Outflow
Q_{sn}	Wm^{-2}	Net incident solar radiation (short wave)
Q_{tot}	Wm^{-2}	Mean total heat flux
RH	%	Relative humidity
RH_{max}	%	Maximum relative humidity
RH_{min}	%	Minimum relative humidity
RH_{mean}	%	Mean relative humidity
Ri	–	Richardson number
s	m	Sector model longitudinal direction
S	Wm^{-2}	Source and sink terms per unit of area due to the discharge
S_T	W	Laterally averaged source/sink term
t	s	Time
T	$^{\circ}C$	Water temperature
T_a	$^{\circ}C$	Air temperature
$T_{a_{max}}$	$^{\circ}C$	Maximum air temperature
$T_{a_{min}}$	$^{\circ}C$	Minimum air temperature
$T_{a_{mean}}$	$^{\circ}C$	Mean air temperature
T_e	$^{\circ}C$	Equilibrium temperature
T_{in}	$^{\circ}C$	Inflow temperature
T_s	$^{\circ}C$	Superficial water temperature
u	ms^{-1}	Flow velocity in the x - or ξ -direction
u_{flow}	ms^{-1}	velocity induced by the flow
u_s^*	ms^{-1}	Surface friction velocity
u_{wind}	ms^{-1}	velocity induced by the wind
U	ms^{-1}	Velocity component in the x coordinate in CE-QUAL-W2
U	ms^{-1}	Wind speed
U_{max}	ms^{-1}	Maximum wind speed
U_{min}	ms^{-1}	Minimum wind speed
U_{mean}	ms^{-1}	Mean wind speed
v	ms^{-1}	Fluid velocity in the y - or ν -direction
V	m^3	Volume
W	–	Wedderburn Number
w	ms^{-1}	Fluid velocity in z -direction
$x; y; z$	m	Cartesian coordinates
Δt	s	Computational time-step
Δx	m	Cell width in the x -direction
Δy	m	Cell width in the y -direction
α	$^{\circ}$	Channel slope
ϕ	$^{\circ}$	Latitude

κ	–	von Karman's constant
τ_{xx}	$\text{kgm}^{-1}\text{s}^{-2}$	Shear stress acting in x direction on the x -face of control volume
τ_{xz}	$\text{kgm}^{-1}\text{s}^{-2}$	Shear stress acting in x direction on the z -face of control volume
ν_s	m^2s^{-1}	Longitudinal eddy viscosity
ν_v	m^2s^{-1}	Vertical eddy viscosity
ν_h	m^2s^{-1}	Horizontal eddy viscosity
ρ	kgm^{-3}	Water density
σ	–	Scaled vertical coordinate; $\sigma = \frac{z-\zeta}{d+\zeta}$
ζ	m	Water level above some horizontal plane of reference (datum)

CONTENTS

1	Introduction	19
1.1	Objectives	20
1.2	Thesis organization	21
2	Heat transport in lakes and reservoirs	23
2.1	Heat transport process	26
2.2	Measurements in lakes and reservoirs	30
2.3	Modeling of heat transport in lakes and reservoirs	34
2.3.1	One-dimensional model	37
2.3.2	Two-dimensional model	41
2.3.3	Three-dimensional model	43
2.3.4	Recent applications	47
2.4	Reservoir classification	49
2.5	Summary of the chapter	50
3	Study site characterization	52
3.1	Vossoroca reservoir	52
3.1.1	Temperature	54
3.1.2	Meteorological data	54
3.1.3	Flow	54
3.2	Passaúna reservoir	54
3.2.1	Temperature	57
3.2.2	Meteorological data	58
3.2.3	Flow and water intake	59
3.3	Capivari reservoir	59
3.3.1	Temperature	60
3.3.2	Meteorological data	60
4	Results of measurements and classification	62
4.1	Measurements in Vossoroca reservoir	62
4.1.1	Vossoroca reservoir data analysis	63
4.2	Measurements in Passaúna reservoir	65
4.3	Heat flux in reservoirs: Capivari study case	68
4.4	Summary of the chapter	70
5	One-dimensional and Sector modeling	71
5.1	Improvements of one-dimensional model	78
5.1.1	Sector model improvements	80
5.1.2	System of reactors	80

5.2	Summary of the chapter	84
6	Three-dimensional modeling	86
6.1	Comparison between heat flux models in Delft3D	86
6.2	Grid influence	88
6.3	Three-dimensional modeling in Vossorooca reservoir	88
6.3.1	Vossorooca reservoir 3D modeling data analysis	95
6.4	Three-dimensional model as a sector model	97
6.5	Comparison between 1D and 3D modeling	97
6.6	Sector model analysis	101
6.7	Summary of the chapter	104
7	Tracer transport modeling	107
7.1	River tracer study	108
7.2	Side arm tracer study	113
7.3	Summary of the chapter	123
8	Conclusions	124
8.1	Recommendations and future studies	126
9	References	128
A	Vossorooca reservoir measurements	136
B	MTCR-1 Model	138
C	Numerical discretization of MTCR-1 Model	141
D	Delft3D Model	142

1 Introduction

Lakes and reservoirs vary widely in their size and number. They comprise approximately 0.02% of the water in the hydrosphere (Martin and McCutcheon, 1999), in contrast of 0.00009% in rivers (Wetzel, 1983). Also, usually there is a distinction between reservoirs and lakes. The former is typically a result of an engineered build solutions (Martin and McCutcheon, 1999) with many purposes as water supply, irrigation, flood control, navigation and power generation (UNESCO/IHA, 2009) and often used for multiple purposes (Martin and McCutcheon, 1999). Lakes may have the same purposes but are natural, and not necessarily are located where water is needed (Martin and McCutcheon, 1999).

Brazil covers 70.1% of the energy demand from hydropower generation (Ministério de Minas e Energia, 2013), with potential to implement more dams to produce energy. In relation to drinking water, it is estimated that 56% of the municipalities use superficial waters as water source. From the environmental perspective, studies about the impacts of the dams are required for licensing these engineered systems. Additionally, reservoirs require the use of management tools for adequate operation and maintenance. In such context, some relevant questions for the management purposes and water quality analysis are:

- Does the reservoir stratify? If yes, when and for how long?
- Which are the consequences of stratification? Does it affect water quality?
- How to assess these situations? Are there horizontal gradients or spatial variabilities? Are resulting fluxes relevant?

To answer these questions before the construction of dams, usually numerical models are applied. In general, there is a lack of measurements in Brazilian reservoirs, therefore numerical model set ups are complex task, on the other hand, very useful to understand the dynamics of the system. Three-dimensional models are usually adopted for short time periods and with a coarse grid, due high processing and post-processing times – seasonal variations are not completely analysed and, from the management point of view, not practical and efficient. The model should be able to represent spatial and time variations with a short time of processing. Therefore, some questions to be answered are:

- Is a complex model necessary to represent the system and periods of interest?
- Is it possible to simplify the model representation?

In this research, the use of simple models is proposed to represent the system and its dynamics – a 1D model, that requires less data for calibration, allows simulations of

seasonal variations with low time processing and analysis of different scenarios. As an expansion of the one-dimensional model, a sector model is proposed, which represents different regions of the reservoir (shallow or deep, for example) and, therefore, allows spatial representation of the system, and has the same advantages of the one-dimensional model.

The main parameter analysed in this thesis is temperature, due its role on the dynamics of the reservoirs and implications for hydrodynamics and water quality. Stratification controls the distribution of heat and substances in lakes and reservoirs. Therefore, water column temperature is an important parameter in studies related to circulation and water quality in reservoirs. In the last years, attention has been given also to the horizontal distribution of temperature, that may also affect transport in lakes and reservoirs, and act as a source of substances to deep waters. This is due to horizontal processes that may induce circulation between shallow and deep water. This circulation could be a source of dissolved oxygen (Hohmann et al., 1997), phosphorus (James and Barko, 1991), for example, which could interfere in the structure of the water column and water quality parameters. Another question related to the heat transport to be answered is:

- Are temperature gradients in the horizontal direction responsible for substances transport?

With all the considerations presented, the hypothesis of this thesis are:

1. Reservoirs present horizontal temperature gradients and they can be modelled;
2. Horizontal temperature gradients may create mass transport;
3. It is possible to quantify these effects with simplified models.

The next section presents the objectives of this thesis, defined to answer the questions and study the hypothesis presented.

1.1 Objectives

The main contribution of this Thesis is the development of a simplified heat transport model that allows the representation of different areas of the reservoir – the sector model, that is based on solving a one-dimensional model in different sectors of the reservoir. The one-dimensional model is applied in each region of the reservoir, that may or may not exchange heat. This simplifies processes in the reservoir, but allows spatial representation of the system, and the amount of input and calibration data are reduced. More complex models, e.g. three-dimensional models, can simulate the entire system and provide local analysis, but they are usually adopted for short time periods, they require more input

and calibration data and the processing time is elevated. As a second objective, one-dimensional and the sector model approaches are complemented with a three-dimensional modelling to understand system dynamics. As a third objective, the role of temperature for mass transport is analysed – how advective and dispersive transport are affected by temperature in a reservoir. To achieve the main objective of this Thesis, the following specific objectives will be addressed:

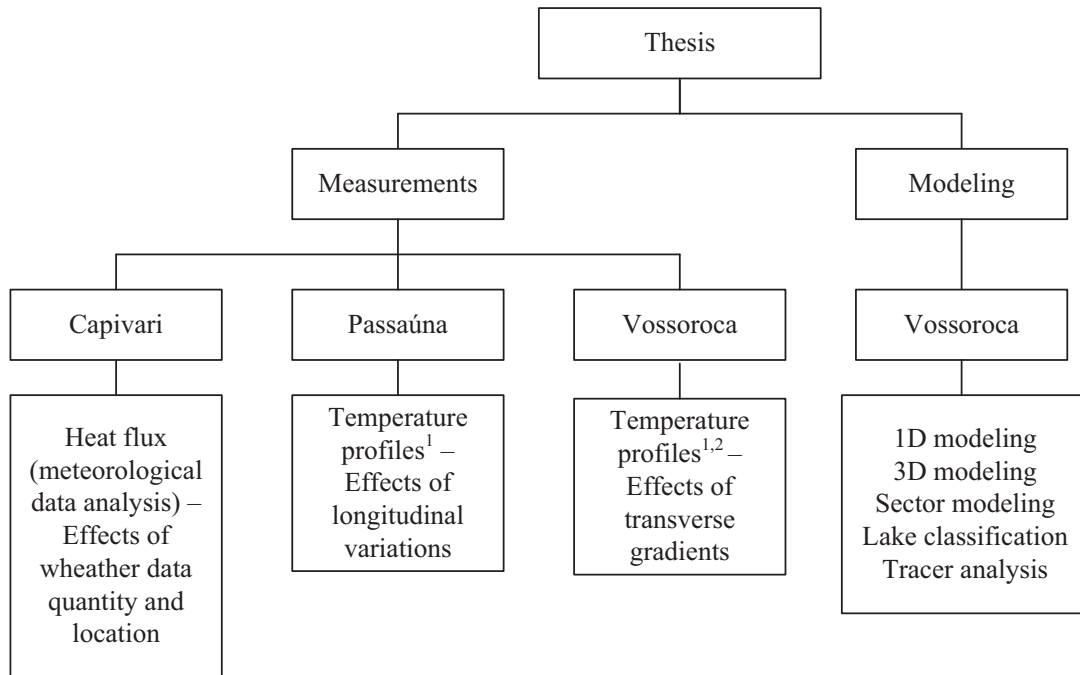
1. Implement a three-dimensional heat transport model to a reservoir, with high resolution;
2. Compare one and three-dimensional models, identifying its limitations and advantages;
3. Calculate physical indices to estimate critical periods in the reservoir (stratification);
4. Develop and implement a sector model, using the advantages of one-dimensional models to simulate temperature spatially in the reservoir;
5. Introduce a conservative tracer in the three-dimensional model to analysis of transport due density differences.

1.2 Thesis organization

To achieve the thesis goals, data from three different reservoirs are used: Vossoroca, Passaúna and Capivari, all located in Paraná State, Brazil. Figure 1 shows a scheme of the way they were applied in the document.

The following measurements were considered from the three reservoirs:

- In Capivari reservoir, data from two meteorological stations were taken to analyse the impacts of heat flux at the air-water interface, to study the influence of different locations of these stations.
- In Passaúna reservoir, temperature profiles are presented with high spatial distribution (and low time resolution), with the aim to identify if there are horizontal temperature gradients in the reservoir.
- In Vossoroca reservoir, some profiles with low time resolution were taken. Also, in Vossoroca reservoir, a floating platform is installed since 2012 and measures temperature with high temporal resolution (in one point, therefore, low spatial resolution). Near the reservoir, a meteorological weather station was installed also in 2012. Since Vossoroca is the reservoir with the most complete set of data, it was chosen for the principal modeling analysis of this Thesis – 1D, 3D and sectorial modeling and related analysis.



¹ Profiles measured with high spatial resolution and low time resolution

² Profiles measured with low spatial resolution and high time resolution

Figure 1 – Thesis organization

The thesis document is organised as it follows:

- Chapter 2: A review about heat transport in lakes, measurements and modeling.
- Chapter 3: The area of study and available data are presented. Data from three reservoirs are presented: Vossoroça, Passaúna and Capivari.
- Chapter 4: Measurements and related analysis are presented: CTD and Secchi depth measurements for Vossoroça and Passaúna reservoirs. A heat flux analysis is presented for Capivari reservoir and shows the differences in heat flux due different location of meteorological measurements.
- Chapter 5: One-dimensional and Sector modeling are presented for Vossoroça reservoir.
- Chapter 6: Three-dimensional modeling of Vossoroça reservoir and related analysis are presented. In this chapter, two heat flux models in the three-dimensional modeling are compared and the number of layers in the modeling is tested. The three-dimensional model is prepared to run as a Sector model and comparisons with one-dimensional modeling and sector model are presented.
- Chapter 7: a tracer modeling is performed with three-dimensional modeling. The tracer is released in a river and in a side arm, and the effects of temperature on mass transport are analysed.

2 Heat transport in lakes and reservoirs

Construction of large reservoirs in Brazil began in the early 1900s (Soares et al., 2008). Brazil is a reservoir-oriented country (Tundisi et al., 1993). According to the National Energy Balance of 2013, hydropower energy corresponds to 70.1% of the Brazilian demand. Between 2011 and 2012 there was a raise of 2.2% in the hydroelectric capacity (Ministério de Minas e Energia, 2013). Also, many of these reservoirs used for hydropower generation have multiple purposes, as water supply, irrigation, and recreation (Soares et al., 2008), therefore water quantity and quality are important for its uses.

According to ANA (2013), flow consumed by multiple purposes in 2010 had the proportion of: 72% to irrigation, 11% to animals consumption, 9% to urban consumption, 7% to industry uses and 1% human rural supply in Brazil. Superficial waters, which includes rivers, lakes, and reservoirs, are still the most used sources for drinking water supply – 56% of the municipalities use superficial waters as a water source (Galli and Abe, 2010). In Curitiba, Iraí and Passaúna reservoirs are used for water supply (Grassi et al., 2014). Table 1 shows the contribution of each system to the water supply in Curitiba and other municipalities that are supplied with the same systems. Passaúna system is responsible for 24% of the water supply, while Iraí, for 35% (from 1.797.408 inhabitants in Curitiba in 2007).

Table 1 – Water supply in Curitiba

System	% of water supply to Curitiba	Water treatment plant flow (Ls⁻¹)	Other municipalities supplied
Iguaçu	38	3200/3300*	São José dos Pinhais, Almirante Tamandaré
Iraí	35	3200/2600*	Piraquara, Quatro Barras, Colombo, Campina Grande do Sul, Pinhais
Passaúna	24	2000/900*	Campo Magro, Campo Largo, Araucária
Miringuava	2	2000/900*	Araucária, São José dos Pinhais, Fazenda Rio Grande

Source: Atlas Brasil – Abastecimento Urbano de Água, ANA (Reference year: 2007)

*Source: Plano diretor SAIC, Sanepar (Reference year: 2013)

Construction of reservoirs may impact physical, chemical and biological characteristics of the water body by affecting residence time, temperature, stratification, reduction in turbulence and often a decrease in particles and turbidity (Friedl et al., 2002). Some water quality issues due river damming are eutrophication (Doan et al., 2015), dissolved oxygen depletion (Schladow and Hamilton, 1997; Antonopoulos and Gianniou, 2003; Bell et al., 2006), manganese release (Bertone et al., 2015) and greenhouse gas emission to the

atmosphere (Barrette and Laprise, 2005; Smits et al., 2009). Knowledge of the physical processes that occur inside the reservoir and its driving forces are important for the management of these systems (Curtarelli et al., 2014).

One of the most important parameters influencing those processes and consequently the management of lakes and reservoirs is temperature. Lakes and reservoirs may present a seasonal behavior and stratify due to hydrological and meteorological conditions, and specially its vertical distribution may be related to water quality. Stratification can control heat and dissolved substance transport (Esteves, 1988). Thermocline depth and its variation over the year may be an indicator of substances distribution over the water column. One example that shows this connection is related to dissolved oxygen concentration. Usually if the reservoir is mixed, the concentration of dissolved oxygen is uniform over depth. If stratification is formed and a thermocline is defined, usually the dissolved oxygen transfer to deeper layers is compromised because mixing is diminished by the stratification. Once the oxygen is consumed at this layers, an anoxic condition may be identified at layers below thermocline. After stratification is broken and thermocline is not defined, due mixing of the water column, dissolved oxygen concentration starts to increase again in deeper layers.

Mannich (2013) measured several temperature and dissolved oxygen profiles in the deepest point of Vossoroça reservoir (Figure 2) on August 2012. According to Mannich (2013), in the first 3 m the water is well mixed, and has a variation of 1 °C over the day. The thermocline is located approximately 4 m from the surface. Dissolved oxygen (DO) showed a characteristic profile – higher concentrations at the top layer and decrease in concentration with depth (Mannich, 2013), but no anaerobic condition was verified (August is the month where stratification starts in Vossoroça reservoir). These profiles show that there is a relation between temperature and DO concentration in the water column – the thermocline corresponds to the point where there is a decrease in DO concentration, meaning that physical stratification corresponds to chemical stratification. Temperature information in the water column allows several associations to water quality – also, temperature is an easier parameter to measure and need less information to be modelled, compared to water quality parameters, that include more processes and parameters to calibrate.

Curtarelli et al. (2014) point out the need of field measurements, as meteorological and limnological data to the understanding of physical processes in lakes and reservoirs. Continuous temperature profiles are key measurements to the understanding of physical processes in a water body, since they allow analysis of the seasonal behavior of the reservoir, identification of mixing and stratification periods and thermocline depth. Continuous measurements have been reported, although measurements including spatial variations are still poorly employed, therefore heat transport between shallow and deeper regions of a reservoir, for example, are often not being measured. Meteorological information is also

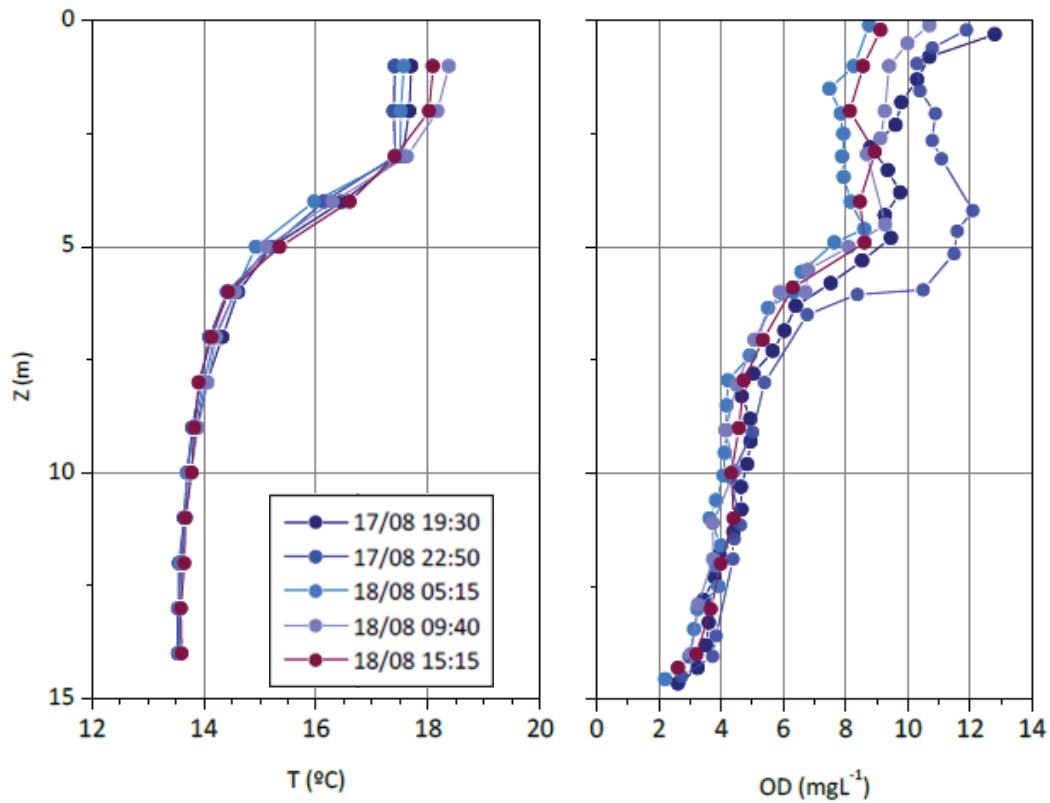


Figure 2 – Temperature and dissolved oxygen (DO) profiles measured in the deepest point of Vossoroca reservoir. Source: Mannich (2013)

significant to heat transport in lakes, and the locations where these measurements are done may not represent the heat exchange between the air-water interface of the water body.

In addition, the use of hydrodynamic models complements the understanding of physical processes (Martin and McCutcheon, 1999). The advantages are related to the possibility of simulating real and hypothetical scenarios and various processes simultaneously or separately (Curtarelli et al.; 2014). Hydrodynamic models have been widely used for this purpose (Curtarelli et al., 2014; Wahl and Peeters, 2014; Marti et al., 2011). For lakes and reservoirs, one, two and three-dimensional models are available for heat transport simulation. Disadvantages of this approach are usually related to the quantity of input and verification data. This is one positive aspect of one-dimensional models – vertical temperature structure and related gradients may be studied with few data and parameters for calibration. Also, they allow long time simulation associated with fine grid resolution, but the disadvantage is the impossibility of studying horizontal gradients. Two-dimensional models, on the other hand, allow the analysis of these gradients in the longitudinal direction and there is the possibility of using these models in a quasi three-dimensional scheme. Advantages of these models are related to the time consumption, which is con-

siderable lower than three-dimensional models and better representation of the system. Three-dimensional models, allow the simulation of the entire system, considering horizontal effects that may impact thermal structure and water quality. Its disadvantages are related to calibration, time consumption and, most of time, impossibility of vertical gradients analysis with fine resolution as in one-dimensional models.

The next section presents the heat transport process, main drivers and consequences to the dynamics in a lake or reservoir. Then, a section about measurements and a section about the models used to the heat transport modeling.

2.1 Heat transport process

Lakes and reservoirs usually show a seasonal behavior related to its physical structure, due to meteorological and hydrological influence. The main heat transfer in a lake or reservoir occurs at the air-water interface due to solar radiation (responsible for heating the surface waters), long wave radiation, sensible and latent heat. Mixing in reservoirs occurs due to: the mixing energy from inflowing waters, the mixing energy from outflows or withdrawals and the energy transfer at the air-water interface, due wind or other meteorological conditions (Martin and McCutcheon, 1999). These energy fluxes at the surface can develop thermal stratification, due to temperature differences between the water layers, i.e., water density, and the lack of sufficient energy to prevent the stratification – solar heating dominates mixing due to wind and flow (Martin and McCutcheon, 1999).

In general, reservoirs show three different layers when stratified: the epilimnion which is the superior layer, well mixed and warm (Horne and Goldman, 1994); the hypolimnion, colder and denser than the epilimnion (Esteves, 1988); and the transition of these two layers is the metalimnion, where it is located the thermocline (Esteves, 1988) that acts as a barrier to the transport between the layers. The knowledge of the variation of these layers and related gradients is essential for the analysis of substances transport (e.g. gas, nutrients) and related water quality issues, as eutrophication (Doan et al., 2015), dissolved oxygen depletion (Schladow and Hamilton, 1997; Antonopoulos and Gianniou, 2003; Bell et al., 2006), manganese (Bertone et al., 2015) and greenhouse gas emissions (Barrette and Laprise, 2005), which are influenced by stratification and mixing processes. Reservoirs are often classified by the number of mixing events during a year. In Brazil, for example, lakes and reservoirs are monomitic, i.e., they are completely mixed once a year (e.g., Vossoroca and Capivari reservoirs, located in Paraná State), while reservoirs in USA (e.g., Onondaga Lake) are dimictic (Prestigiacomo et al., 2015), with two episodes of mixing in a year. There are also oligomictic reservoirs, that rarely have circulation periods, and polimictic lakes and reservoirs which have continuous or frequent circulation (Wetzel, 1983). Polymictic lakes react within a few hours to a forcing – meteorological forcing, for example, and this may affect great part of the water column (Soulignac et

al., 2017). This is a different pattern than monomitic lakes and reservoirs, studied in this Thesis – the reservoir responds to a forcing in a seasonal time scale.

The pattern of flows and mixing in a lake is affected by bathymetry, thermal structure, inflows, outflows and wind mixing (Martin and McCutcheon, 1999). Monismith et al. (1990) measured temperature profiles in three different regions of the Wellington reservoir (in shallow and deeper regions) and found out there is a non-one-dimensional response of the reservoir to heating and cooling, due to sloping bathymetry generating gravity currents (Wells and Sherman, 2001). Figure 3 shows measurements performed by Monismith et al. (1990) in which horizontal temperature gradients are identified due to difference in depth in the reservoir.

This response is due differential cooling and/or heating. The former is, for a given heat flux out of the water surface, temperature of the water column decreases more rapidly in the shallower regions where the water column has less thermal mass than the deeper regions (Wells and Sherman, 2001). This produces a horizontal temperature gradient (i.e., water density) which is driven to the bottom as a cold gravity current that transports denser water and even contaminants, from the shallow to the deeper regions (Wells and Sherman, 2001). The differential heating, on the other hand, occurs when solar radiation heats shallow waters faster than open waters (Horsch and Stefan, 1988). The effects of differential cooling/heating depends on the weather conditions and may be switched on or off within minutes or hours (Imboden and Wüest, 1995).

In Figures 3.a and 3.b the dominant process presented is differential cooling. In Figure 3.a, temperature gradients at the surface are small (measurements at 16:15 h). In Figure 3.b, however, the temperature gradients are between 0.3 and 0.4 °C (or a difference between 0.08 and 0.1 kgm⁻³). Also in this figure, the isotherms in the deeper water are forced down, indicating water movement between the littoral and pelagic zone. Figure 3.c shows a time serie between three points in the reservoir (location of the points is indicated in Figure 3.a and 3.b). The graph shows that shallow water warms faster during the day and cools faster during the night in relation to deeper points. This is an evidence that differential cooling/heating could occur in the reservoir and affect transport of heat and substances. Curtarelli et al. (2014) investigated the effects of cold front activity in Itumbiara reservoir (Brazil) with three-dimensional modeling and identify that cold fronts may increase temperature gradients between littoral and pelagic zones, enhancing the possibility of transport by differential cooling.

James and Barko (1991) measured temperature transects in Eau Galle reservoir (USA) and used a tracer (Rhodamine WT red fluorescent dye) to analyse horizontal transport due differential cooling. With the results of the hourly volumetric flow rates estimated from the tracer (between littoral and pelagic regions), they calculated the total phosphorus (TP) exchange rates, assuming that TP moves with the tracer. The measurements by James and Barko (1991) show that the higher the horizontal temperature gradients, higher the

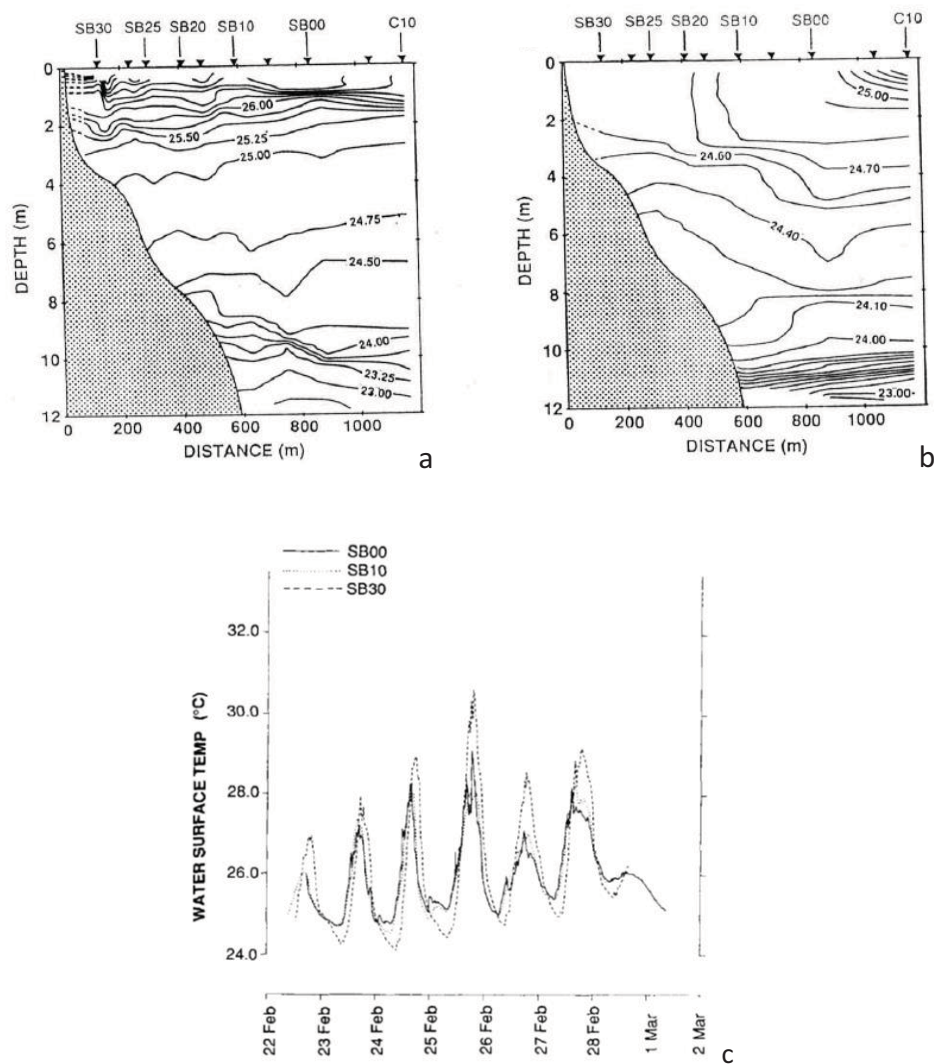


Figure 3 – Temperature measurements in a section of Wellington reservoir (Australia) (Monismith et al., 1990) a) Longitudinal transects at 16:15 hours, 23 February b) 24:00 hours, 23 February c) Water surface temperatures (stations are identified in a and b)

hourly volumetric flow rates. Figure 4 shows temperature and tracer distribution along a section in the Eau Galle reservoir.

Inflows contribute to the mixing of lakes and they are a primary source of dissolved and particulate materials (Martin and McCutcheon, 1999). Density differences between the inflow and lake may be due to differences in temperature, concentrations (of dissolved and suspended substances) or a combination of these (Marti et al., 2011). If the density differences are due to differences in temperature or dissolved materials, inflows entering the reservoir are called density currents (Martin and McCutcheon, 1999). Although, if density differences are a result of particulate loads, inflows are referred as turbidity currents (Martin and McCutcheon, 1999).

The depth at which inflowing water will enter the reservoir depends on its density and the lake density. If inflowing water has lower density than the surface water of the lake, an overflow occurs. If, on the other hand, the inflowing density is larger than the density

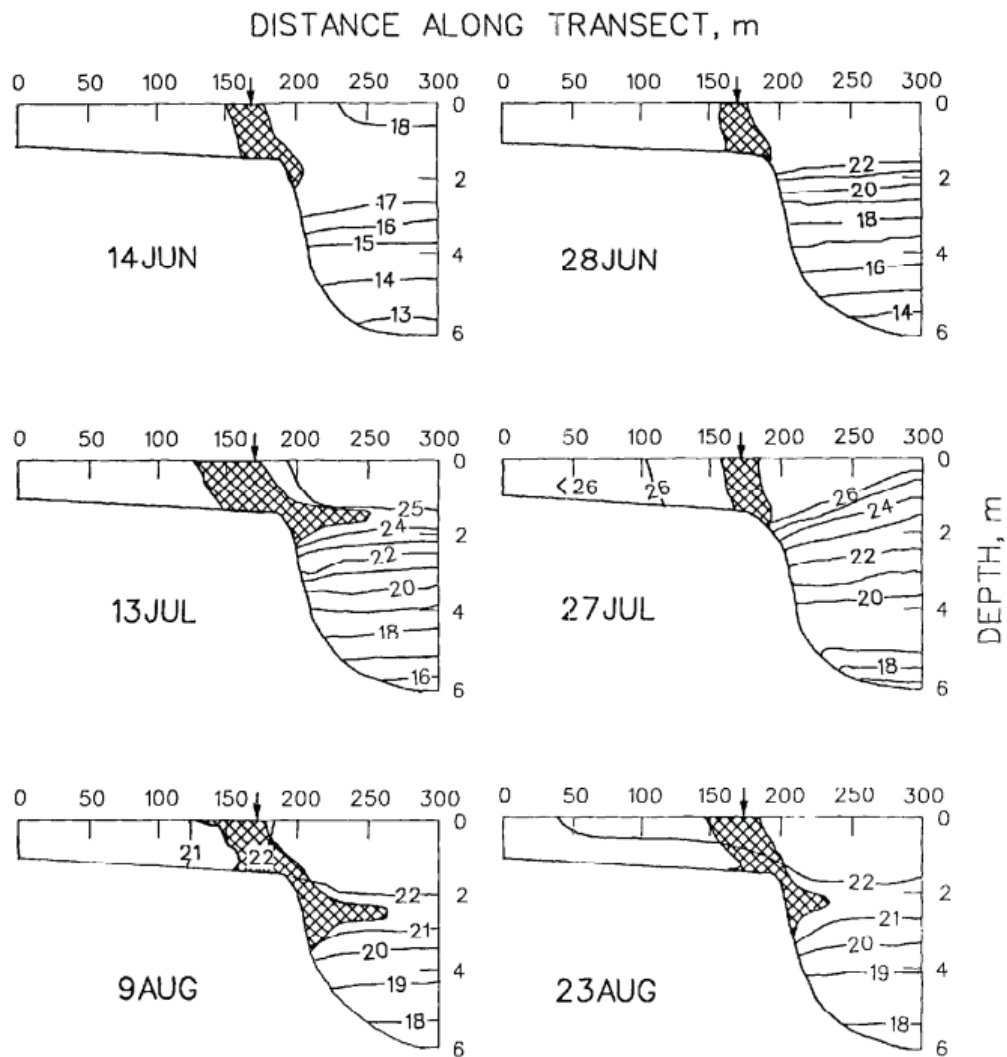


Figure 4 – Temperature and tracer distribution in a section of Eau Galle reservoir (USA) measured by James and Barko (1991)

of the bottom of the lake, an underflow occurs (Marti et al., 2011). When inflow density is between the density of surface and bottom of the lake, an interflow occurs into the depth of similar density. According to Martin and McCutcheon (1999), small lakes that weakly stratify are often completely mixed during high-flow events. Li et al. (2015) identified that high density inflows could weaken thermal stratification. Martin and McCutcheon (1999) also point out to the strong impact of inflows on circulation and water quality of lakes and reservoirs.

Meteorological events are also significant influences on water quality in lakes and reservoirs (Martin and McCutcheon, 1999), which includes thermal energy due to radiation, sensible heat, evaporation and mechanical energy transfer due the wind (Tuan et al., 2009). Wind stress and convective turbulence maintain mixing and, therefore, tend to remove stratification and homogenize the surface layer while solar radiation strengths the stratification (Wüest and Schmid, 2013). Wind also induces motions depend of the

spatial-temporal variation of wind forcing interacting with bathymetry and density distribution. These motions include basin-scale internal waves driven by temporal variations and basin-scale mean circulation driven by spatial variations on the wind stress (Laval et al., 2003).

Figure 5 shows an scheme of the main processes affecting heat transport in lakes and the objective and significance of this thesis. Figure 5.a exhibits a reservoir with varying bathymetry, which receives and releases low inflows and outflows and is influenced by meteorological forcing. The main heat transfer occurs at the air-water interface, mixing occurs mainly by the wind and little mixing by inflows/outflows is expected. Solar radiation may keep warmer shallow regions than deeper regions due to differential heating or, if the reservoir is losing heat, differential cooling could happen in the reservoir.

Figure 5.b shows the same scheme, but the reservoir has higher inflows and outflows, as a run-of-a-river reservoir, which may induce velocities and affect mixing processes and thermal structure of the reservoir. Figure 5.c, on the other hand, presents a simplified scheme of the objective of this thesis. The schemes on Figures 5.a and 5.b shown none distinction between shallow and deeper regions of the reservoir, which are the purpose of this thesis, the sector approach, allowing the analysis of the heat transport in lakes, considering the variations of depth.

The assessment of the main contribution to the heat transport in lakes depends on measurements, which allow the spatial and temporal analysis of the daily and seasonal behavior of the water body. As described in this section of the main physical processes, data required are temperature profiles, inflows and outflows information and meteorological data, which will be discussed in the next section, bearing in mind the importance of measurements for the spatial and temporal characterization and modeling of the heat transport.

2.2 Measurements in lakes and reservoirs

This section describes some of the newest works and a discussion regarding measurements in lakes and reservoirs and the approach used to measure variables related to heat transport to support future measurements.

Table 2 presents information about other reservoirs regarding measurements, used for comparison with Vossoroça reservoir, located in Paraná State, Brazil. Table 2 describes the reservoir studied by Huang et al. (2014), which has area with the same magnitude of Vossoroça reservoir, although its maximum depth is almost six times of Vossoroça's. The largest reservoir, in terms of surface area, is studied by Curtarelli et al. (2014) and Curtarelli et al. (2013), also in Brazil, where the surface area is almost 247 times Vossoroça reservoir surface area and its maximum depth is greater than four times Vossoroça's maximum depth. Only by this comparison it is feasible to analyse the great variability in

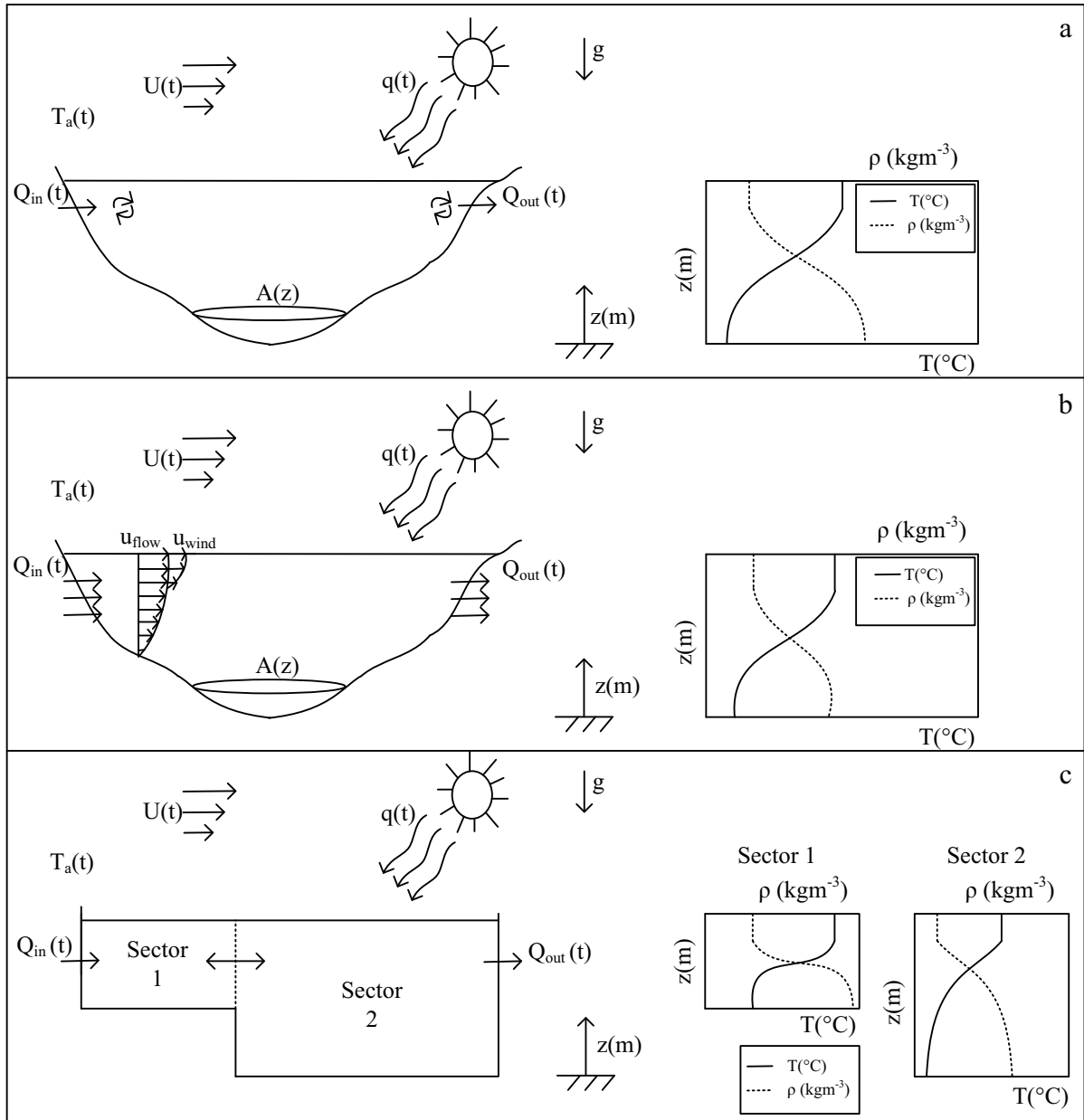


Figure 5 – Representation of the main heat transport parameters in lakes. a) Low inflows and outflows, b) High inflows and outflows, c) Sector approach.

sizes and shapes of lakes and reservoirs, that result in different boundary effects (Imboden and Wüest, 1995).

Curtarelli et al. (2014) point out the need of continuous and frequently collection of meteorological and limnological data, that is costly and requires complex logistic when performed using only conventional methods (Curtarelli et al., 2014). This section will describe the most important variables to measure when working with heat transport in lakes, related to the temperature of the water column, temperature of the inflowing/outflowing water (and the inflow/outflow) and meteorological variables.

Table 2 – Reservoirs monitoring comparison

Reference	Study site	Lake	A (km ²)	Maximum depth (m)	Monitoring period	Floating platform	Monitoring points	Frequency	Equipment	Meteorological monitoring
Li et al. (2015)	China	Shibianyu	–	60	2011–2013	0	3	Weekly	Hydrolab DS5X multi probe sonde	–
Huang et al. (2014)	China	Jinpen	4.55	94	2011–2012	0	4	Weekly	Hydrolab DS5X multi probe sonde	–
Bertone et al. (2015)	Australia	Advancetown	15	50	2008–2012	1	1	3h	YSI Sonde	Water (3 h)
Prestigiacomo et al. (2015)	USA	Onondaga	12	20	2007, 2009, 2010, 2012	0	36	Weekly	SBE 37-SI MicroCAT	–
Curtarelli et al. (2014)	Brazil	Itumbiara	814	78	1 day	2	2	1 h	Two chains of temperature sensors	✓ (1 h)
Curtarelli et al. (2013)	Brazil	Itumbiara	778	78	49 days	2	2	1 h	Two chains of temperature sensors	Water (1 h)
Marti et al. (2011)	Australia	Thomson	22.3	165	4 days	2	2	3 min	Two chains of temperature sensors and one of DO	Water (3 min)
Yang et al. (2010)	China	Dianchi	308.6	>4.4	2003–2007	0	8	Monthly	–	–
Yu et al. (2010)	Korea	Daecheong	–	–	03–11.2002–2003	0	5	Monthly	–	Land (Daily)
Yu et al. (2010)	Japan	Biwa	23	30	2002–2004	0	1	1 h	Fine-Scale Profiler (F-probe)	✓ (1 h)
Tuan et al. (2009)	Japan	Shikinawa	4.92 10 ⁻²	2.5	3 days	1	3	2 min	Thermocouple system	Water (2 min)
Morillo et al. (2008)	USA	Coeur d’Alene	129	64	12 days	1	71	Daily	F-Probe and SCAMP (fluctuations)	Water (1 min)
Elçi (2008)	Turkey	Tahtali	20	27	08–12.2006	0	1	Monthly	Multiparameter water-quality meter	Land
Vossoroca reservoir	Brazil	Vossoroca	3.3	17	since 2012	1	1	15 min	One chain of temperature sensors	Land (2 min)
Passaúna reservoir	Brazil	Passaúna	11	17	2016	1	5	Monthly	Chain of temperature sensors, DO, ADCP, ABT, Fluoroprobe, OPUS, nanoFlu	Land (1 h/ 1 min)
Capivari reservoir	Brazil	Capivari	12.6	35	2012–2013	1	–	1 h	One chain of temperature sensors	Water/Land (1h)

Temperature of the water column may be measured continuously in a point or taken as a punctual measurement in time (daily, weekly or monthly measurements). Table 2 presents a comparison between strategies to measure temperature in a few recent studies related to heat transport in lakes. As Table 2 shows, there is not just one strategy to measure temperature and even recent studies adopt only weekly or monthly measurements, which can cover a large area of the reservoir, but its temporal variation is not well represented. From Table 2, continuous temperature measurements is not yet fully explored, although it has been reported the importance of diurnal cycles of stratification and mixing (Curtarelli et al., 2014). Also, from Table 2, the higher the frequency of measurements, the lower the study period, therefore the full cycle of stratification and mixing is not investigated in recent studies. The main conclusion for temperature profile measurements is that, even being reported that the knowledge of thermal structure of the reservoir is important to understand physical processes, high frequency temperature measurements are not adopted. In addition, when they are applied, spatial variation of the water temperature is not covered.

Inflows act as a primary source of dissolved and particulate materials (Martin and McCutcheon, 1999). In relation to overflows, they can contribute substantially to water quality variations, since they add materials directly to the more productive surface zones of the lake or reservoir (Martin and McCutcheon, 1999). From the studies shown in Table 2, only Li et al. (2015), Huang et al. (2015), Marti et al. (2011) and Morillo et al. (2008) controlled the inflowing waters. The temperature of the inflowing water should be measured, since the density of the water determines if the water enters as an overflow, and interflow or a underflow (Marti et al., 2011) and several studies have investigated the distribution of inflows in lakes, as Huang et al. (2014), Marti et al. (2011), Yu et al. (2010) and Chung et al. (2009). In addition, it has been reported that large inflows can increase turbulence – decreasing water stability and weaken stratification and may introduce oxygen in deeper layers. Depending on the density of the inflows and the lake, inflows may be distributed in the water column or be confined in some region, affecting water quality.

Meteorological data are the most important driving forces of the heat exchanged between air-water interface in reservoirs. Table 2 shows a comparison between meteorological variables measured in different regions of the world. Frequency of monitoring varies from 1 min to daily measurements (Vossoroca reservoir has frequency of 2 min) and the location of meteorological data monitoring is, most of the time, over the water surface than in an onshore weather station (some of the studies do not specify the location and/or neither the frequency of monitoring). León et al. (2007) performed a sensitivity analysis in a three-dimensional heat transport model to provide information on the impact of meteorological inputs on the simulation of surface temperature and heat fluxes – increasing 10% in air temperature and solar radiation produce 3.08% and 8.27% increase in the water

surface temperature, respectively, and 8.5% decrease in the evaporative heat flux (León et al., 2007).

Measurements of meteorological data may present differences according the place they are taken. Usually these measurements are made in an onshore weather station instead over the water surface. These different locations may give different measurements – wind speed could be affected by the presence of obstacles and relative humidity over the water surface is usually higher than in the onshore weather station. Therefore, since the main heat transfer in a reservoir occurs at the air-water interface, it may affect heat transfer and, when working with heat transport modeling, differences between the actual heat transfer could result in non reliable findings and do not represent the system or expected events of mixing and stratification. Analysis of the heat transfer between air-water interface with data from different meteorological stations were performed in this thesis to the analysis of the impact of the location of measurements. The results will be present in the section 4.3.

To complement the understanding of the system and its physical processes, measurements are usually combined with modeling, which allows analysis of scenarios, sensitivity due some change and the importance of each forcing in the system. The next section approaches the modeling of heat transport in lakes, the state-of-art and issues related to modeling.

2.3 Modeling of heat transport in lakes and reservoirs

Heat transport in lakes may be modeled by one, two or three-dimensional models. This section describes the main differences between each approach and their strengths and weaknesses.

The first group are one-dimensional models that have been widely used to simulate seasonal thermal structure behavior of reservoirs, identification of mixing periods and coupled with water quality (Martin and McCutcheon, 1999; Weinberger et al., 2012). These models assume horizontal homogeneity, vertical turbulent diffusivity is a relation of the wind speed at the surface and usually not uniform (Jassby et al., 1975; Sundaram and Rehm, 1971; Henderson-Sellers, 1986), there is no flux of energy at the bottom (Gianniou and Antonopoulos, 2003; Babajimopoulos and Papadopoulos, 1986), although that could not be true for shallow reservoirs (Wetzel, 1983) and the energy flux at the surface is parametrized (Edinger et al., 1986; Sundaram and Rehm, 1971) or calculated term-by-term (Henderson-Sellers, 1986). Polli (2014) reviewed one-dimensional models and concluded that none is capable of simulating all physical processes that happen in the water column and the more complex models need more parameters to calibrate. Some of the well known models are: DYRESM (Weinberger et al., 2012; Hocking et al., 1991; Imerito, 2007), SIMSTRAT (Peeters et al., 2002; Goudsmit et al., 2002), FLake (Mirinov,

2003) and GLM (Hipsey et al., 2014). GLM, the General Lake Model, for example, is a one-dimensional hydrodynamic model for water balance and vertical stratification of lakes and other standing water bodies simulations, and it is an open source model (Hipsey et al., 2014). The model is suitable for investigations where the horizontal variability is not a requirement of the study. The model can be coupled with ecological models to support simulations of lake water quality and ecosystems processes. The model couples with the Framework for Aquatic Biogeochemical Models (FABM) and is able to simulate turbidity, oxygen, nutrients, phytoplankton, zooplankton, pathogens and chemical variables (Hipsey et al., 2014). Polli (2014) also developed an one-dimensional heat transport model called MTCR-1, described in Section 2.3.1.

Laterally averaged two-dimensional models simulate water quality changes in the longitudinal and vertical directions (Martin and McCutcheon, 1999). They are applicable to stratified reservoirs where lateral variations are negligible (Martin and McCutcheon, 1999). Two-dimensional models solve the two-dimensional laterally averaged equations of continuity, momentum and transport. CE-QUAL-W2 is the well known laterally averaged model and has been widely used in problems related to thermal stratification (Modiri-Gharehveran et al., 2014; Zouabi-Aloui et al., 2014; Bonalumi et al., 2012).

Three-dimensional models solve the full continuity, momentum and transport equations. Some well known three-dimensional models are ELCOM and Delft3D. Both models solve Reynolds Averaged Navier Stokes equations, assuming hydrostatic and Boussinesq approximation (Deltares, 2014; Lee et al., 2013). Numerical approach used in ELCOM is finite volume method (Chung et al., 2009) while in Delft3D, finite difference method (Deltares, 2014). Both models use a staggered grid (Deltares, 2014; Lee et al., 2013) which means velocities are defined on cell faces and scalars on cell centres and both models follow the stability criterion of Courant-Friedrichs-Lewy condition (Deltares, 2014; Lee et al., 2013). Delft3D has five different heat flux models (Deltares, 2014), while ELCOM has one heat flux model that calculates all heat fluxes at the air-water interface separately (Lee et al., 2013). One difference in the heat flux models is in the heat absorption in the water surface – if a grid cell is lower than 1 m, the heat is distributed in the first one meter from the free surface in ELCOM (Lee et al., 2013) while in Delft3D the absorption is in the first grid cell from the surface (Deltares, 2014). Delft3D has four models of turbulence closure for vertical viscosity and diffusivity, from a uniform value defined by the user up to a $k - \epsilon$ model that solves two transport equations for production and dissipation of turbulent kinetic energy (Deltares, 2014). ELCOM takes an approach derived from the mixing energy budgets used in 1D lake modeling (Lee et al., 2013). ELCOM estimates an energy budget between the energies available for mixing, required for mixing, and dissipated based upon the 3D turbulent kinetic energy transport equation (Hodges, 2000).

Table 3 shows a comparison between one, two and three-dimensional models, summa-

rizing the main information related to assumptions, equations and formulations applied in these models. The question of each model to use is always an issue to be discussed. All models have their strengths and weaknesses, and the choice should be related to the system, main forcings, available data and the degree of detail in the modeling. Table 4 shows the equations used to solve one and three-dimensional models (since both models are used in this thesis) – 1D equations from MTCR-1 model and 3D equations from Delft3D model, presented in detail later in this section.

One-dimensional models have the ability to simulate fast and efficiently, with a high spatial and temporal resolution, heat transport in lakes. If a great detail in the vertical structure is necessary and the horizontal effects are not important, this kind of model is capable of simulating with good resolution and precision temperature in the water column. If a process become important (e.g., high inflows/outflows), one-dimensional models could be not representative of the system.

Two-dimensional models, on the other hand, allow the simulation of vertical and longitudinal direction. These models advantages are related to the time consumption for computation (which is considerable lower than for three-dimensional models) and input data.

Three-dimensional models are capable to simulate all processes in the vertical and horizontal directions. Despite the fact of being more complete than one and two-dimensional models, there are some limitations in their application. Grid resolution could be a limiting factor in three-dimensional modeling when working with heat transport, where vertical resolution is of great importance, and the increase of layers increases the computational time, which is not practical for the engineering point of view (even for daily or seasonal variations). In addition, the definition of the number of layers and their arrangement may be difficult to define.

For practical purposes of engineering or system management, modeling of temperature has several applications. In the case of drinking water purposes, modeling is a tool for the analysis of where to intake water and at which depth (which temperature is required). One-dimensional models are capable to answer the depth of intake, but can not answer the best location spatially in the reservoir. Also, one-dimensional models have the ability to simulate several scenarios of the thermal structure in a short period of time. Two-dimensional models, on the other hand, could answer the depth and location on the longitudinal direction. Three-dimensional models will answer the location of the intake and depth (as explained before, depth could be a limiting factor of the modeling), but the time required to this application from the practical point of view may not be the optimum solution. The choice of the location where to intake water may reduce treatment costs and optimize the management.

Additionally, other issue related to reservoirs, thermal structure and different regions of the reservoir, which have been widely studied in the last years is the greenhouse gas

emissions. Emissions could be associated with heat transport modeling and the most suitable regions of emissions could be identified. Also, the effects of discharging cooling water from industry, that may affect physical processes could be modelled with a heat transport model. Other examples of applications are related to the impacts on the water body due to climate change and, for large water bodies, surface water temperatures may be used in weather forecasting models.

All the issues described before require spatial representation in a model. One-dimensional models are not suitable for that kind of application, although three-dimensional models are not appropriate when a fast response of the system is necessary. Therefore, the sector model proposed in this thesis could be an option to problems where fast response of the system and spatial resolution is required, since will adopt the fast response of one-dimensional models and the spatial variation in the reservoir.

The next sections show a description of the one-dimensional model MTCR-1, the two-dimensional model CE-QUAL-W2 and the three-dimensional model, Delft3D. In addition, section 2.2.3 presents applications regarding measurements and modeling in lakes and reservoirs.

2.3.1 One-dimensional model

This thesis continues using and improving the model developed by the author. Polli (2014) developed an one-dimensional heat transport model for lakes called MTCR-1 ("*Modelo de transporte de calor para reservatórios - 1D*") which solves the 1D heat transport equation. The main forcings of the model are meteorological and hydrological data. Temperature of Vossocora lake was simulated and the error obtained was 0.26 ± 1.42 °C (Polli, 2014).

Governing Equations

The main equation used, that solves one-dimensional heat transport in lakes is (Polli, 2014)

$$A \frac{\partial T}{\partial t} = \frac{\partial}{\partial z} \left[EA \frac{\partial T}{\partial z} \right] + \frac{1}{\rho c_p} \frac{\partial Aq(z)}{\partial z} + \frac{Q_{in}AT_{in} - Q_{out}AT}{V} \quad (1)$$

in which A is the area (m^2), T is the temperature ($^{\circ}\text{C}$), t is the time (s), z is the depth (m), E is the eddy diffusivity coefficient (m^2s^{-1}), ρ_w is the water density (kg m^{-3}), c_p is the specific heat of water ($\text{Jkg}^{-1}\text{K}^{-1}$), $q(z)$ is a heat source term represented by solar radiation ($\text{Jm}^{-2}\text{s}^{-1}$), Q_{in} is the inflow (m^3s^{-1}), Q_{out} is the outflow (m^3s^{-1}) e V is the volume (m^3).

Boundary conditions are related to energy fluxes at the surface and the bottom. At the surface, heat fluxes are due solar radiation, evaporation, conduction and emission (from water and atmosphere), described as (Babajimopoulos and Papadopoulos, 1986):

Table 3 – Comparison between one, two and three-dimensional models

	One-dimensional models	Two-dimensional models	Three-dimensional models
Equations	Transport	RANS +Transport	RANS +Transport
Assumptions	Horizontal homogeneity	Hydrostatic and Boussinesq approximation; Lateral homogeneity	Hydrostatic and Boussinesq approximation
Discretization	Finite volume or finite difference	Finite difference	Finite volume or finite difference
Grid	Staggered	Staggered	Staggered
Coordinates	Cartesian	Cartesian	Cartesian/Spherical
Turbulence	In general, a function of Ri (there are also models that adopt $k - \epsilon$ turbulence model)	Formulations: Nickuradse; Parabolic, W2, W2 with mixing length of Nickuradse; RNG; $k - \epsilon$	Constant coefficient; Algebraic eddy viscosity closure model; $k - L$ turbulence closure model; $k - \epsilon$ turbulence closure model
Heat flux model	Parametrized or calculated term-by-term; Solar radiation absorbed over depth	Parametrized or calculated term-by-term; Solar radiation absorbed over depth	Calculated term-by-term; Solar radiation absorbed at the surface or over depth
Light extinction	Constant	Constant	Constant
Sediment heat exchange	Not considered	Considered	Not considered

Reynolds Averaged Navier-Stokes Equations

Richardson number

Models available in CE-QUAL-W2

Table 4 – Set of equations solved by one and three-dimensional models MTCR-1 and Delft3D

Model	Equation
1D	Continuity No continuity equation is solved ($u, v, w = 0$)
1D	Momentum No momentum equation is solved ($u, v, w = 0$)
1D	Transport $A \underbrace{\frac{\partial T}{\partial t}}_{\text{unsteady term}} = \underbrace{\frac{\partial}{\partial z} \left[EA \frac{\partial T}{\partial z} \right]}_{\text{mixing term}} + \underbrace{\frac{1}{\rho c_p} \frac{\partial A q(z)}{\partial z} + \frac{Q_{in} AT_{in} - Q_{out} AT}{V}}_{\text{source term}}$
3D	Continuity $\frac{\partial \zeta}{\partial t} + \frac{\partial(d + \zeta)u}{\partial x} + \frac{\partial(d + \zeta)v}{\partial y} + \frac{\partial(d + \zeta)w}{\partial z} = Q$
3D	Momentum x $\frac{\partial u}{\partial t} + u \frac{\partial u}{\partial x} + v \frac{\partial u}{\partial y} + w \frac{\partial u}{\partial z} - f v = M_x - \frac{1}{\rho} \frac{\partial P}{\partial x} + \frac{1}{(d + \zeta)^2} \frac{\partial}{\partial \sigma} \left(\nu_v \frac{\partial u}{\partial \sigma} \right) + \nu_h \left(\frac{\partial^2 u}{\partial x^2} + \frac{\partial^2 u}{\partial y^2} \right)$
3D	Momentum y $\frac{\partial v}{\partial t} + u \frac{\partial v}{\partial x} + v \frac{\partial v}{\partial y} + w \frac{\partial v}{\partial z} - f u = \underbrace{M_y}_{\text{sources/sinks of momentum}} - \underbrace{\frac{1}{\rho} \frac{\partial P}{\partial y}}_{\text{pressure term}} + \underbrace{\frac{1}{(d + \zeta)^2} \frac{\partial}{\partial \sigma} \left(\nu_v \frac{\partial v}{\partial \sigma} \right) + \nu_h \left(\frac{\partial^2 v}{\partial x^2} + \frac{\partial^2 v}{\partial y^2} \right)}_{\text{viscosity term}}$
3D	Momentum z $\frac{\partial P}{\partial \sigma} = -\rho H$ <i>Hydrostatic pressure</i>
3D	Transport $\frac{\partial(d + \zeta)T}{\partial t} + \underbrace{\frac{\partial(d + \zeta)uT}{\partial x} + \frac{\partial(d + \zeta)vT}{\partial y} + \frac{\partial(wT)}{\partial \sigma}}_{\text{advective term}} = \underbrace{d + \sigma \left[\frac{\partial}{\partial x} \left(D_H \frac{\partial T}{\partial x} \right) \right] + (d + \sigma) \left[\frac{\partial}{\partial y} \left(D_H \frac{\partial T}{\partial y} \right) \right]}_{\text{mixing term}} + \underbrace{\frac{1}{d + \zeta} \frac{\partial}{\partial \sigma} \left(D_V \frac{\partial T}{\partial \sigma} \right) + \frac{1}{\rho c_p} S}_{\text{source term}}$

$$\rho c_p E \left. \frac{\partial T}{\partial z} \right|_{z=H} = -q_n \quad (2)$$

where q_n is the net heat flux. At the bottom, there are no energy fluxes (Gianniou and Antonopoulos, 2003; Babajimopoulos and Papadopoulos, 1986)

$$\left. \frac{\partial T}{\partial z} \right|_{z=0} = 0. \quad (3)$$

Heat flux model

Heat flux at the air-water interface is due solar radiation, long wave radiation (from atmosphere and water), sensible heat and evaporation (Henderson-Sellers, 1986). Edinger et al. (1968) proposed the energy flux is

$$q_n = K(T_e - T_s) \quad (4)$$

in which K is the heat transfer coefficient ($\text{WK}^{-1}\text{m}^{-2}$), T_e is the equilibrium temperature ($^{\circ}\text{C}$) and T_s is the superficial water temperature ($^{\circ}\text{C}$). If $T_s < T_e$, the water body receives heat.

Eddy diffusivity coefficient

Sundaram and Rehm (1971) proposed for the eddy diffusivity coefficient E , in stable thermal stratification

$$E = E_0 f(Ri) \quad (5)$$

$$f(Ri) = \frac{1}{1 + 37Ri^2} \quad (6)$$

$$E_0 = \frac{\kappa u_s^* z}{P_0} \exp(-k^* z) \quad (7)$$

where E_0 is the neutral eddy diffusivity coefficient (m^2s^{-1}), f is a function of Richardson Number (Ri) (a relation between buoyancy forces and turbulence generation), κ is the von Karman's constant, u_s^* is the surface friction velocity (ms^{-1}), P_0 is the neutral Prandtl number, k^* is a function for different latitudes ($k^* = 6.6\sqrt{\sin\phi}U^{-1.84}$), ϕ is latitude and U is the wind speed (ms^{-1}). MTCR-1 has an additional term of turbulence due to the inflowing waters, calculated by the mean vertical mixing coefficient by Fischer et al. (1979).

Assumptions and limitations

One-dimensional heat transport models assume the vertical direction is representative of the heat transport. The main assumption is the homogeneity in the horizontal direction. Stratification occurs due the temperature differences between the layers, i.e. water density. These models allow high spatial and temporal resolution simulation. The numerical method applied to solve MTCR-1 is implicit finite volume method. MTCR-1

can not simulate seiches.

For more detailed information about MTCR-1 model, see Appendix B and C.

2.3.2 Two-dimensional model

The two-dimensional model described in this section is CE-QUAL-W2, which is a free and open source model, developed by Cole and Wells (2015) and used to simulate longitudinal/vertical, hydrodynamic and water quality in water bodies. The model assumes that lateral variations in velocities, temperatures, and constituents are negligible. CE-QUAL-W2 also assumes hydrostatic pressure and the Boussinesq approximation. CE-QUAL-W2 has been applied to rivers, lakes, reservoirs, estuaries, and combinations of these (Cole and Wells, 2015).

Governing Equations

The hydrodynamic system of equations solves the unsteady shallow water equations in two dimensions. The equations solved are the continuity, momentum in x and z directions and transport. The following equations are solved by CE-QUAL-W2 for a rectangular grid system.

Continuity equation

$$\frac{\partial UB}{\partial x} + \frac{\partial WB}{\partial z} = qB \quad (8)$$

In equation (8), U and W are the velocity components in the x and z coordinates, B is the average cross-sectional width and q is the net lateral inflow per unit volume.

Momentum equation

$$\frac{\partial UB}{\partial t} + \frac{\partial UUB}{\partial x} + \frac{\partial UWB}{\partial z} = gB \sin \alpha - \frac{B}{\rho} \frac{\partial P}{\partial x} + \frac{1}{\rho} \frac{\partial B \tau_{xx}}{\partial x} + \frac{1}{\rho} \frac{\partial B \tau_{xz}}{\partial z} \quad (9)$$

$$\frac{1}{\rho} \frac{\partial P}{\partial z} = g \cos \alpha \quad (10)$$

In equations (9) and (10), t is time, g is the gravity acceleration, α is the channel slope, ρ is the water density, P is the pressure and τ_{xx} and τ_{xz} are the shear stress.

Transport equation

$$\frac{\partial BT}{\partial t} + \frac{\partial UBT}{\partial x} + \frac{\partial WBT}{\partial z} - \frac{\partial}{\partial x} \left(BD_x \frac{\partial T}{\partial x} \right) - \frac{\partial}{\partial z} \left(BD_z \frac{\partial T}{\partial z} \right) = \frac{1}{\rho c_p} q_T B + \frac{1}{\rho c_p} S_T B \quad (11)$$

In equation (11), T is the temperature, D_x and D_z is the longitudinal and vertical temperature dispersion coefficients, q_T is the lateral inflow or outflow mass flow rate per unit volume and S_T is the laterally averaged source/sink term.

Turbulence model

CE-QUAL-W2 has six different turbulence models: Nickuradse, Parabolic, W2, W2

with mixing length of Nickuradse, RNG and TKE. The turbulence models implemented in CE-QUAL-W2 (Cole and Wells, 2015):

1. *Nickuradse*, two equations are used to solve the mixing length and eddy viscosity. The mixing length is corrected for stability effects, according to the Richardson number;
2. *RNG*, the eddy viscosity is calculated as a function of the mixing length and the turbulent energy dissipation rate. This model was adjusted to account for stratified flow conditions by using the Richardson number;
3. *Parabolic*, assumes a parabolic distribution of the eddy viscosity;
4. *W2*, a equation is used to solve the eddy viscosity and the mixing length is assumed to be the layer thickness;
5. *W2N*, uses the same formulation as in the model W2, except that the mixing length is not the layer thickness, but is computed using mixing length of Nickaradse model;
6. *TKE*, which is the application of a $k - \epsilon$ model. The model solve two equations for the production of turbulent energy, k , and the dissipation rate, ϵ ;

A recommendation is to use the models W2 and W2N in waterbodies with deep sections that could be stratified. The other models should be used for estuary or river systems (Cole and Wells, 2015).

Heat flux model

Heat transfer at the air-water interface can be calculated term-by-term or parametrized by the equilibrium temperature, as in the model MTCR-1. In this model, solar radiation is absorbed at the water column as a function of the extinction coefficient. If no data of solar radiation is available, the model estimates the clear sky solar radiation, according to the latitude of the water body.

Different from the other models (including MTCR-1 and Delft3D), CE-QUAL-W2 calculates the heat exchange between the water and the sediment. It is a small contribution in relation to the exchange at the surface, but according to Cole and Wells (2015), investigations on several reservoirs have shown the process must be included to accurately reproduce hypolimnetic temperatures. To include this contribution, the temperature in the sediment is a input data.

Computational Grid

The model allows the simulation of any number of waterbodies (river, lake, estuary, a combination of then – more than one waterbody). Each waterbody is divided in branches, and each branch is divided in segments. See Figure 6 which shows a scheme of waterbodies, branches and segments, as defined in CE-QUAL-W2.

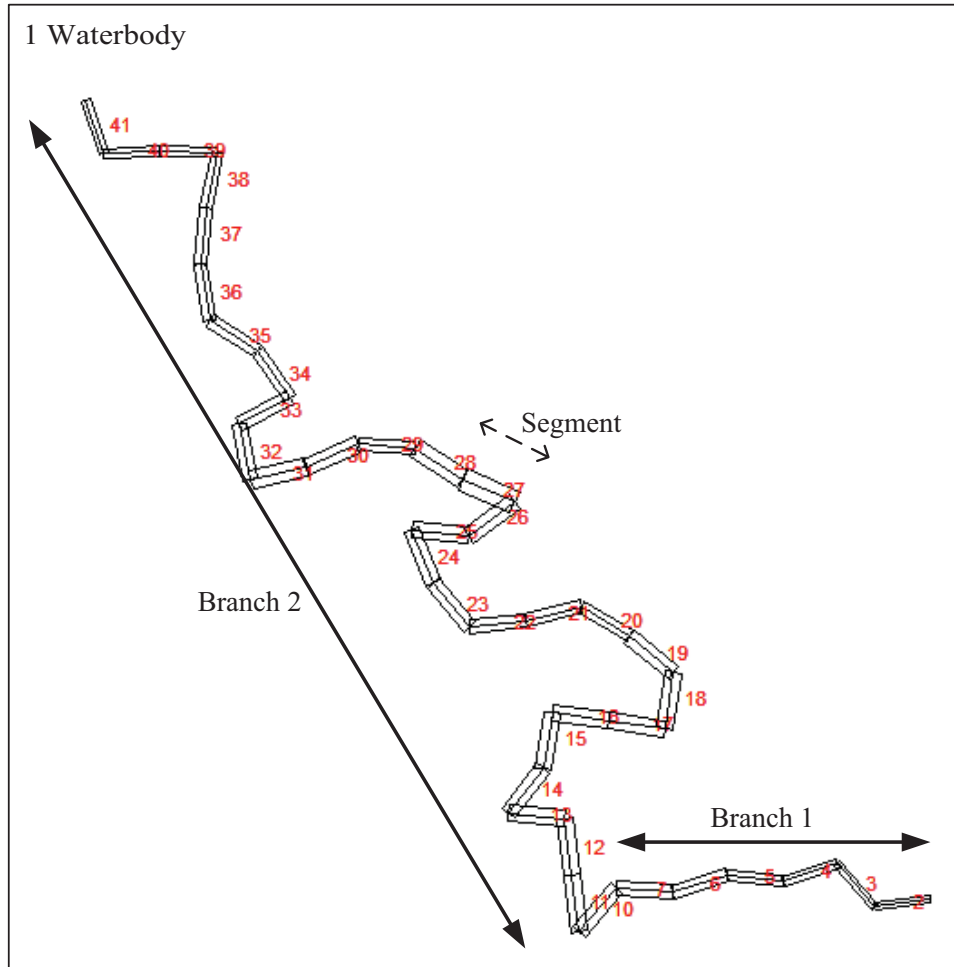


Figure 6 – CE-QUAL-W2 waterbody division for simulations – Waterbody, Branches and Segments. Adapted from Cole and Wells (2015) – examples from CE-QUAL-W2

The variables are arranged as follows on the grid – width, density, pressure and water quality state variables are defined at cell centers; horizontal velocity, longitudinal eddy viscosity and diffusivity and longitudinal shear stress are defined at the right hand side of the cell; and vertical velocity and vertical diffusivity are defined at the bottom of the cell (Cole and Wells, 2015).

Stability

Equations on CE-QUAL-W2 may be solved by implicit or explicit methods. The time step for numerical stability is reduced when solving the momentum equations using an explicit numerical method (Cole and Wells, 2015). Also, if the dimensions of a grid cell decreases, the timestep should also decrease to maintain numerical stability.

2.3.3 Three-dimensional model

The 3D modeling will be performed with Delft3D. Delft3D was chosen because it is an open source model and has been widely used to solve problems related to reservoirs and thermal stratification (Soulignac et al., 2015; Wahl and Peeters, 2014; Smits et al., 2009).

The hydrodynamic module Delft3D-FLOW simulates two-dimensional (depth averaged) and three-dimensional unsteady flow and transport resulting from tidal and/or meteorological forcing, and includes the effect of density differences (due non-uniform temperature and salinity). The flow model can be used to predict the flow in shallow seas, coastal areas, estuaries, lagoons, rivers and lakes (Deltares, 2014). Table 5 shows the assumptions and approximations applied in Delft3D.

Table 5 – Delft3D assumptions

Hydrostatic pressure	In the σ co-ordinate system the depth is assumed to be much smaller than the horizontal length scale. The shallow water assumption is valid – the vertical momentum equation is reduced to the hydrostatic pressure relation. Vertical accelerations are assumed to be small compared to the gravitational acceleration and are therefore not taken into account.
Boussinesq approximation	The effect of variable density is only taken into account in the pressure term
Turbulent scales	The equations solve the turbulent scales (large eddy simulation), but usually the hydrodynamic grids are too coarse to resolve the fluctuations. Therefore, the basic equations are Reynolds-averaged introducing so-called Reynolds stresses. These stresses are related to the Reynolds-averaged flow quantities by a turbulence closure model.
Eddy viscosity	The eddy viscosity is an-isotropic. The horizontal eddy viscosity and diffusivity coefficients should combine both the effect of the 3D turbulent eddies and the horizontal motions that cannot be resolved by the horizontal grid. The horizontal eddy viscosity is generally much larger than the vertical eddy viscosity.

Source: Adapted from Deltares (2014)

Delft-3D has two options for the vertical coordinates: σ and Z models. According to Deltares (2014) the vertical grid system determines the accuracy of the discretization of the vertical exchange processes. The vertical grid should (Deltares, 2014): resolve the boundary layer near the bottom to allow an accurate evaluation of the bed stress; be fine around pycnocline (where the greatest density gradient is located); avoid large truncation errors in the approximation of strict horizontal gradients. The σ grid does not meet all these requirements since it is boundary fitted and not always have enough resolution around the pycnocline (Deltares, 2014). Therefore, the recommendation is to use the cartesian Z co-ordinate system, which has horizontal coordinate lines (nearly parallel with density interfaces) in regions with steep bottom slopes (Deltares, 2014). This is important to reduce artificial mixing of scalar properties such as salinity and temperature (Deltares, 2014).

Governing Equations

The hydrodynamic modeling system solves the unsteady shallow water equations (in two or three dimensions). The system of equations is composed by the equations of motion, the continuity equation and the transport equation for conservative constituents

(Deltares, 2014). The following equations present the equations solved by Delft3D-FLOW for a rectangular grid.

Continuity equation

$$\frac{\partial \zeta}{\partial t} + \frac{\partial(d + \zeta)u}{\partial x} + \frac{\partial(d + \zeta)v}{\partial y} + \frac{\partial(d + \zeta)w}{\partial z} = Q \quad (12)$$

In equation (12), t is the time (s), ζ is the water level above some horizontal plane of reference (m), d is the depth below some horizontal plane of reference (m), u , v and w are the fluid velocity components in the x , y and z coordinates, respectively, and Q is the global source or sink per unit of area (ms^{-1}).

Momentum equation

$$\frac{\partial u}{\partial t} + u \frac{\partial u}{\partial x} + v \frac{\partial u}{\partial y} + \frac{w}{d + \zeta} \frac{\partial u}{\partial \sigma} - fv = M_x - \frac{1}{\rho} \frac{\partial P}{\partial x} + \frac{1}{(d + \zeta)^2} \frac{\partial}{\partial \sigma} \left(\nu_v \frac{\partial u}{\partial \sigma} \right) + \nu_h \left(\frac{\partial^2 u}{\partial x^2} + \frac{\partial^2 u}{\partial y^2} \right) \quad (13)$$

$$\frac{\partial v}{\partial t} + u \frac{\partial v}{\partial x} + v \frac{\partial v}{\partial y} + \frac{w}{d + \zeta} \frac{\partial v}{\partial \sigma} - fu = M_y - \frac{1}{\rho} \frac{\partial P}{\partial y} + \frac{1}{(d + \zeta)^2} \frac{\partial}{\partial \sigma} \left(\nu_v \frac{\partial v}{\partial \sigma} \right) + \nu_h \left(\frac{\partial^2 v}{\partial x^2} + \frac{\partial^2 v}{\partial y^2} \right) \quad (14)$$

In equations (13) and (14), f is the Coriolis parameter (s^{-1}), M_x and M_y are the depth-averaged mass fluxes due to Stokes drift (kg ms^{-1}) in x and y direction, respectively, ρ is the water density (kgm^{-3}), P is the hydrostatic water pressure ($\text{kg m}^{-1}\text{s}^{-2}$), σ is the scaled vertical coordinate $\sigma = \frac{z - \zeta}{d + \zeta}$ and ν_v and ν_h are the vertical and horizontal eddy viscosity (m^2s^{-1}). The vertical momentum equation is reduced to a hydrostatic pressure equation, since it is considered the shallow water assumption on Delft3D.

Transport equation

$$\begin{aligned} \frac{\partial(d + \zeta)T}{\partial t} + \frac{\partial(d + \zeta)uT}{\partial x} + \frac{\partial(d + \zeta)vT}{\partial y} + \frac{\partial(wT)}{\partial \sigma} &= (d + \sigma) \left[\frac{\partial}{\partial x} \left(D_H \frac{\partial T}{\partial x} \right) \right] \\ &+ (d + \sigma) \left[\frac{\partial}{\partial y} \left(D_H \frac{\partial T}{\partial y} \right) \right] + \frac{1}{d + \zeta} \frac{\partial}{\partial \sigma} \left(D_V \frac{\partial T}{\partial \sigma} \right) + \frac{1}{\rho c_p} S \end{aligned} \quad (15)$$

In equation (15), T is the water temperature ($^{\circ}\text{C}$), D_H and D_V are the horizontal and vertical diffusivity coefficients (m^2s^{-1}), respectively, and S is a source or sink term per unit area due to discharge (Wm^{-2}).

Turbulence model

Delft3D-FLOW solves the Navier-Stokes equations for an incompressible fluid. Usually the grid (horizontal and/or vertical) is too coarse and the time step too large to resolve the turbulent scales of motion – the turbulent processes are "sub-grid".

For 3D shallow water flow the stress and diffusion tensor are an-isotropic. The horizontal eddy viscosity coefficient ν_H and eddy diffusivity coefficient D_H are much larger

than the vertical coefficients ν_V and D_V .

The horizontal coefficients are assumed to be a superposition of three parts: 1) a part due to molecular viscosity; 2) due to "2D turbulence", associated with the contribution of horizontal motions and forcings that cannot be resolved by the horizontal grid (Reynolds averaged or eddy resolving computations) and 3) due to "3D turbulence", is referred to as the three-dimensional turbulence and is computed following one of the turbulence closure models available. Delft3D-FLOW has four implemented turbulence closure models to determine D_V and ν_v :

1. *Constant coefficient*, specified by the user (a constant eddy viscosity will lead to parabolic vertical velocity profiles – laminar flow);
2. *Algebraic Eddy viscosity closure Model (AEM)*, called zero order closure scheme is a combination of two algebraic formulations. This model uses analytical (algebraic) formulas to determine k (turbulent kinetic energy) and L (mixing length);
3. *$k - L$ turbulence closure model*, this closure model for the eddy viscosity involves one transport equation for k and is called a first order turbulence closure scheme. The mixing length L is prescribed analytically (the same formulation as used for the AEM turbulence model);
4. *$k - \epsilon$ turbulence closure model*, is a second order turbulence closure model. In this model both the turbulent energy k and dissipation rate of turbulent kinetic energy ϵ are calculated by a transport equation (Deltares, 2014).

For more detailed information about $k - \epsilon$ turbulence closure model in Delft3D, see Annex D.

Heat flux model

In Delft3D-FLOW the heat exchange at the surface is modelled by taking into account the separate effects of solar (short wave) and atmospheric (long wave) radiation, and heat loss due to back radiation, evaporation and convection (Deltares, 2014). In Delft3D-FLOW, five heat flux models are implemented:

1. *Heat flux model 1*, the incoming (short wave) solar radiation for a clear sky is prescribed. The net atmospheric (long wave) radiation and the heat losses due to evaporation, back radiation and convection are computed by the model;
2. *Heat flux model 2*, the combined net (short wave) solar and net (long wave) atmospheric radiation is prescribed. The terms related to heat losses due to evaporation, back radiation and convection are computed by the model;
3. *Excess temperature model*, the heat exchange flux at the air-water interface is computed; only the background temperature is required;

4. *Murakami heat flux model*, The net (short wave) solar radiation is prescribed. The effective back radiation and the heat losses due to evaporation and convection are computed by the model. The incoming radiation is absorbed as a function of depth;
5. *Ocean heat flux model*, The fraction of the sky covered by clouds is prescribed (in %). The effective back radiation and the heat losses due to evaporation and convection are computed by the model. Additionally, when air and water densities and/or temperatures are such that free convection occurs, free convection of latent and sensible heat is computed by the model. This model formulation typically applies for large water bodies (Deltares, 2014).

For more detailed information about Murakami and Ocean heat flux models in Delft3D, see Annex D.

Computational Grid

The numerical method of Delft3D-FLOW is based on finite differences. The grid is assumed orthogonal and well-structured. Variables as water level and velocity (u , v , w) describe the flow. To discretise the 3D shallow water equations, the variables are arranged in a special way on the grid (velocities perpendicular to the grid cell faces and water level centred in a grid cell). The pattern is called a staggered grid. This particular arrangement of the variables is called the Arakawa C-grid.

Stability

A robust solver of the shallow water equations satisfy the demands: robustness (unconditionally stable), accuracy, suitable for both time-dependent and steady state problems and has to be computationally efficient (Deltares, 2014). An explicit time integration of the shallow water equations on a rectangular grid is subject to a time step condition based on the Courant number for wave propagation (Deltares, 2014):

$$CFL_{wave} = 2\Delta t \sqrt{gH} \sqrt{\frac{1}{\Delta x^2} + \frac{1}{\Delta y^2}} < 1 \quad (16)$$

where where Δt is the time step, g is the acceleration of gravity, H is the total water depth and Δx and Δy are the smallest grid spaces.

2.3.4 Recent applications

Heat transport has been widely modelled for different objectives, as analysis of water quality, periods of mixing and stratification, impacts of climate change on seasonal behavior of water temperature, analysis of vertical thermal structure and horizontal gradients. In this wide range of studies, one, bi and three-dimensional models have been used for these purpose. This section present some studies that have been done and the use of modeling to analyse heat transport in reservoirs, focusing in three-dimensional modeling.

Zouabi-Aloui et al. (2015) analysed with CE-QUAL-W2 the effects on stratification and water quality of the different depths of water withdrawal. Usually when the withdrawals are done near the bottom, there is a decrease in water stability and the exchange between surface and bottom it is facilitated. If the withdrawal is at the surface, this usually increases thermal stability and stratification, decreasing the exchange between the layers (Zouabi-Aloui et al. 2015). Zouabi-Aloui et al. (2015) analysed the effects on thermal stratification and water quality of different configurations of water withdrawal. Kim et al. (2006) used CE-QUAL-W2 to simulate density currents in a lake in Korea due to storm rainfall events.

Liu et al. (2009) simulated hydrodynamics and water quality in Mingder Reservoir in Taiwan with CE-QUAL-W2, since the lake is eutrophic, with the objective of obtaining information about nutrient loads and supporting decisions for the reservoir management. Chung et al. (1998) analysed with CE-QUAL-W2 the path and dilution of pesticides from the river to the reservoir, influenced by the density.

Soullignac et al. (2015) measured (continuously, in three points) and simulated temperature profiles in a polymictic lake with a three-dimensional model (Delft3D) for three years and compared simulated data with measured temperature data (each 30 s), with errors lower than 10%. The periods of mixing, daily stratification were defined on a daily maximum and minimum differences between subsurface and bottom temperatures at the central station of temperature measurements (Soullignac et al., 2015).

Wahl and Peeters (2014) apply a 3D hydrodynamic model (Delft3D) to investigate the effect of climatic changes focusing on vertical transport and deep-water exchange in the reservoir, considering homogeneous wind field and neglect the tributaries, and compared the results also performing a 1D simulation with SIMSTRAT model. In relation to the three-dimensional model, grid resolution was investigated and it was identified that coarse grid may enhance mixing in the hypolimnion. Sensitivity of the 3D model in relation to wind speed was performed – increasing the wind speed deep waters were warmer and a decrease in water stability was verified. The sensitivity analysis of increased air temperature showed an increase in water stability. The comparison of the models showed that increasing air temperature occurs a large reduction in vertical mixing in the upper hypolimnion in the 1D simulation, whereas 3D modeling showed a lower reduction in vertical mixing.

Curtarelli et al. (2014) analyse the heat budget and thermal structure on a diurnal time scale in a tropical reservoir with a three-dimensional model (ELCOM) and identified temperature gradients at the surface between littoral zone (colder) and the pelagic zone. The gradients were pronounced during the night and early morning when the heat loss was higher (Curtarelli et al., 2014). Also, Curtarelli et al. (2014) showed the river temperature exerts influence on the thermal structure and contribute to water stability.

León et al. (2007) performed a sensitivity analysis of the impact of meteorological

information on modeling (ELCOM). The objective is to include lake modeling and the heat transfer in weather forecasting – the sensitivity analysis was performed with measured data in the lake and data from a climate model. The potential error simulation with data from the climate model was approximately 15% (emphasizing the importance of the lake component in weather forecasting). The sensitivity analysis of measured data, on the other hand, showed that increasing 10% in air temperature and solar radiation produce 3.08% and 8.27% increase in the water surface temperature, respectively, and 8.5% decrease in the evaporative heat flux (León et al., 2007).

Marti et al. (2011) using a three dimensional model (ELCOM), analyse the path of multiple inflows into a reservoir. They also identified surface temperature gradients between two points of measurements. The signatures of inflow waters were analysed by vertical salinity profiles, since the salinity of inflows were distinct from the main reservoir and the modeling was capable of simulating the location and depths of intrusion.

Chung et al. (2009) using ELCOM-CAEDYM (Computational Aquatic Ecosystem Dynamics Model), simulate particle dynamics and modelled the propagation of turbid density inflows into a stratified reservoir and the subsequent spatial variability of reservoir turbidity with the aim of reservoir management, analysis of selective withdrawal – the reduction of costs in water treatment (avoiding turbid regions) and water quality (reservoir and downstream). Huang et al. (2014) also evaluate the storm-rainfall events and its effects in water temperature and the path of a turbid density flow to identify the proper intake to reduce the costs of the drinking water treatment plant (optimizing the depth of water withdrawal), but no modeling was performed.

2.4 Reservoir classification

Lakes and reservoirs may be classified according to its periods of mixing and stratification. Read et al. (2011) developed the software Lake Analyzer, that quantifies important parameters related to these periods in lakes and reservoirs, based on measurements. The characterization of the lake according mixing and stratification periods can be performed using Lake Number and Wedderburn Number. The Wedderburn Number is a relationship between buoyancy and mixing induced by wind shear, calculated by (Imberger et al., 1989):

$$W = \frac{g'}{L} \left(\frac{z_e}{u^*} \right)^2 \quad (17)$$

in which g' is the reduced gravity ($g' = g\Delta\rho/\rho_h$), g is the acceleration of gravity, $\Delta\rho$ is the density difference between the hipolimnion (ρ_h) and epilimnion (ρ_e), z_e is the epilimnion thickness (m), L is the reservoir fetch length (m). If $W \ll 1$, the increase of the mixed layer depth is dominated by the internal production of turbulence. In this case, upwelling can occur upwind and strong gradients at downwind (Imberger et al., 1989). On the other hand, if $W \gg 1$, the isothermal inclination by the wind is small and horizontal

variations are negligible (Imberger et al., 1989). Stratification is strong and the mixed layer will deepen slowly (Read et al., 2011).

The Lake Number describes relevant process for mixing in lakes induced by wind action, according to (Read et al., 2011)

$$L_N = \frac{S_t(z_e + z_h)}{2\rho_h u_*^2 A_s^{1/2} z_v} \quad (18)$$

where S_t is the Schmidt Stability that relates the resistance to mechanical mixing due to the potential energy on the stratification of the water column, z_h is the hypolimnion thickness (m), A_s is the surface area of the reservoir (m²) and $z_v = \int_{z=0}^{z=z_D} z A_z dz / \int_0^{z_D} A_z dz$ (Read et al., 2011). If $L_N > 1$, stratification is strong and any disturbance produced by the wind at the surface is minimized. Otherwise, if $L_N < 1$ indicates weak stratification and potential to mixing (Imberger et al., 1989).

2.5 Summary of the chapter

This chapter showed the importance of temperature for the physical processes in lakes and reservoirs. Temperature is a well known parameter which affects physical processes and water quality. Despite the fact of that importance, few measurements related to spatial temperature gradients have been done, so there is a lack in this kind of measurement. In addition, most of time, control of inflows and outflows is not carried out, it is done by researchers interested in density currents, although regarding heat transport in lakes, this is not yet fully adopted.

The most important set of data for heat transport is concerning meteorological effects. The location of measurements may affect models results, since measurements in onshore and floating platforms weather stations may present differences in wind speed (affecting mixing), relative humidity and air temperature. These differences could alter heat fluxes at the air-water interface, but no study about these differences has been done, although there are discussions about measurements and models sensitivity.

In relation to modeling of heat transport in lakes and reservoirs, this chapter showed the main contributions of each approach and limitations that may restrict some engineering applications. One-dimensional models are widely used for applications related to water quality, climate change and other cases considering horizontal homogeneity. As it was presented, this simplification is, sometimes, not feasible – therefore, usually three-dimensional models are applied. Although three-dimensional models represent in more detail the processes, for practical applications it may not be desirable due the computational time required to run the model and the number of layers, which could be a limiting factor.

This thesis will connect measurements and modeling. The former will allow the anal-

ysis of the most important parameters regarding heat transport – different locations of meteorological measurements and model response, effects of inflows/outflows and also the spatial analysis of temperature, since few measurements have been done in more than one location in the reservoir with high spatial and temporal resolution. The sector modeling proposed in this thesis will have the ability of one-dimensional models to simulate fast and efficiently the heat transport in lakes, with the possibility to analyse horizontal temperature variations and effects of bathymetry in water temperature. This may allow fast tools for management in lakes and reservoirs that may receive discharge from industries, for drinking water purposes and even water quality issues.

3 Study site characterization

This section describes the study areas for this thesis – Vossoroça, Passaúna and Capiuari reservoir, all located near to Curitiba (see Figure 7), in Paraná State, Brazil. The monitoring consists of meteorological and hydrological data, continuous temperature profiles monitoring, with high temporal and spatial resolution, and measurements with a CTD sensor (conductivity, temperature and depth) at the reservoir. In this section, data was obtained through GHG Apine Project, data from literature, and COPEL and Sanepar companies. Figure 8 shows the available data for each reservoir, that are presented in this section. Chapter 4 will present further data, obtained during this thesis.

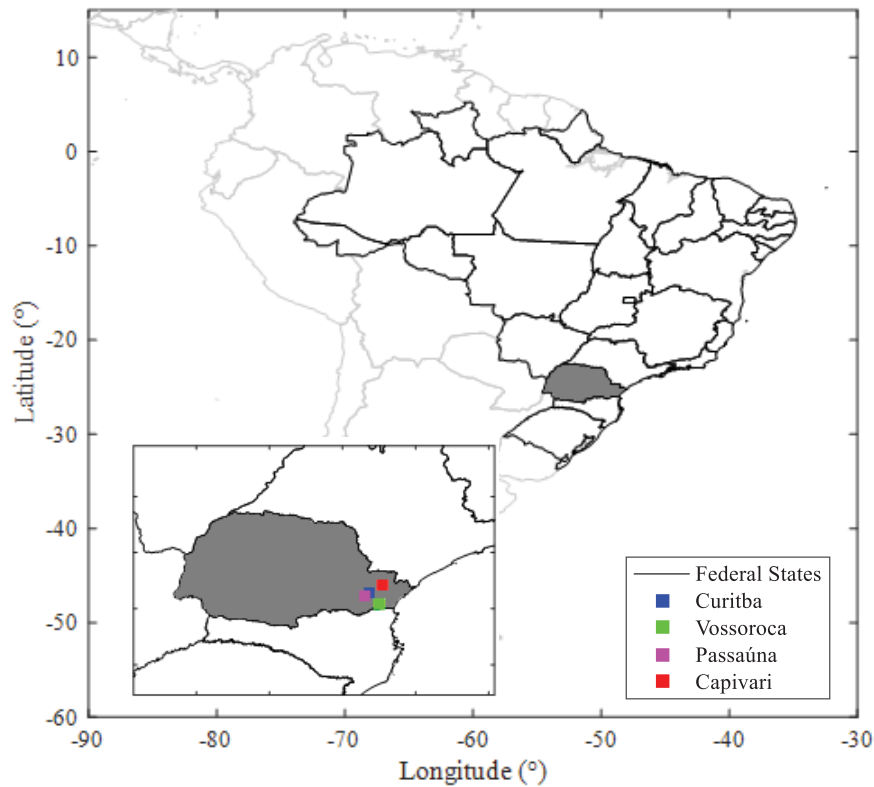


Figure 7 – Location of Vossoroça, Passaúna and Capiuari reservoirs in Brazil

3.1 Vossoroça reservoir

Vossoroça reservoir (see Figure 9) was built in 1949 by the impoundment of São João river, located in Tijucas do Sul – PR (80 km from Curitiba), Brazil. The reservoir has a surface area of 3.3 km², volume of 35.7 10⁶ m³, maximum and mean depths of 17 m and 8 m, respectively and its detention time is 117 days. The reservoir function is to regulate the

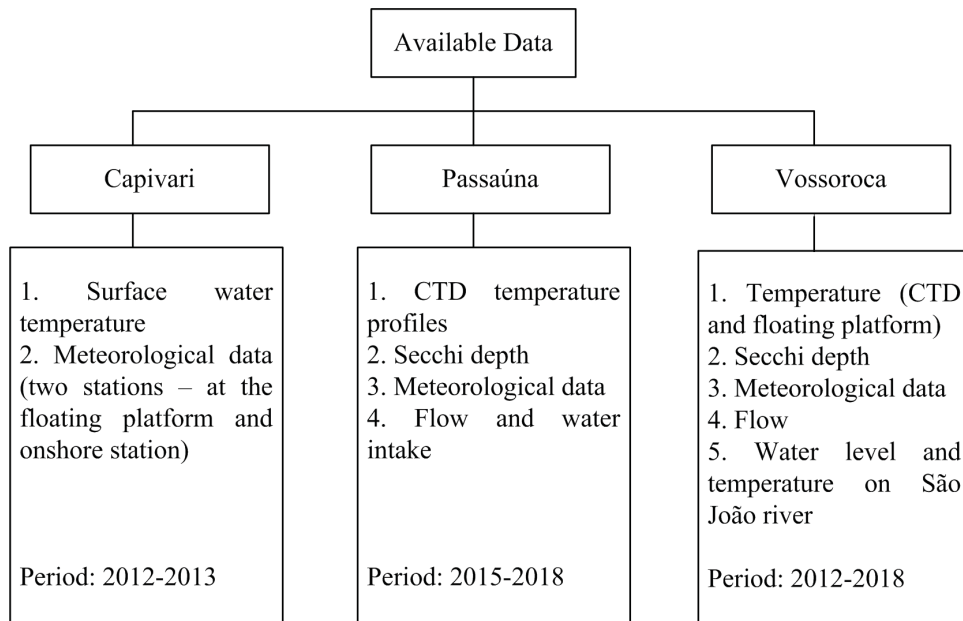


Figure 8 – Available data of Vossoroca, Passaúna and Capivari reservoirs

flow to Chaminé hydropower plant (with capacity of 18 MW) (COPEL, 1999). Vossoroca is a monomitic lake, mixed during winter. Dissolved oxygen profile follows temperature profiles, with anoxic periods during stratification (IAP, 2008).

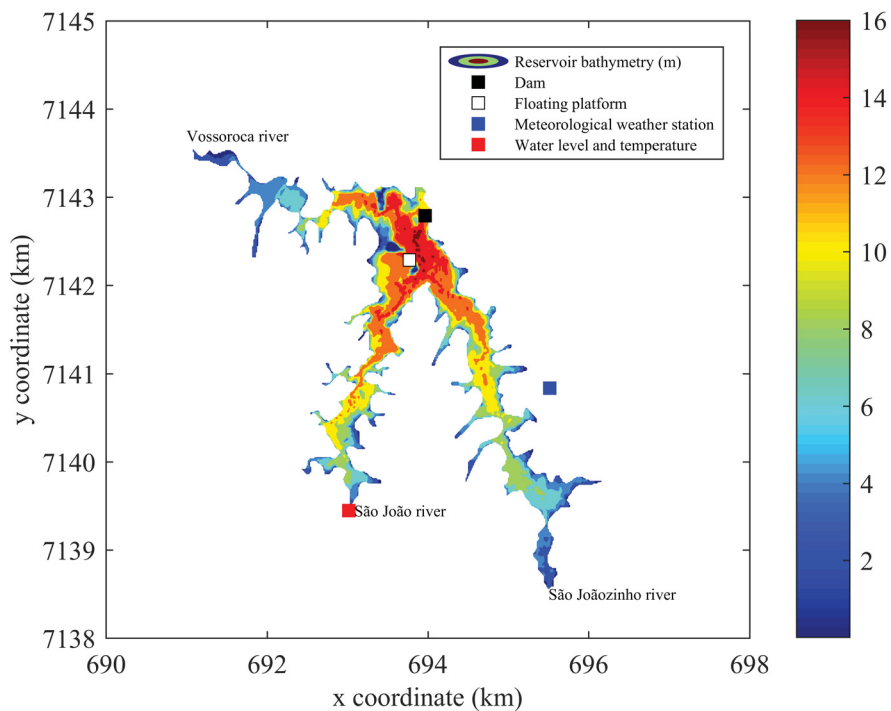


Figure 9 – Vossoroca reservoir bathymetry and monitoring sites

Chaminé hydropower plant is located in the left margin of São João river, between São José dos Pinhais and Tijucas do Sul, in an environmental protection area (COPEL,

1999). The climate of this region is classified as humid subtropical and its annual average temperatures are 22 °C during the hot months and lower than 18 °C during the cold months. Vossoroça reservoir is monitored since 2012. Its monitoring includes temperature, meteorological measurements and the control of inflow/outflow.

3.1.1 Temperature

Temperature is measured in a floating platform (see Figure 9) installed in the reservoir using seven temperature sensors (Männich, 2013). The depths measured (from surface) are: 1, 3, 5, 7, 9, 11 m and 1 m from the bottom, with time step of 15 minutes (see Figure 10.a for the location of the floating platform) and Figure 11 show temperature measurements between 2012 and early 2013. During Winter in South Hemisphere the reservoir is well mixed, with lower temperatures. Then, the reservoir warms at the surface, developing thermal stratification. At the end of December, the entire water column warms up (Summer in South Hemisphere).

See also appendix A for additional measurements of temperature in the floating platform.

3.1.2 Meteorological data

Meteorological data is measured with 2 min time step in an onshore weather station (see Figure 9). The meteorological weather station measures precipitation, air temperature, relative humidity, solar radiation, pressure, wind speed and wind direction (see Table 6 for information about equipments and resolution of the sensors and Figure 10.b for the location of the meteorological weather station). Figure 12 shows measured data in the meteorological weather station used in the heat transport modeling. Figure 13 also shows wind direction measured in Vossoroça reservoir. See also appendix A for additional meteorological measurements.

3.1.3 Flow

Figure 14 shows inflows/outflows and water level in Vossoroça reservoir (provided by COPEL). The main rivers contributing to Vossoroça reservoir are São João, São Joãozinho and Vossoroça. São João is monitored since August/2015. Figure 15 shows the water level and temperature in São João river.

3.2 Passaúna reservoir

Passaúna reservoir (see Figure 16) was formed in 1990. It is located in Araucária – PR, near to Curitiba, Brazil. The reservoir has a surface area of 11 km², maximum and



Figure 10 – Vossoroca reservoir monitoring sites a) floating platform and b) meteorological weather station in Vossoroca reservoir and c) Limnometric station in São João river

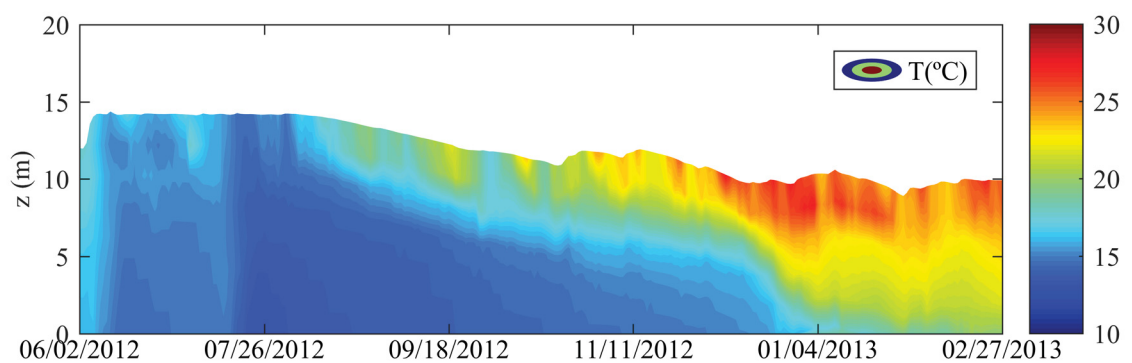


Figure 11 – Temperature measured in Vossoroca reservoir in the floating platform

mean depths of 16 m and 9.4 m, respectively, volume of 71.6 hm³ and detention time of 2 years. The reservoir function is water supply for Curitiba and region. Passaúna reservoir has 13 inflows – flow and drainage area are described in Table 7. According to Carneiro et al. (2016) thermal stratification occurs in the deeper parts of the reservoir and anoxic

Table 6 – Meteorological sensors installed at Vossoroça reservoir

Equipment	Variable	Manufacturer	Resolution
Tipping Bucket Rain Gauge - H 340	Precipitation	Water Log	± 0.2 mm - 0.001 mm
Thermistor Temperature Probe - H 377	Temperature	Water Log	± 0.2 °C - 0.1 °C
HygroClip S3	Relative Humidity	Rotronic	$\pm 1\%$ RH - 0.02% RH ± 0.2 °C - 0.06 °C
CMP3-L Pyranometer	Solar radiation	Campbell Scientific	$\pm 5\%$ - 1 Wm ⁻²
Barometric Pressure Transducer - Model 278	Pressure	Setra	± 1.0 mb - 0.01 mb
Wind Monitor	Wind speed and direction	Young	± 0.3 ms ⁻¹ or 1% ± 2 °C

Source: Adapted from Männich (2013)

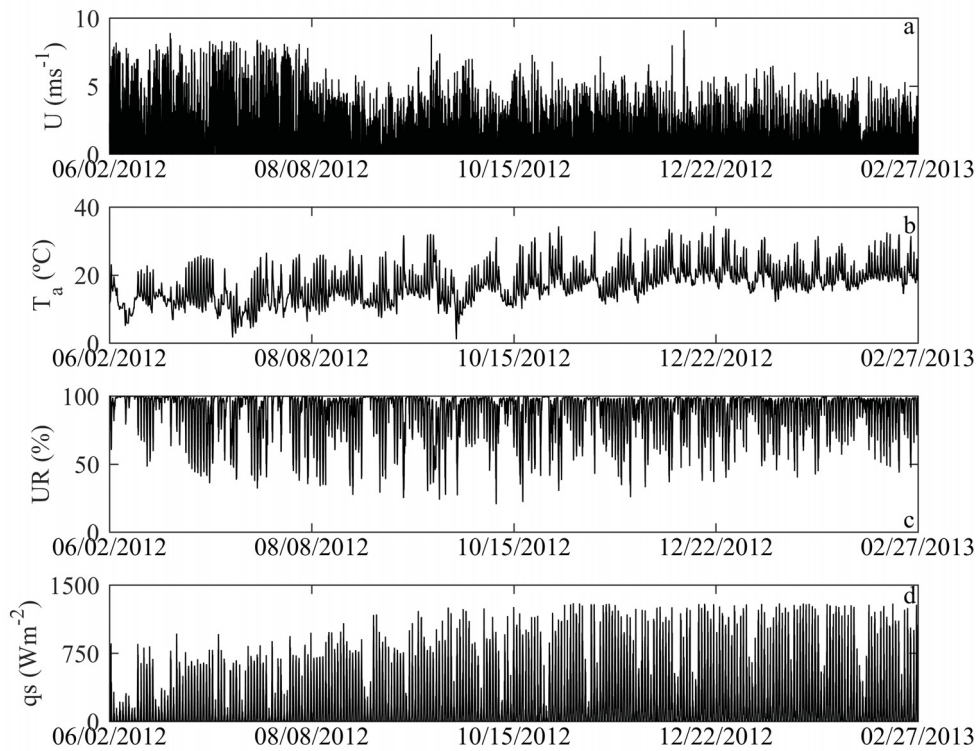


Figure 12 – Meteorological data near to Vossoroça reservoir. a) Wind speed, b) Air temperature, c) Relative Humidity and d) Shortwave radiation

conditions are verified in the deepest zones of the reservoir during warm periods (between September and March).

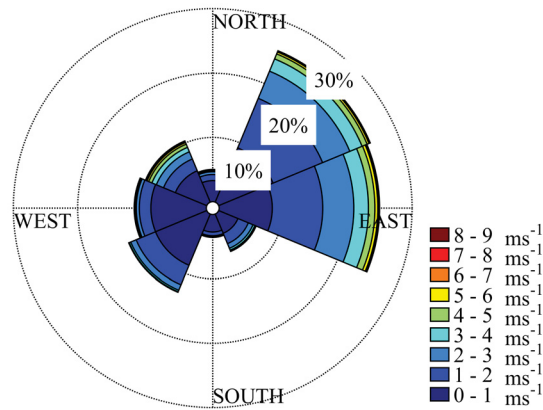


Figure 13 – Wind speed and direction measured in the meteorological weather station in Vossoroca reservoir

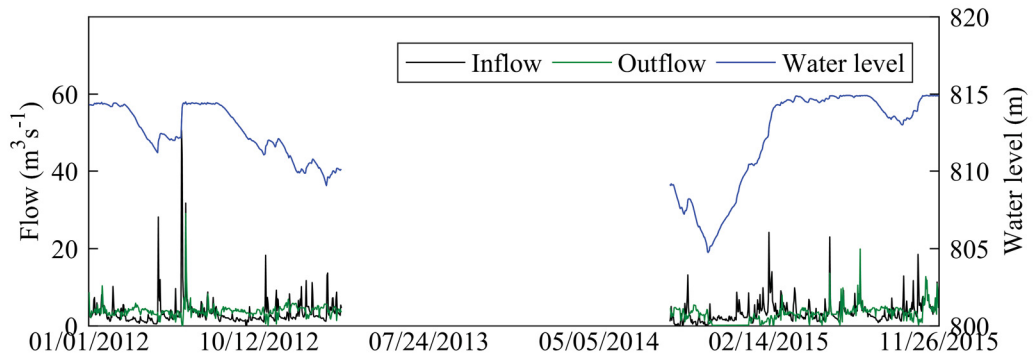


Figure 14 – a) Inflow/Outflow and b) Water level from Vossoroca reservoir

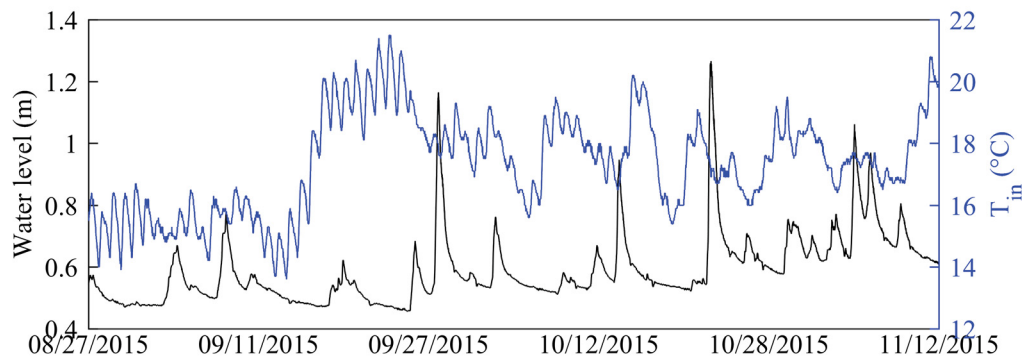


Figure 15 – Water level and temperature in São João river

3.2.1 Temperature

Continuous temperature measurements are not taken in Passaúna reservoir. Temperature profiles measured with a CTD are presented in Section 4.2.

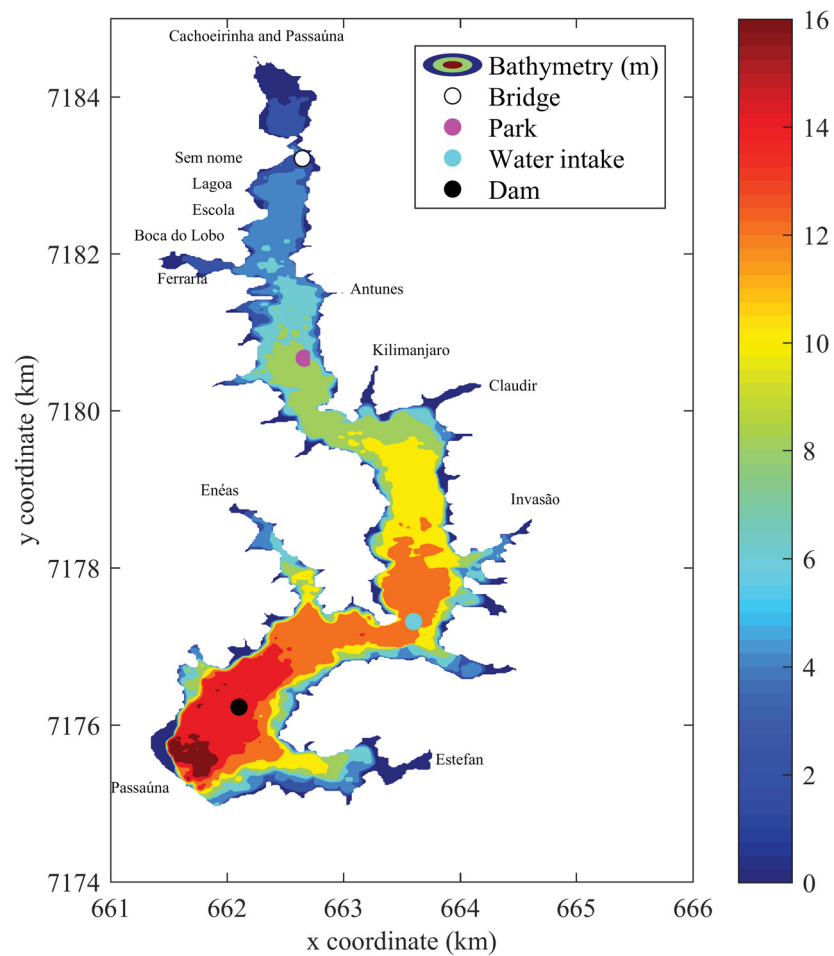


Figure 16 – Passaúna reservoir

Table 7 – Flow and drainage area in Passaúna reservoir (Veiga and Dzedzic, 2010)

River	Flow (m^3s^{-1})	Drainage Area (km^2)
Passaúna upstream	1.36	82.73
Cachoeira	0.18	10.82
Sem nome	0.05	3.14
Lagoa	0.01	0.67
Escola	0.01	0.42
Lobo	0.01	0.94
Ferraria	0.18	11.07
Enéas	0.04	2.53
Antunes	0.07	4.01
Kilimanjaro	0.02	1.16
Claudir	0.03	2.04
Invasão	0.01	0.60
Estefan	0.09	5.9

3.2.2 Meteorological data

Meteorological data is measured at Assis station (in Araucária). Figure 17 shows data measured at the station in 2015. Data is available since 2011. In the period shown,

mean wind speed is 1.9 ms^{-1} , mean air temperature is $17.78 \text{ }^\circ\text{C}$, mean relative humidity is 82.13% and mean solar radiation, 125.84 Wm^{-2} .

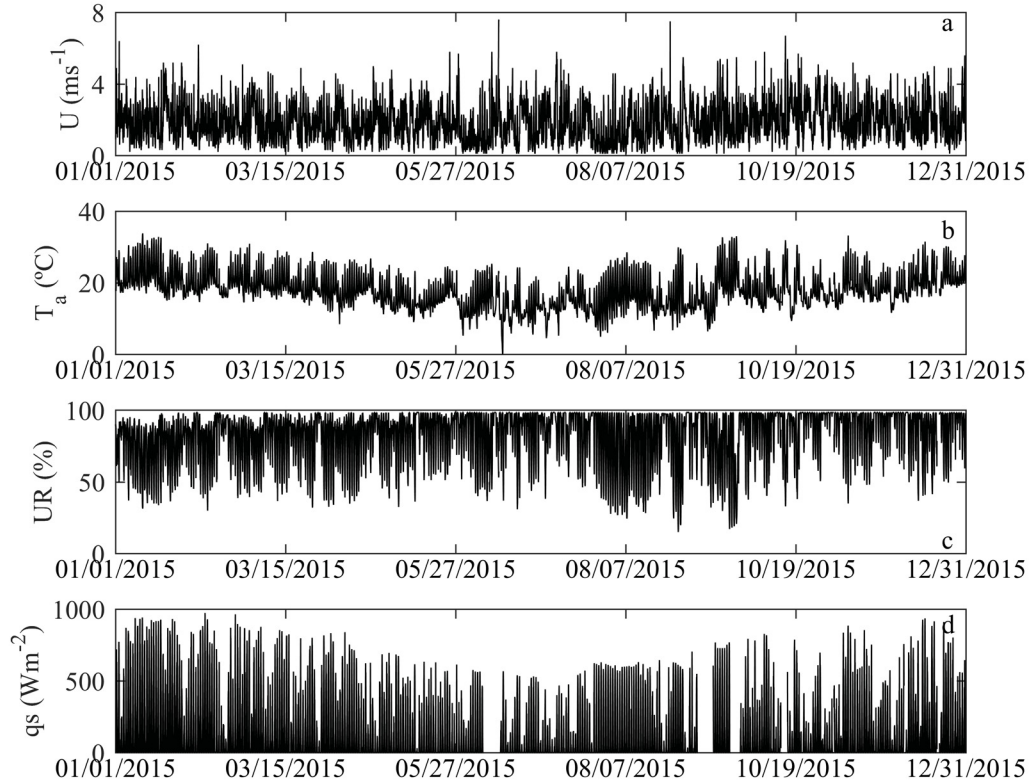


Figure 17 – Meteorological data near to Passaúna reservoir. a) Wind speed, b) Air temperature, c) Relative Humidity and d) Shortwave radiation

3.2.3 Flow and water intake

Data related to the water intake and water level was provided by Sanepar. Figure 18 show the flows and water level in 2016. The water level in this year do not vary more than 0.5 m. Figure 19 shows the mean air temperature and the volume of water intake in 2016. Also, the depth of the water intake is 2.3 m.

3.3 Capivari reservoir

Capivari reservoir was formed by the impoundment of Capivari river, located in Campina Grande do Sul (50 km from Curitiba). In this thesis, data measured in Capivari reservoir is used to estimate heat fluxes at the air-water interface.

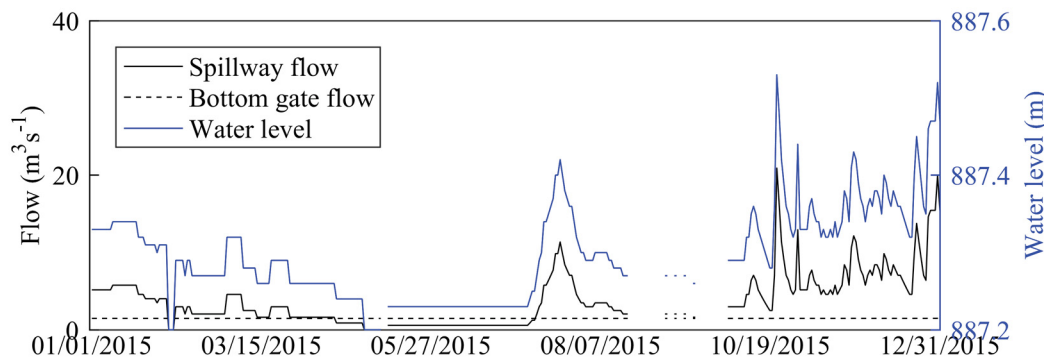


Figure 18 – Flow and water level in Passaúna reservoir

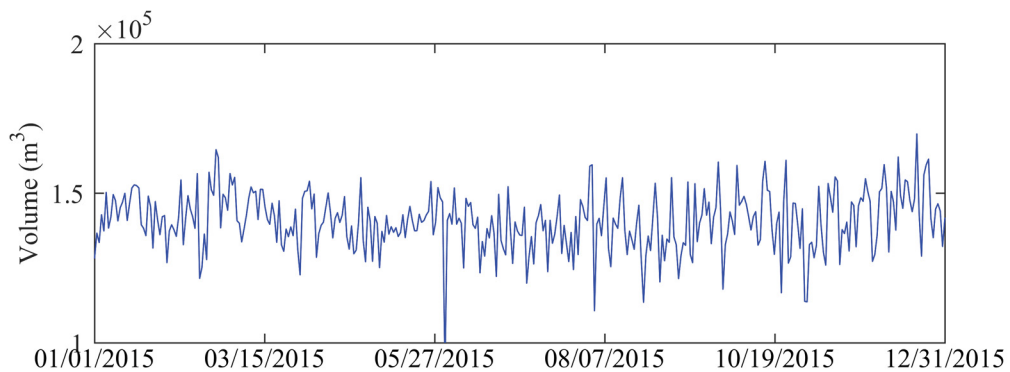


Figure 19 – Water intake volume in Passaúna reservoir

3.3.1 Temperature

Temperature was measured in Capivari reservoir at surface and 1, 2 and 4 m from the surface. In this thesis, surface temperature is used to estimate heat fluxes. Figure 20 shows surface water temperature between December 2012 and January 2013.

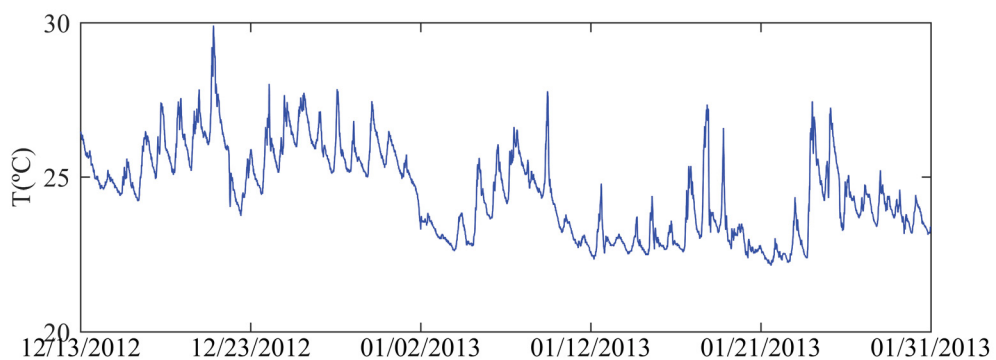


Figure 20 – Surface temperature in Capivari reservoir

3.3.2 Meteorological data

Meteorological data was measured in Capivari reservoir in two points – one onshore weather station and in a floating platform. The distance between the weather stations

was 1 km. Figure 21 shows the measurements between December 2012 and January 2013.

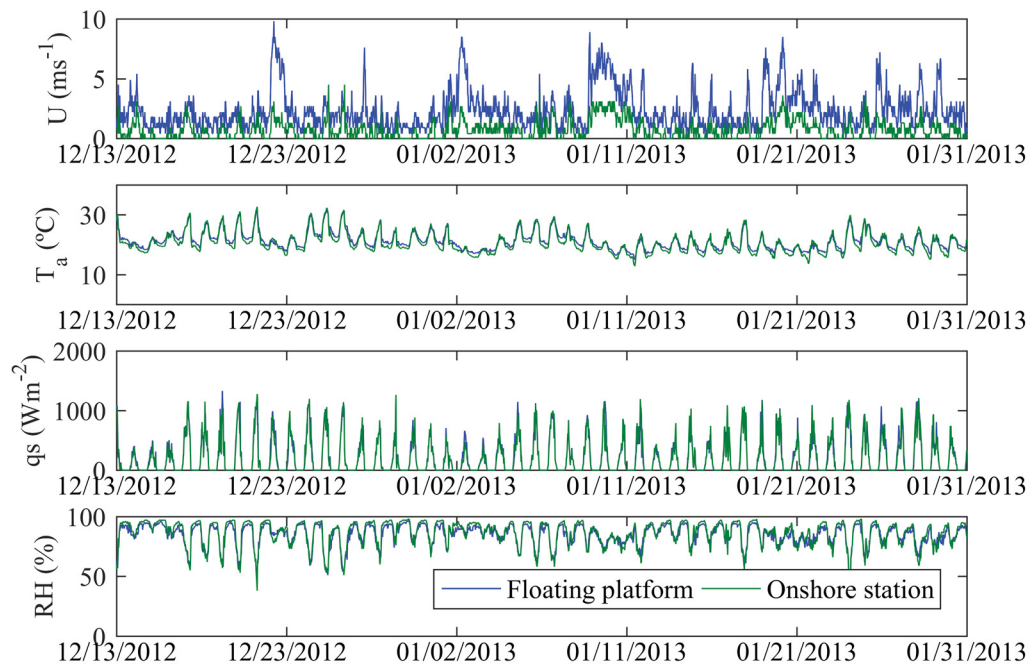


Figure 21 – Meteorological data from Capivari reservoir a) Wind speed, b) Air temperature, c) Relative Humidity and d) Shortwave radiation

4 Results of measurements and classification

Regarding the thesis objectives, in addition to the data from Chapter 3, further measurements were undertaken. CTD (CastAway-CTD) (conductivity, temperature and depth – although CTD sensors do not measure depth but pressure (Roget, 2013)) profiles were measured at Vossoroca and Passaúna reservoirs, with the objective of analysis of temperature variations in different regions (that may be caused by the bathymetry or inflows, for example), including Secchi depth measurements, to the analysis of depth of penetration of solar radiation. Also, section 4.3 shows an analyse of air-water heat fluxes due differences in meteorological measurements – stations that are 1 km distant (in Capivari reservoir), but present significant differences in heat fluxes.

4.1 Measurements in Vossoroca reservoir

Figure 22 shows the points where CTD measurements were taken. At the floating

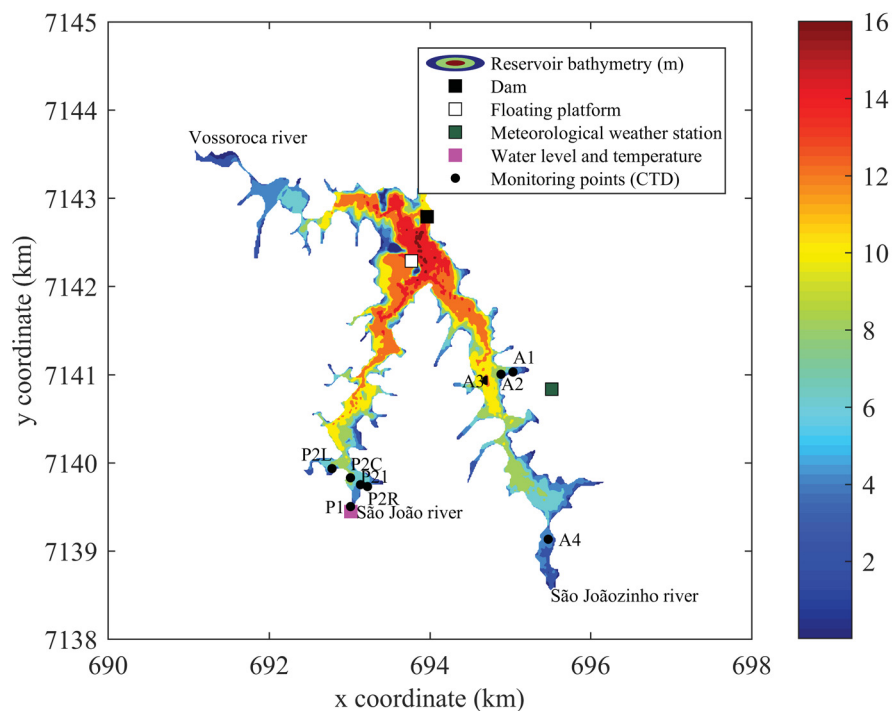


Figure 22 – Location of CTD measurements in Vossoroca reservoir

platform, near São Joãozinho river (A4) and a section of three profiles with different depths – A1, A2 and A3 (see also the points location in Figure 22). Figure 23.a shows the temperature at the floating platform: the differences at the profile occur mainly at the surface. Figure 23.a also shows the water temperature near São Joãozinho river (point A4), which could be influenced by the temperature of the inflowing water (the temperature

of São João river was 19°C). Figure 23.b shows three temperature profiles measured at a section from shallow to deeper regions – there is a gradient of 2°C at the superficial layer. Figure 23.c shows all profiles, highlighting the gradients of the shallow regions of the reservoir and near the entrance.

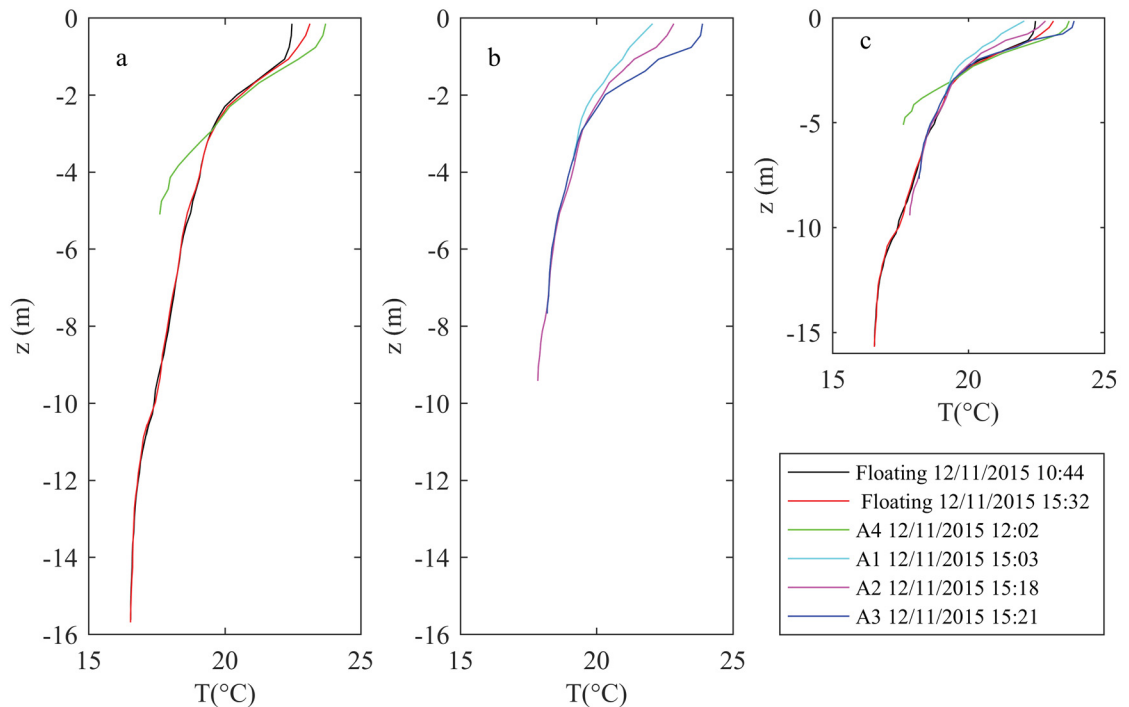


Figure 23 – Temperature profiles in different regions of Vossoroca reservoir at 11/12/2015. a) Profiles in the floating platform and São Joãozinho river. b) Section from shallow to deeper region. c) All measured profiles

Figure 24 shows a second set of data measured at the floating platform, near São João river (P1) and a section from shallow to deeper regions (P2L, P2C, P21 and P2R) (see Figure 22 for the location of the points). The gradients at the surface from deep to shallow waters and from entrance to deeper waters were again verified. These few measures in Vossoroca reservoir showed horizontal temperature gradients that may interfere in water quality and dynamic into the reservoir and should be considered.

Combined with temperature profiles measurements, Secchi depth was measured in the points already described. Table 8 shows the coordinates of the measured points and Secchi depth, which are non uniform in the reservoir, therefore, the absorption of solar radiation and the depth of penetration may vary in different points and could increase horizontal temperature gradients.

4.1.1 Vossoroca reservoir data analysis

Wedderburn number and Lake number were calculated to Vossoroca reservoir, using temperature measurements (Figure 11) and meteorological data (Figure 12) and are

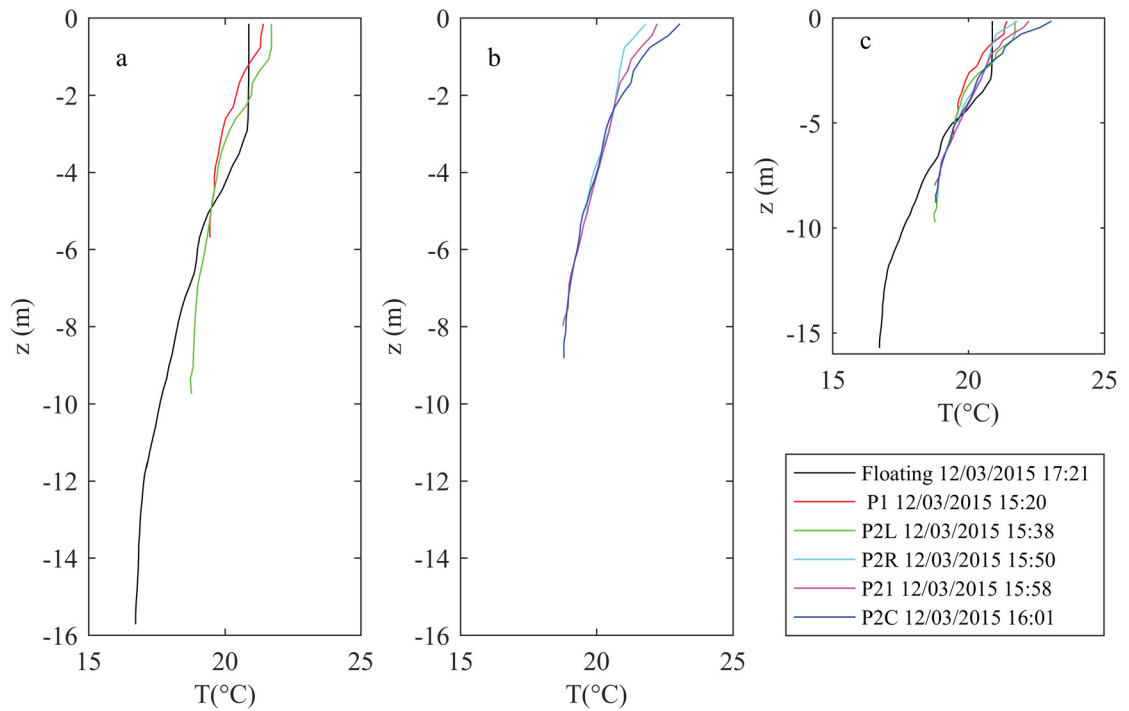


Figure 24 – Temperature profiles in different regions of Vossoroca reservoir at 12/03/2015. a) Profiles in the floating platform, São João river and a point in the reservoir P2. b) Section from shallow to deeper region. c) All measured profiles

Table 8 – Coordinates of measurement points and Secchi depth

Point	Latitude (°)	Longitude (°)	Secchi depth (m)	Date
Floating platform	-25.8247	-49.0669	1.50 ¹ /2.10 ²	11/12/2015 10:44 ¹ 12/03/2015 17:21 ²
P1	-25.8500	-49.0740	0.3	12/03/2015 15:20
P2L (left)	-25.8461	-49.0764	0.86	12/03/2015 15:38
P2R (right)	-25.8479	-49.0719	0.50	12/03/2015 15:50
P21	-25.8477	-49.0728	0.71	12/03/2015 15:58
P2C (centre)	-25.8470	-49.0740	1.00	12/03/2015 16:01
A1	-25.8359	-49.0541	1.30	11/12/2015 15:03
A2	-25.8362	-49.0555	–	11/12/2015 15:18
A3	-25.8368	-49.0573	1.10	11/12/2015 15:21
A4	-25.8530	-49.0494	–	11/12/2015 12:02

present in Figure 25. These indices were calculated using the software Lake Analyzer (Read et al., 2011). In general, Wedderburn number is higher than 1, with exception of the beginning of the period showed here, where high wind speeds and low differences in temperature in the water column are verified. In August, the superficial layer starts to warm, and the increase in temperature gradients combined with low wind speeds result in higher Wedderburn numbers, corresponding to strong stratification. Lake number shows the same behavior – low numbers at the beginning of the period, indicating weak strat-

ification and allowing mixing in the water column – which is suppressed by the strong stratification after August.

Table 9 presents an estimation of the number of days in which a certain temperature gradient (between surface and bottom) is verified in the reservoir. Gradients higher than 2°C , for example, occur in 69 days (from 94 days of measurements). Also, $W>1$ occur in 91 days and $L_N>1$ in 91 days, indicating that during this period the reservoir is stratified.

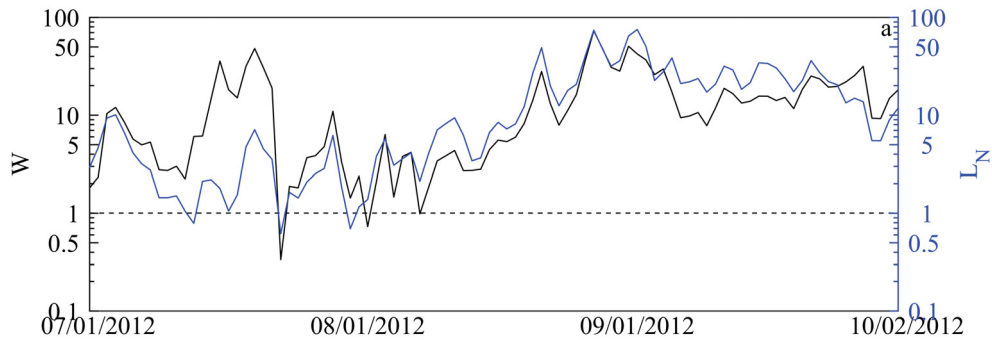


Figure 25 – Wedderburn number and Lake number in Vossoroca reservoir

Table 9 – Number of days that $\Delta T > 1, 2$ and 3°C , $W>1$ and $L_N>1$ to measured data from Vossoroca reservoir (from 94 days)

$\Delta T > 1^{\circ}\text{C}$ (days)	86
$\Delta T > 2^{\circ}\text{C}$ (days)	69
$\Delta T > 3^{\circ}\text{C}$ (days)	56
$W > 1$ (days)	91
$L_N > 1$ (days)	91

4.2 Measurements in Passaúna reservoir

Measurements were performed at Passaúna reservoir in February 2017. This measurements include the main points showed in the section 3.2 and side arms that may have or not inflows contributing to the reservoir (see Figure 26 which shows the points measured).

Figure 27 shows the measurements in the longitudinal direction of the reservoir. The measurements show that the water entering the reservoir is colder than the water in the reservoir and a temperature gradient is identified. The profile at the bridge shows that the water is probably entering the reservoir near the bottom, due the colder temperatures in this region. Also, the measurements show a difference in the mixed layer depth between the bridge and the dam – in the first there is no well defined mixed layer, while at the dam the mixed layer is around 6 m. Secchi depth measurements were performed with CTD measurements, and the general behavior was the increasing of Secchi depth along the reservoir: at the bridge 0.8 m and at the Dam, 2.1 m. The point at the water intake, on the other hand, had a Secchi depth higher than the measured at the Dam, 2.3 m.

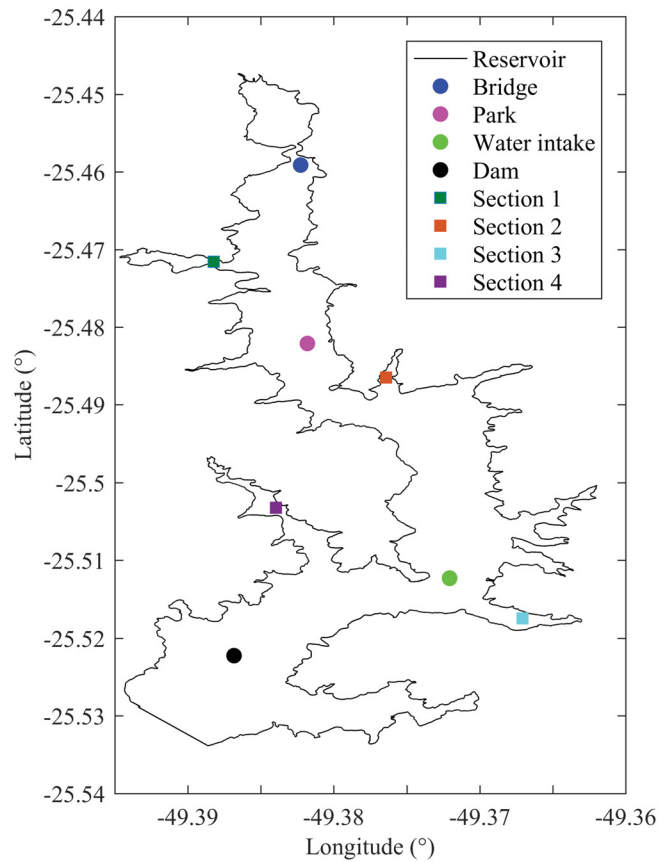


Figure 26 – Points of temperature measurements in February 2017 in Passaúna reservoir

Figure 28 shows the sections in side arms measured in February 2017. The main gradients appear at the surface, but in sections 2 e 4, gradients at the bottom of shallower waters were also identified. This gradients may be caused by depth difference, influence of inflowing waters and also by vegetation around the side arms, that could prevent solar radiation to penetrate the water and decrease wind velocities.

Figure 29 shows temperature profiles measured with a CTD in three days in Passaúna reservoir. Figure 29.a shows that the reservoir is stratified at the Dam during February. The gradient between surface and bottom is approximately 6°C . Also in this graph, it is possible to observe the difference in thermocline depth between the points in the reservoir – (e.g. 8 m from the surface at Dam and 6 m at Park) and horizontal temperature gradients were also observed (0.80°C between Dam and Bridge at the surface). Figure 29.b also shows vertical temperature gradient around 6°C in April, but the depth of the mixed layer was lower than the mixed layer observed in February. In Figure 29.c, the points near to the Water Intake and the Dam were not stratified and the thermocline is not well defined. However, the measurement points near the inflow (Bridge, closest to the inflow) and the point Park had gradients around 1°C between surface and bottom and the horizontal gradients at surface between the point Bridge and Dam are around 1°C .

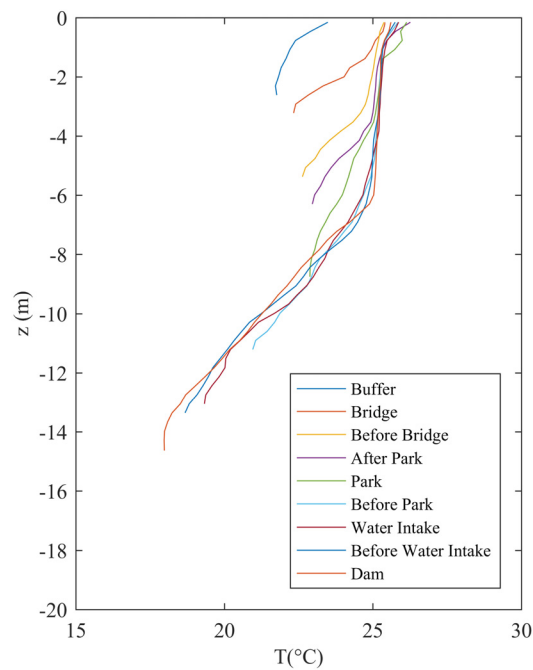


Figure 27 – Temperature measurements in the longitudinal direction in Passaúna reservoir

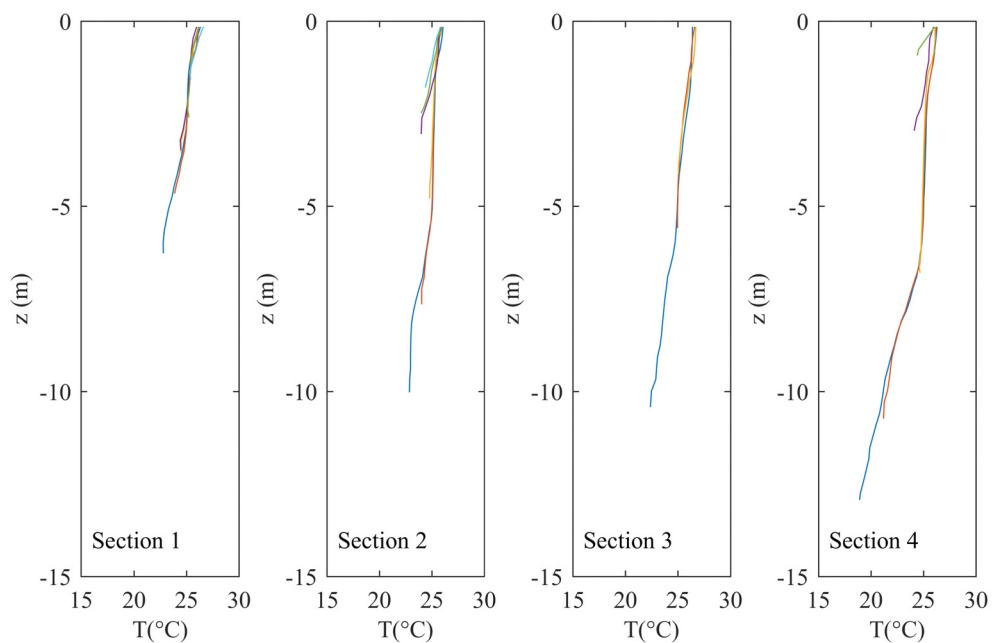


Figure 28 – Side arms temperature sections in Passaúna reservoir (see Figure 26)

Combined with temperature profiles, Secchi depth measurements were taken in Passaúna reservoir as it is shown in Table 10. The measurements show that the Secchi depth increases with the distance of the inflow, the same behavior as Vossoroca reservoir.

Some surface temperature measurements were done also during 2014 in the reservoir. In May 2014, the temperature measured at Bridge was 19.3°C and 20.1°C at the point

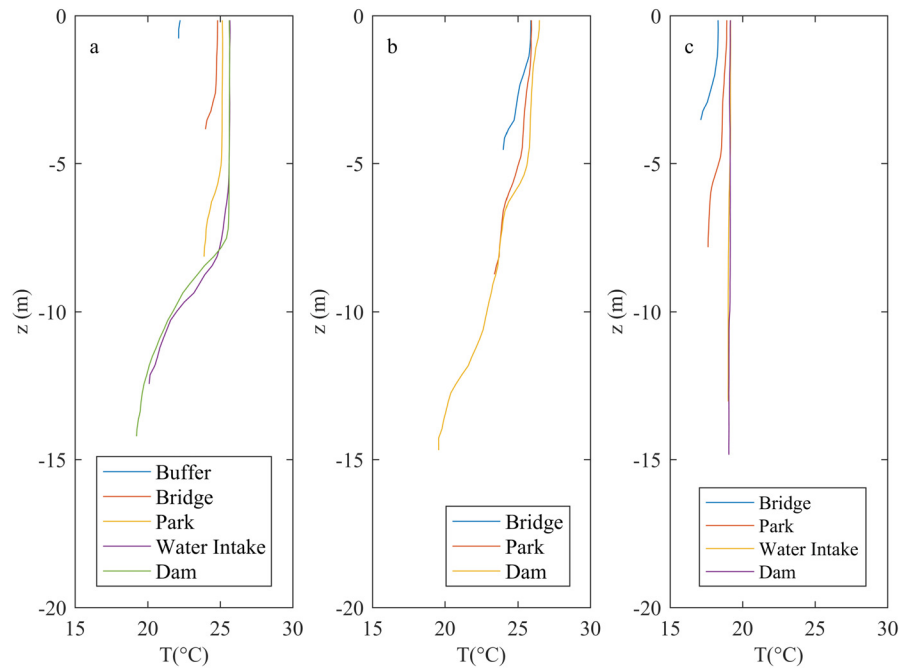


Figure 29 – Temperature in Passaúna reservoir. a) 02/28/2016, b) 04/18/2016 and c) 05/23/2016.

Table 10 – Coordinates of measurement points and Secchi depth in Passaúna reservoir

Point	Latitude (°)	Longitude (°)	Secchi depth (m)	Date
Buffer	-25.4489519	-49.3852956	–	02/28/2016 12:03
Bridge	-25.4618553	-49.3825732	1.28	02/28/2016 11:42
Park	-25.4783881	-49.382162	1.57	02/28/2016 11:21
Water intake	-25.5120249	-49.3710491	2.20	02/28/2016 10:51
Dam	-25.5311913	-49.3894425	2.20	02/28/2016 10:16

Park (Secchi depth of 2.5 m). During June 2014, the gradients between these points decreased – the surface temperatures were 17.3°C and 17.9°C, at Bridge and Park, respectively (Secchi depth of 3 m). In July 2014, a horizontal gradient of 1°C was measured between these two points (15.3°C at Bridge and 16.3°C at Park, and Secchi depth of 3 m).

4.3 Heat flux in reservoirs: Capivari study case

To investigate the effect of the meteorological data measured over a floating platform and an onshore weather stations (distance between the station was 1 km), meteorological data from Capivari reservoir (UFPR and Lactec, 2015) available for approximately two months (see Figure 21) was compared and the heat transfer between the air-water interface was calculated. This reservoir was chosen for this analysis since it is the only reservoir that has meteorological measurements both at an onshore and a floating platform weather

Table 11 – Differences between meteorological data measured in the onshore and floating platform stations in Capivari reservoir

Station	U_{\max} (ms^{-1})	U_{\min} (ms^{-1})	U_{mean} (ms^{-1})	$T_{a\max}$ ($^{\circ}\text{C}$)	$T_{a\min}$ ($^{\circ}\text{C}$)	$T_{a\text{mean}}$ ($^{\circ}\text{C}$)
Onshore	4.50	0	0.72	32.70	12.80	20.57
Floating	9.8	0	2.33	32.30	15.00	21.22
Station	RH_{\max} (%)	RH_{\min} (%)	RH_{mean} (%)	$q_{s\max}$ (Wm^{-2})	$q_{s\min}$ (Wm^{-2})	$q_{s\text{mean}}$ (Wm^{-2})
Onshore	98	38	86.09	1278	0	202.14
Floating	97	42	84.70	1329	0	206.64

*max – maximum values; min – minimum values and mean – averaged values; wind speed (U); air temperature (T_a); relative humidity (RH); shortwave solar radiation (q_s)

stations.

The graphs (Figure 21) show there is difference between measurements in the onshore and floating platform stations, therefore the energy fluxes estimated from these data could present differences. Table 11 presents maximum, minimum and mean value for each measurement for the variables: wind speed (U), air temperature (T_a), relative humidity (RH) and shortwave solar radiation (q_s).

For the wind, the highest wind speed measured in the floating platform is 9.8 ms^{-1} while in the onshore station is 4.50 ms^{-1} . The mean wind speed also has a significant difference – 0.72 ms^{-1} in the onshore station and 2.33 ms^{-1} in the floating platform. Therefore, the mixing promoted by the wind could not be sufficient to mix the water column as expected, in the case of meteorological measurements in the onshore station. The other meteorological variables showed difference in its maximum and minimum values, but the averaged values did not present more than 4% difference.

The results of heat flux for each set of data was estimated with Heat Flux Analyzer (Woolway et al., 2015). Figure 30 shows the total energy flux calculated for Capivari reservoir. There is a difference between the fluxes according each set of data: while mean total heat flux (Q_{tot}) with meteorological data from measurements at the floating platform is $-126.16 \pm 86.60 \text{ Wm}^{-2}$ (the reservoir losses heat), the heat flux estimated by measurements at the onshore station is $-89.76 \pm 56.05 \text{ Wm}^{-2}$. The maximum heat flux estimated is 236.62 Wm^{-2} (floating platform) and 271.37 Wm^{-2} (onshore station), while minimum is -462.46 Wm^{-2} (floating platform) and -234.04 Wm^{-2} (onshore station). These differences in heat fluxes are mainly due to sensible heat ($-10.03 \pm 8.06 \text{ Wm}^{-2}$ – onshore station; $-16.51 \pm 15.96 \text{ Wm}^{-2}$ – floating platform) and latent heat ($-38.81 \pm 20.37 \text{ Wm}^{-2}$ – onshore station; $-73.15 \pm 50.46 \text{ Wm}^{-2}$ – floating platform).

Table 2 in Section 2.2 showed that the meteorological monitoring in some studies was performed in stations over the water surface (Bertone et al., 2015; Curtarelli et al. (2013); Marti et al. (2011); Tuan et al. (2009); Morillo et al. (2008)), or close to the reservoir (Yu et al. (2010); Elçi (2008)). This section showed that the measurements may

influence estimation of heat fluxes – therefore, the location meteorological measurements are performed may affect the heat fluxes estimation at the reservoir surface, temperature of the water column and mixing processes.

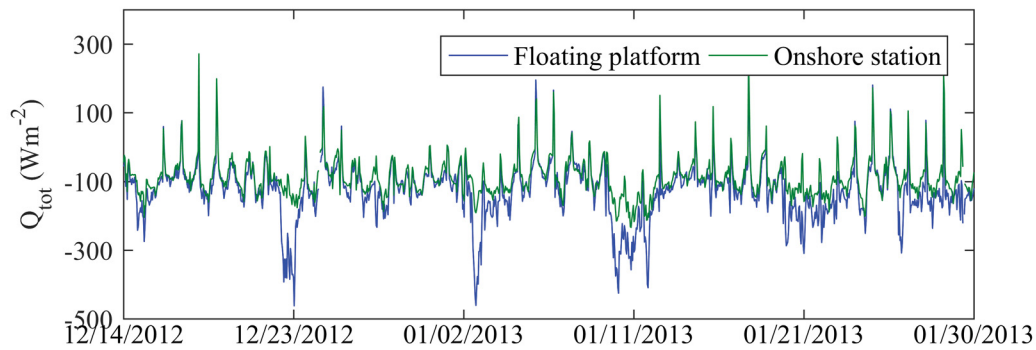


Figure 30 – Energy fluxes calculated for Capivari reservoir

4.4 Summary of the chapter

This chapter showed that lakes and reservoirs may present vertical and horizontal temperature gradients, which may interfere in mass transport or water quality, for example. The cause of these gradients is related to the influence of inflows, bathymetry and meteorological forcing. Close to river entrance, gradients were identified at the bottom layer. In side arms, temperature gradients occurred at the surface layer, that may be caused by differential cooling/heating. This is an evidence that temperature has an influence on circulation and mass transport in Vossoroca and Passaúna reservoirs. This is investigated in more detail for Vossoroca reservoir in Section 7. This section also presented the influence of different location of meteorological measurements (onshore weather station and floating platform weather station) on air-water interface heat fluxes – the most important heat fluxes in lakes and reservoirs. The meteorological measurements showed differences that may result in different heat fluxes – which can have an impact in heat transport modeling in lakes and reservoirs. This topic is also investigated in Section 6.

5 One-dimensional and Sector modeling

One of the questions to be answered in this thesis is that if it is possible to apply an one-dimensional model in different regions of the reservoir (simplifying system representation) and obtain reliable results of the heat transport. The challenge is to define how the exchange between the sectors will occur, and if it is possible to model them separately or not. Figure 31 shows an scheme of the sector model. The proposed tests are:

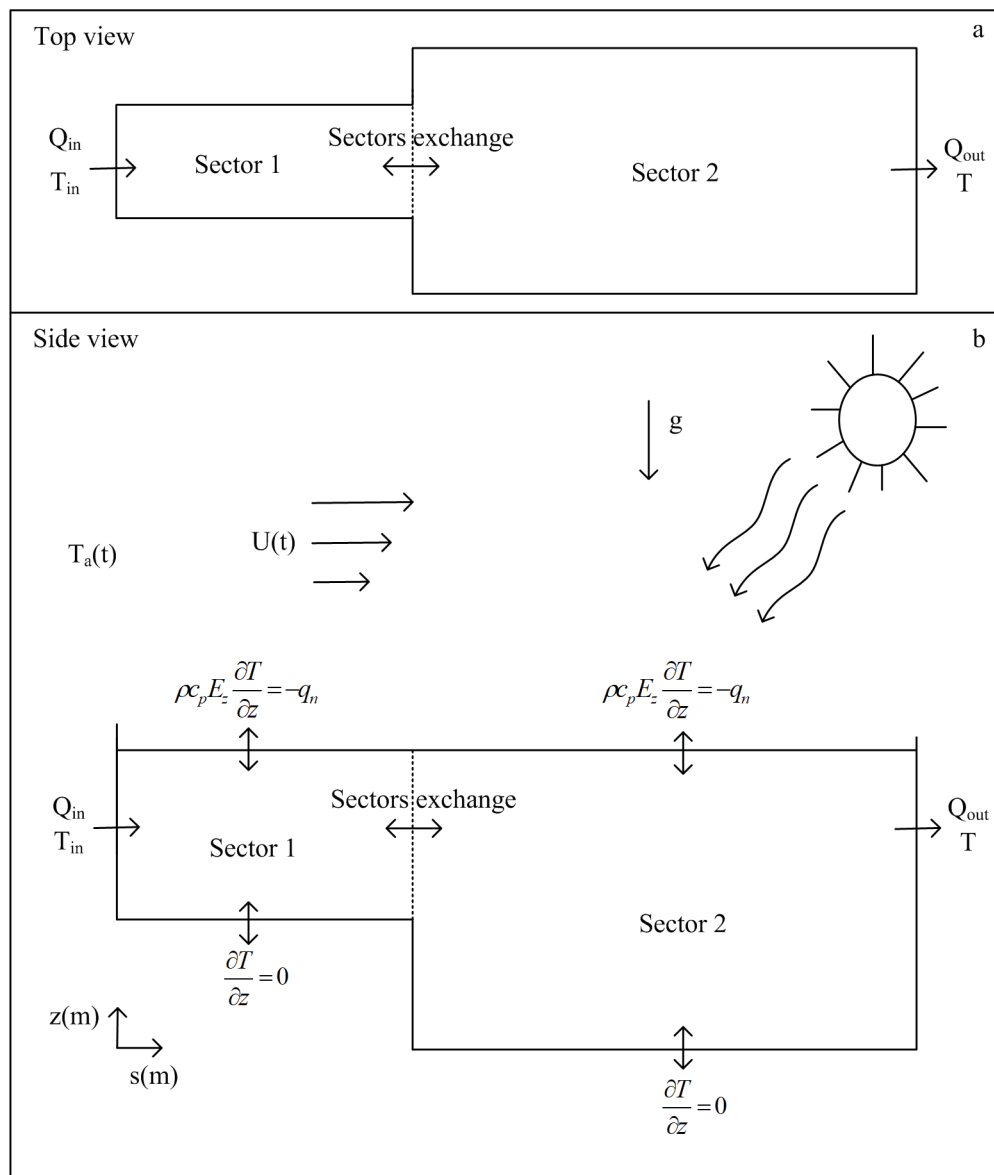


Figure 31 – Scheme of the sector model. a) Top view and b) Side view and boundary conditions

- No exchange between sectors;
- Exchange related to the difference in temperature between the sectors;

- Allow exchange between sectors related to temperature gradients, using a system of reactors, as in Chapra (1997).

The one-dimensional model, MTCR-1, was already implemented in Vossoroca reservoir (Polli, 2014) and compared against measured data and showed good agreement and high temporal resolutions. The grid in MTCR-1 model was defined with a maximum of 85 fixed layers, which corresponds to 0.2 m each layer for Vossoroca reservoir. The model considers the variation of area with depth. UNESCO equation is used to calculate water density for fresh water. Solar radiation is absorbed as a function of depth – Secchi depth is a calibration parameter for the model. Secchi depth was set as 1.8 m, that is close to the measurements at the deepest point of the reservoir. The mean absolute error (MAE) and standard deviation (SD) were calculated for estimation of errors in relation to the measurements. The time step for the simulation was 2 min. In July, Vossoroca reservoir is mixed, therefore initial condition of temperature is 14.5 °C. In these conditions, the time to run MTCR-1 model was less than 2 min. Table 12 shows the main information about the modeling and calibration parameters for the 1D modeling in Vossoroca reservoir. Table 13 shows required data in the 1D modeling in Vossoroca reservoir and where in the model the data is used.

Table 12 – MTCR-1 model set-up and calibration parameters for Vossoroca reservoir modeling

	Description	MTCR-1 set-up
Δt	Time step of the modeling	2 min
Δz	Vertical grid size	0.2 m
T_0	Initial condition of temperature	14.5 °C
Period	Period of simulation	94 days
Processing time	–	< 2 min
H_{Secchi}	Secchi depth (calibration parameter)	1.8 m
β	Solar radiation absorbed at surface	0.45
α	Albedo	0.07

Table 13 – MTCR-1 model required data for Vossoroca reservoir modeling

Data	Description
Maximum depth	Point where the 1D model is applied. In Vossoroca, 16 m
Area	The model considers the area variation with depth
Inflows/outflow	In Vossoroca, three rivers contribute to flow – São João, São Joãozinho and Vossoroca. São João is the main river. Inflow temperature is also required. Daily data is available. In the 1D model, the flow of the three rivers is accumulated.
Meteorological data	Solar radiation, wind speed, air temperature and relative humidity are required in the heat flux model at the air-water interface. Wind speed is also required for eddy diffusivity calculations. In Vossoroca, the time step of measurements is 2 min

Figure 32 shows temperature results (see also Figure 11 that shows measured data). The starting period of the simulation is in July (Winter in South Hemisphere), therefore,

the water column is mixed – this is represented by MTCR-1 model. The model tend to increase temperature in deeper layers, but simulate the initial period of stratification and mean temperatures. Table 14 shows the mean absolute and relative error for the 1D modeling of Vossoroca reservoir – MAE is 1.18 ± 0.84 °C and the mean relative error, 0.21 ± 1.44 °C.

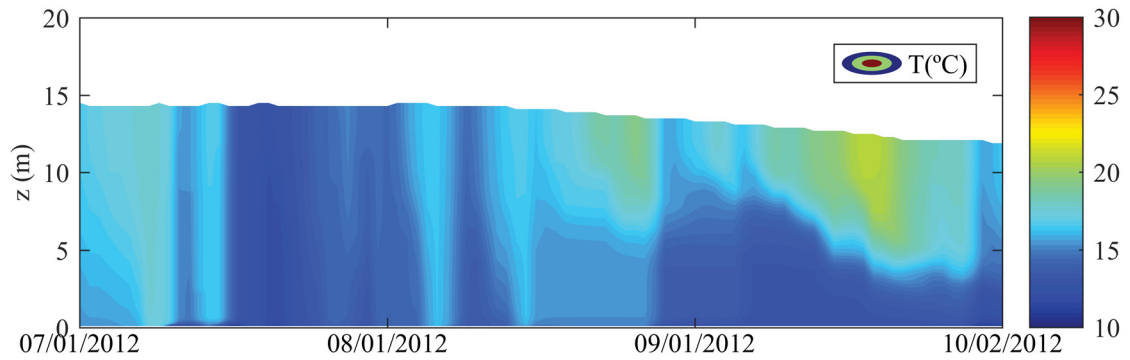


Figure 32 – Vossoroca reservoir 1D heat transport modeling (Polli, 2014)

Table 14 – Mean absolute and relative error in the 1D modeling

Mean absolute error (°C)	Mean relative error (°C)
1.18 ± 0.84	0.21 ± 1.44

Temperature gradients simulated by one-dimensional model MTCR-1 were close to measured data (see also Figure 11). Table 15 shows the number of the days a certain temperature gradient is expected – gradients higher than 1°C, for example, were observed in 79 days, while the model reproduced it in 49 days. In general, the model follow the expected behavior from the measured data but, most of the time, MTCR-1 model underestimate temperature gradients.

Table 15 – Number of days that $\Delta T > 1, 2$ and 3 °C, $W > 1$ and $L_N > 1$ of Vossoroca reservoir 1D modeling (from 94 days)

$\Delta T > 1$ °C (days)	49
$\Delta T > 2$ °C (days)	42
$\Delta T > 3$ °C (days)	25
$W > 1$ (days)	93
$L_N > 1$ (days)	83

Wedderburn number and Lake number were calculated for the one-dimensional model results (Figure 33 and Table 15). Most of time, the results of physical indices are higher than the critical number ($W=1$ and $L_N=1$), indicating stability of the water column and stratification – the results are close to the results from the measurements. In 93 days, Wedderburn number is $W > 1$ and in 83 days, $L_N > 1$.

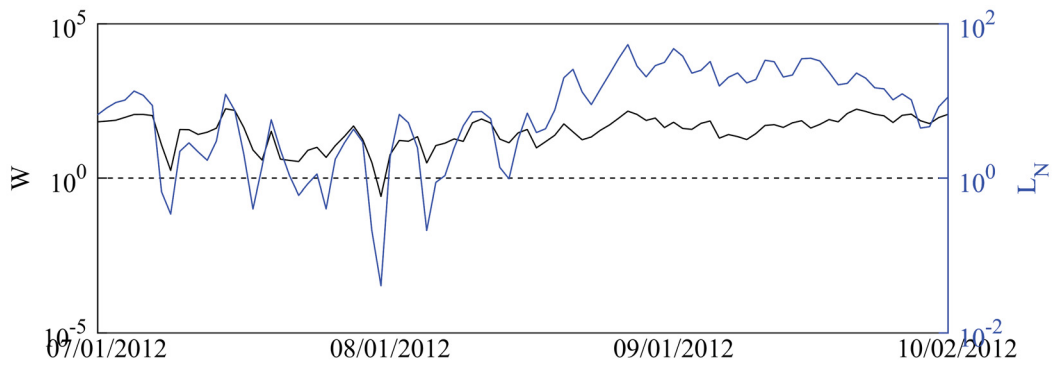


Figure 33 – Wedderburn number and Lake number in Vossoroca reservoir with data of the 1D modeling

Usually in environmental studies in lakes and reservoirs the main interest is to obtain temperature profiles in different points, as showed in Figure 34. Point 3 is located in the region of maximum depth, while points 1 and 2 are shallower. The 1D model previously showed does not allow this kind of evaluation, since only one point in the reservoir is modelled. In the case of Vossoroca reservoir, the one-dimensional model is applied to the deeper area, do not representing shallow regions that may present different temperature profiles. Also, there is no attempt in the literature to model different regions of the reservoir simplifying the system representation. In rivers, on the other hand, Keupers and Willems (2017) developed a fast conceptual river water quality model, where the river branch is represented by reservoirs in series with divisions based on key locations of interest. Therefore, this representation allows fast response of the system.

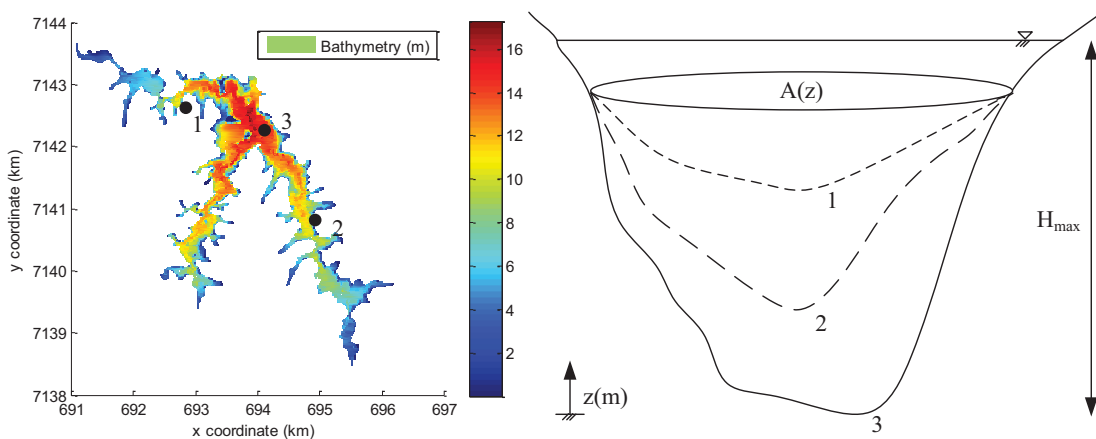


Figure 34 – Scheme showing regions of Vossoroca reservoir with different depths

The sector model may allow the evaluation of different regions. In Vossoroca reservoir, the first approach to apply a sector model is to divide the arms of the reservoir. Figure 35 show a scheme on how the connection and the simulation works.

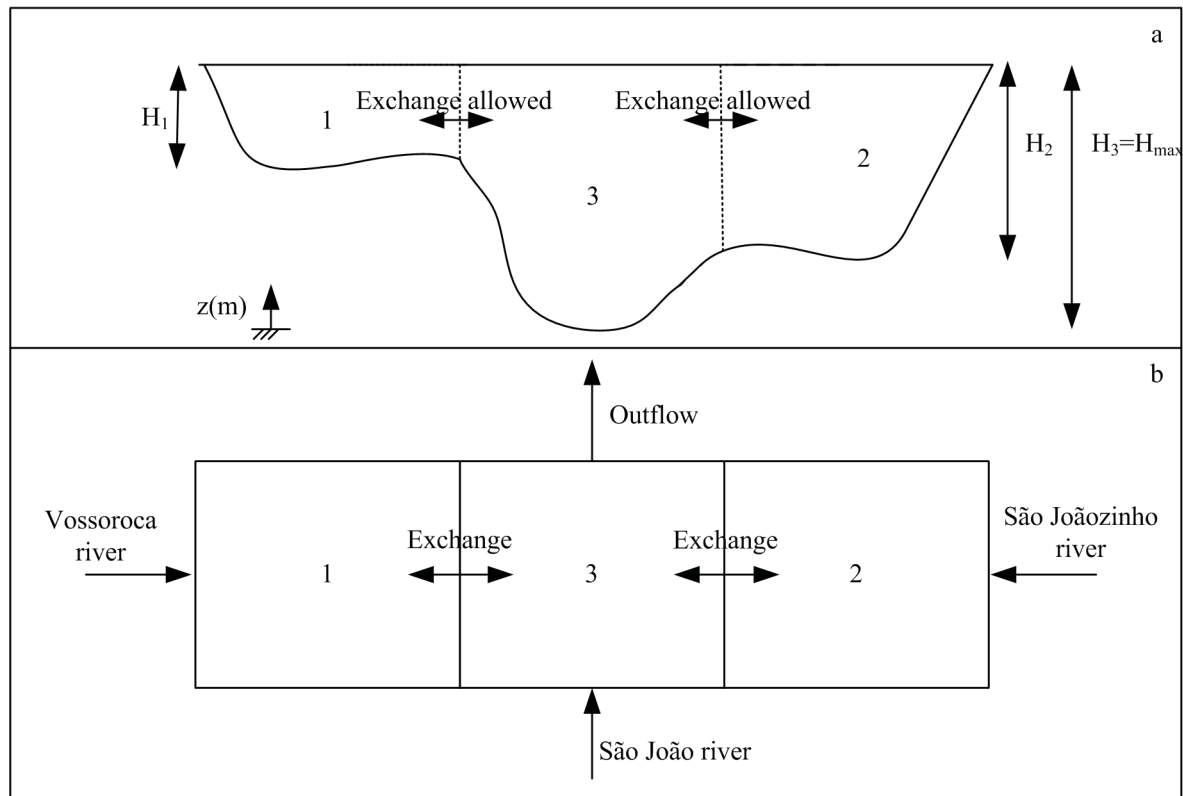


Figure 35 – Scheme showing the approach to the Vossoroca reservoir sector model. a) Side view of the sectors and b) flows and exchange in each sector

Sector 1 receives inflowing water from Vossoroca river and may exchange heat with sector 3 (just the depth directly connected with sector 1 may exchange heat). Sector 2 receives inflowing water from São Joãozinho river and may exchange heat with sector 3 (just the depth directly connected with sector 2 may exchange heat). Sector 3 receives inflowing water from São João river and has an outflow corresponding to the dam in Vossoroca reservoir.

To test the model, first simulations were performed without the exchange between the sectors, just considering differences in depth. After that, it was considered an exchange based on the mean difference in temperature between the sectors directly connected. The basic configuration of number of layers, time step, initial condition is the same as in the one-dimensional modeling (see Table 12). In relation to required data (see Table 13), the flow is not accumulated in the sector model – each sector receives de flow related to the contribution of the rivers – São João river (56% of the total flow), São Joãozinho (28% of the total flow) and Vossoroca river (16% of the total flow).

Figure 36 shows the sector model for three regions of Vossoroca reservoir without exchange between the sectors. Figure 37 shows the results considering the exchange calculated according the mean difference in temperature of each layer between the sectors. Some differences may be identified from the results of Figure 36 and 37 – temperature of sector 1 increases when exchange occurs. The same is observed in sector 2. In general,

temperature of sector 3 decreases. Both simulations with and without exchange in the sector model can simulate the beginning of stratification in the reservoir. Table 16 shows the error calculated for the two simulations of the sector model. Mean absolute and relative error diminished in the simulation considering exchange between the sectors. MAE for the modeling without exchange is 1.22 ± 1.07 °C, and with exchange 1.16 ± 0.90 °C.

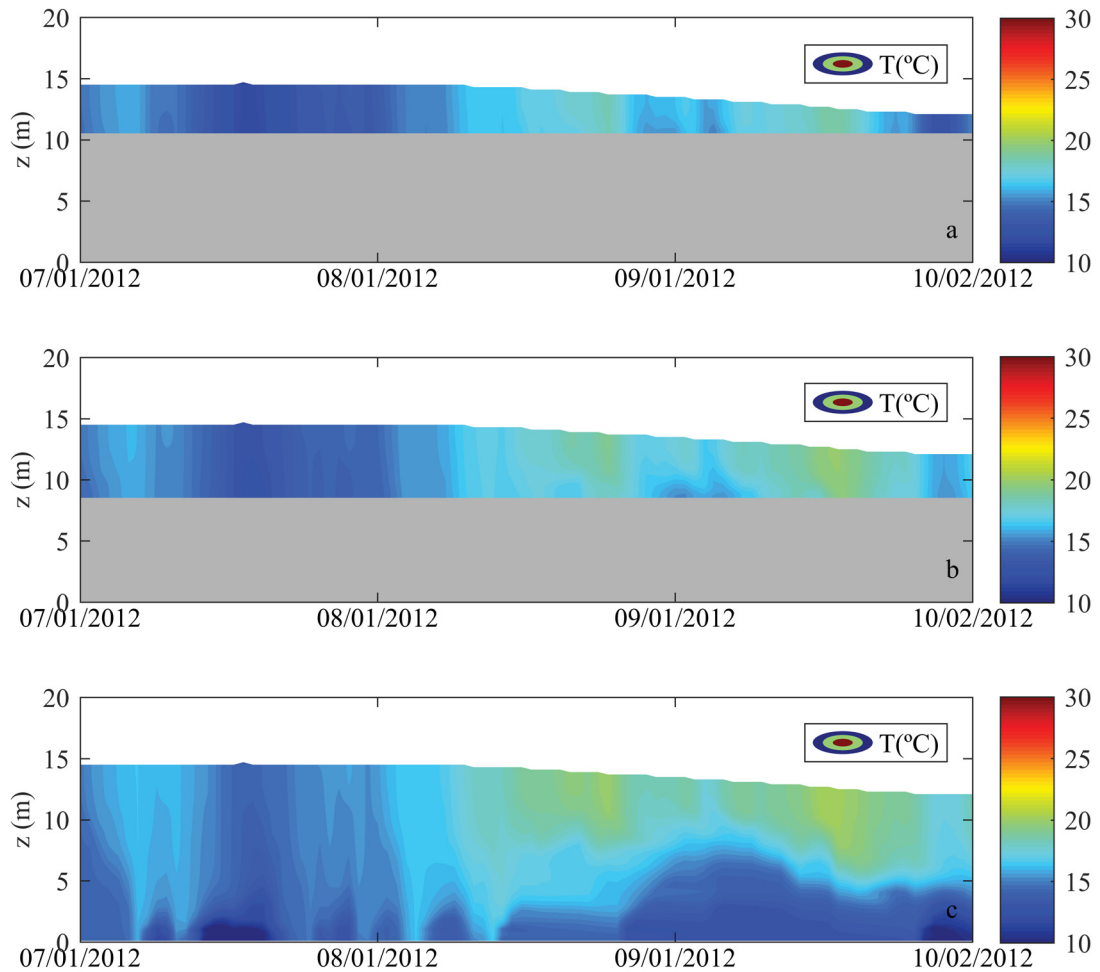


Figure 36 – Sector model of Vossoroca reservoir without exchange between sectors a) Sector 1, b) Sector 2 and c) Sector 3

Table 16 – Mean absolute and relative error in the sector modeling of Vossoroca reservoir

Mean error	No exchange	With exchange
Absolute (°C)	1.22 ± 1.07	1.16 ± 0.90
Relative (°C)	0.54 ± 1.53	0.17 ± 1.46

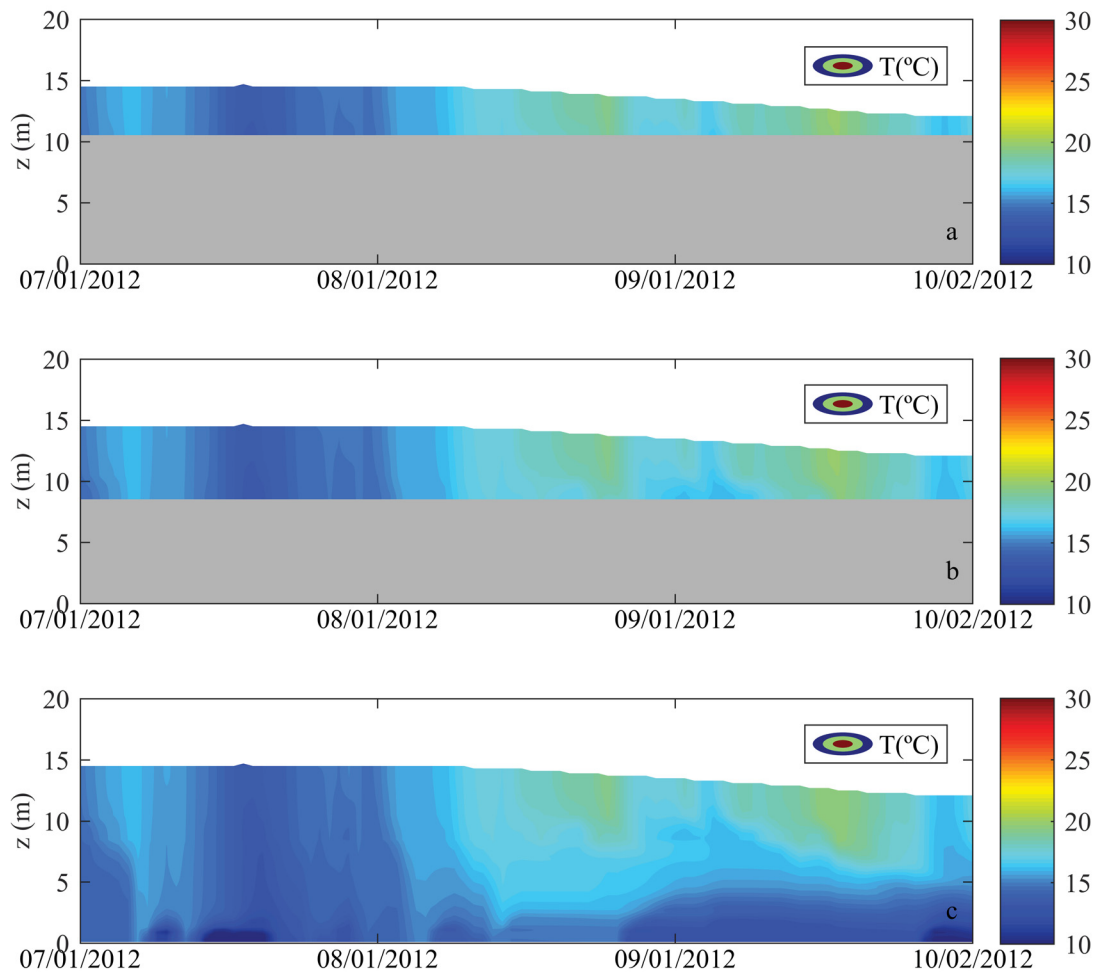


Figure 37 – Sector model of Vossoroca reservoir with exchange according the mean difference in temperature of each sector a) Sector 1, b) Sector 2 and c) Sector 3

Surface temperature is compared in Figure 38 and Table 17 shows mean temperature of the surface layer for each sector. In the simulation without the exchange, temperature of sector 1 is lower in relation to the other sectors – the heat flux at surface is the same in the three sectors, but the effect of this flux is higher in sector 1 due its depth. The difference in mean surface temperature between the sectors is 1.89 °C. In the simulation considering exchange between the sectors by the mean difference in temperature, sectors mean temperature should be the same, as it is shown on Table 17. There is an increase of temperature in sectors 1 and 2, and decrease in sector 3.

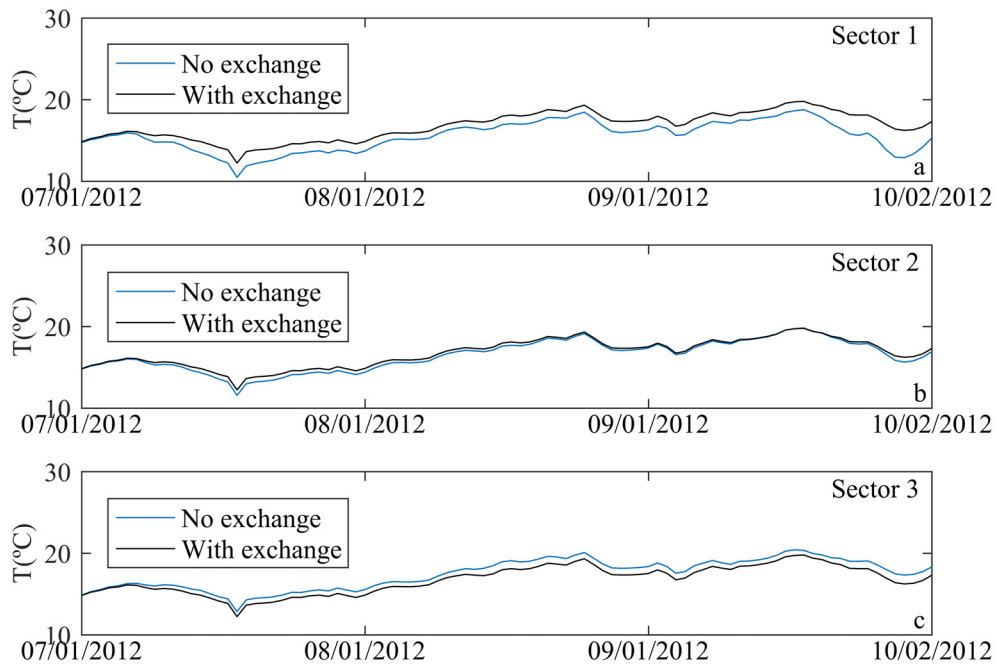


Figure 38 – Surface temperature with and without exchange between sectors in a) sector 1, b) sector 2 and c) sector 3

Table 17 – Mean surface temperature in the sectors of Vossoroca reservoir

Sectors	Sector 1	Sector 2	Sector 3
Without exchange (°C)	15.53	16.45	17.42
With exchange (°C)	16.74	16.74	16.74

5.1 Improvements of one-dimensional model

The 1D model is highly sensitive to inflows/outflows when bathymetry is considered in the modeling. If the inflow has higher density than the bottom layer of the reservoir, the water enters the reservoir in the bottom layer. If the inflow has lower density than the surface layer, the water enters the reservoir in the surface layer. If an intrusion occurs, the current approach is to identify the layer with similar density and distribute inflows equally above this layer. Since bathymetry is considered in the modeling, the effect of a forcing at the layers close to the bottom increases due the lower volume of these layers.

The effects of including bathymetry in one-dimensional models was already reported by Stepanenko et al. (2014). Three one-dimensional models were tested considering the surface area representing the system and also considering the bathymetry. The results of the modeling were better considering the surface area as representative of the system, considering measured data. In the first case, with surface area, the lake showed thermal stratification as expected from measurements for the three models. With bathymetry, the three models showed similar behavior – temperature increased more than expected

in the bottom layers and lower temperature gradients between surface and bottom were simulated. The bathymetry in the modeling increased temperature in deeper regions due the lower volume compared to layers close to the surface. This is also verified in MTCR-1 model (see Figure 32) – temperature gradients are underestimated by the model. The models tested by Stepanenko et al. (2014) do not consider inflows/outflows in the heat transport equation. Some tests were already performed by Polli (2014) in MTCR-1 model, and the 1D model showed to be highly sensitive to inflows/outflows when bathymetry is considered. A new approach to distribute the flow is tested in this section. Figure 39 shows the current approach used and the new approach to distribute the flow in the water column. Now, if the inflow has higher density than the bottom layer of the reservoir, the inflow is distributed proportionality to the layer volume in the entire water column. If a intrusion occurs, the layer of similar density is identified and the inflow is distributed above this layer, proportionality to the layer volume.

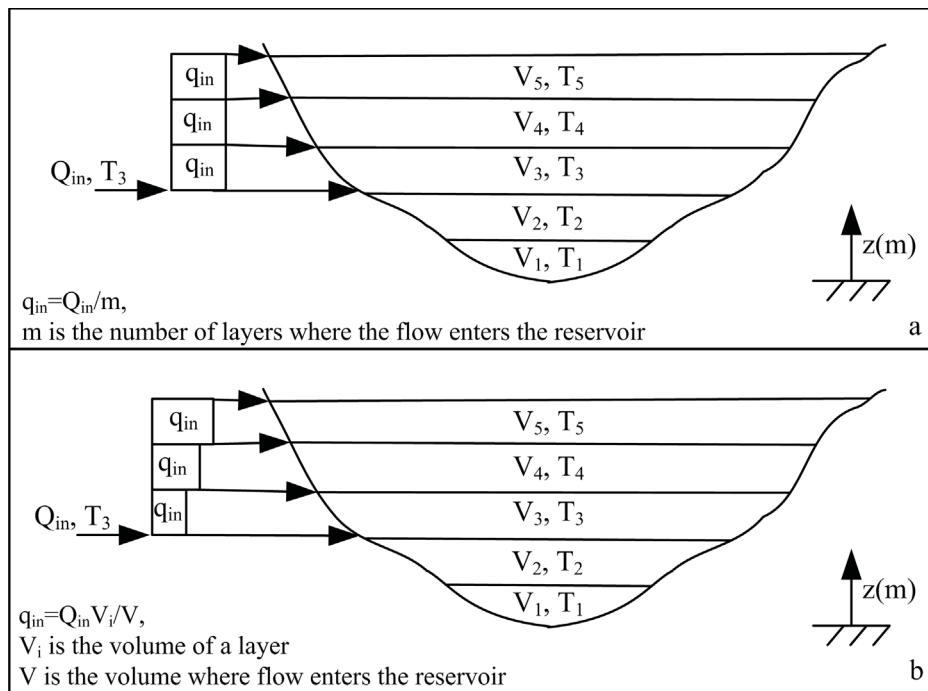


Figure 39 – Scheme on MTCR-1 model of inflow entering the reservoir. a) Current approach distributing equally inflows in the water column b) New approach distributing inflows in relation to the volume of layers

Figure 40 shows the results of the modeling distributing the flow according the volume of each layer. The mean absolute error (MAE) increased in relation the results of Figure 32, $1.45 \pm 0.97^\circ\text{C}$, however the representation of temperature gradients and physical indices is improved, as presented in Table 18.

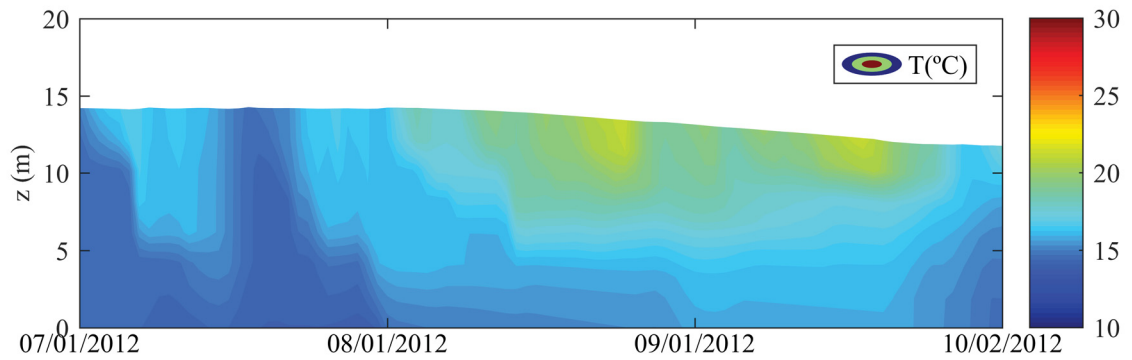


Figure 40 – Vossoroca reservoir 1D heat transport modeling – inflow distributed according the volume of the layers

Table 18 – Number of days that $\Delta T > 1, 2$ and 3°C , $W > 1$ and $L_N > 1$ of Vossoroca reservoir 1D modeling (from 94 days) with inflow distributed according the volume of the layers

$\Delta T > 1^\circ\text{C}$ (days)	87
$\Delta T > 2^\circ\text{C}$ (days)	71
$\Delta T > 3^\circ\text{C}$ (days)	50
$W > 1$ (days)	91
$L_N > 1$ (days)	91

5.1.1 Sector model improvements

The approach presented in the last section is applied now to the sector model and the three proposed tests for heat exchange between the sectors: no exchange and exchange related to the difference in temperature between the sectors.

Figure 41 shows the results of the modeling do not considering exchange between the sectors and Figure 42 the results with exchange according the mean difference in temperature of each sector. In both simulations, the decrease in temperature in deeper layers is lower due the new approach to distribute inflows – results are closer to measured temperature profiles. Table 19 shows the mean absolute and relative error for the two simulations – the error diminished in relation to the error calculated for the previous modeling (see Table 16).

Table 19 – Mean absolute and relative error in the sector modeling of Vossoroca reservoir with inflow distributed according the volume of the layers

Mean error	No exchange	With exchange
Absolute ($^\circ\text{C}$)	0.84 ± 0.70	0.90 ± 0.72
Relative ($^\circ\text{C}$)	0.03 ± 1.09	-0.39 ± 1.09

5.1.2 System of reactors

In this section, it is presented the equations and tests applied to the sector model, to simulate the exchange between the sectors as a system of reactors, as in Chapra (1997).

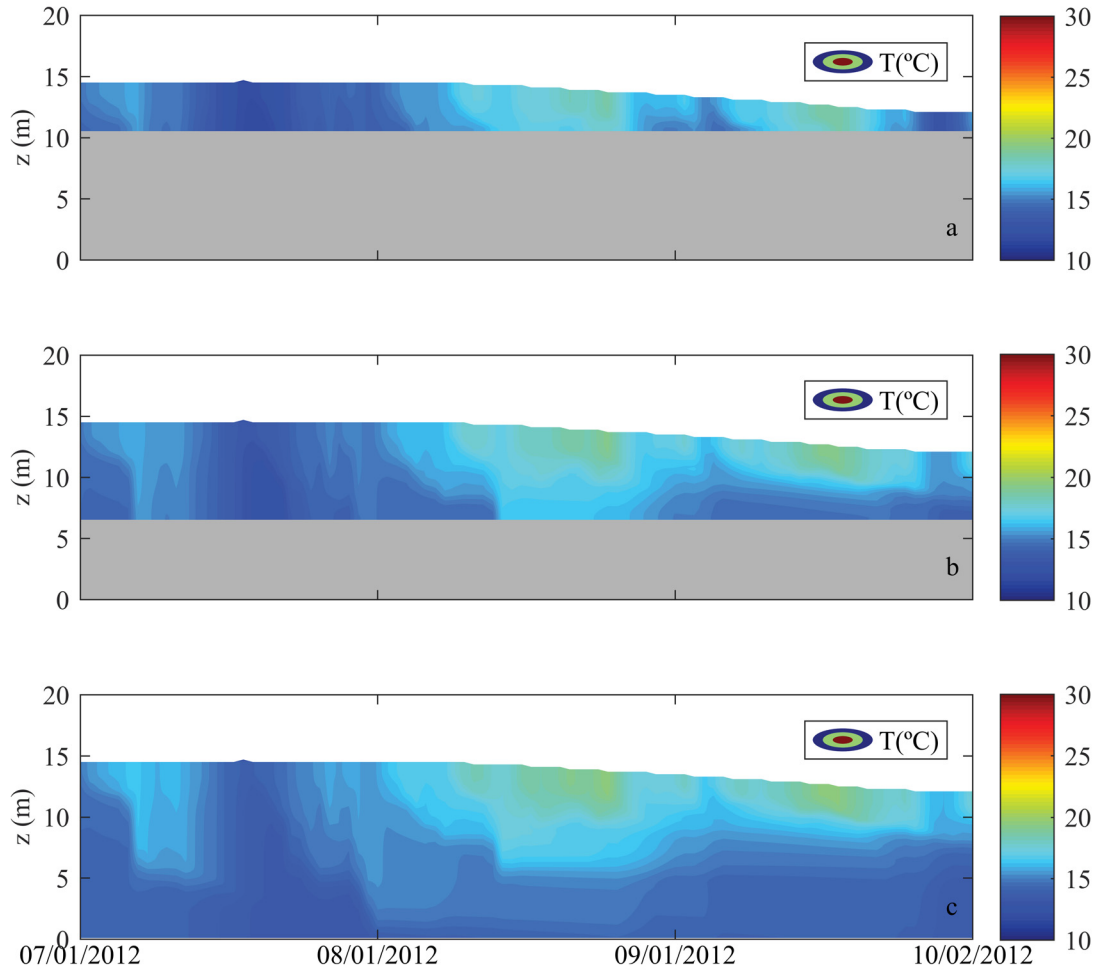


Figure 41 – Sector model of Vossoroca reservoir without exchange between sectors – inflow distributed according the volume of the layers a) Sector 1, b) Sector 2 and c) Sector 3

Figure 43 shows an scheme of the sectors for Vossoroca reservoir. For Sector 1, 2 and 3:

$$\rho_1 c_{p1} V \frac{dT_1}{dt} = Q_{in1} \rho_{in1} c_{pin1} T_{in} - Q_{13} \rho_1 c_{p1} T_1 \quad (19)$$

$$\rho_2 c_{p2} V \frac{dT_2}{dt} = Q_{in2} \rho_{in2} c_{pin2} T_{in} - Q_{23} \rho_2 c_{p2} T_2 \quad (20)$$

$$\rho_3 c_{p3} V \frac{dT_3}{dt} = Q_{in3} \rho_{in3} c_{pin3} T_{in} + Q_{13} \rho_{13} c_{p13} T_1 + Q_{23} \rho_{23} c_{p23} T_2 - Q_{out} \rho_3 c_{p3} T_3 \quad (21)$$

in which the indices 1, 2 and 3 correspond to sectors 1,2 and 3, respectively, ρ is the water density, c_p is the specific heat of water, V is the volume, T is temperature, t is time, Q_{in} is the inflow, ρ_{in} is the density of inflow, c_{pin} is the specific heat of the inflow, T_{in} is the temperature of inflow, Q_{13} is the flow between sector 1 and 3 and Q_{23} is the flow between

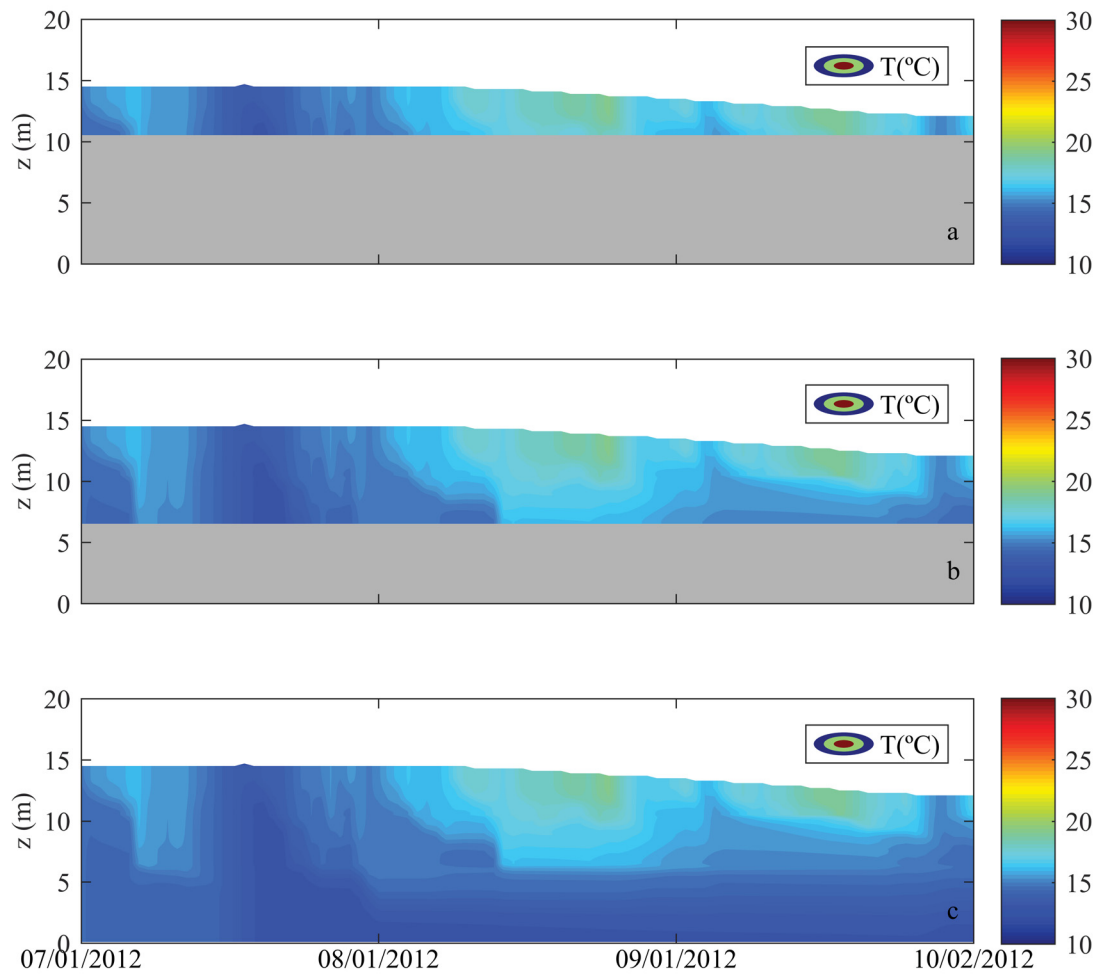


Figure 42 – Sector model of Vossoroca reservoir with exchange according the mean difference in temperature of each sector – inflow distributed according the volume of the layers
 a) Sector 1, b) Sector 2 and c) Sector 3

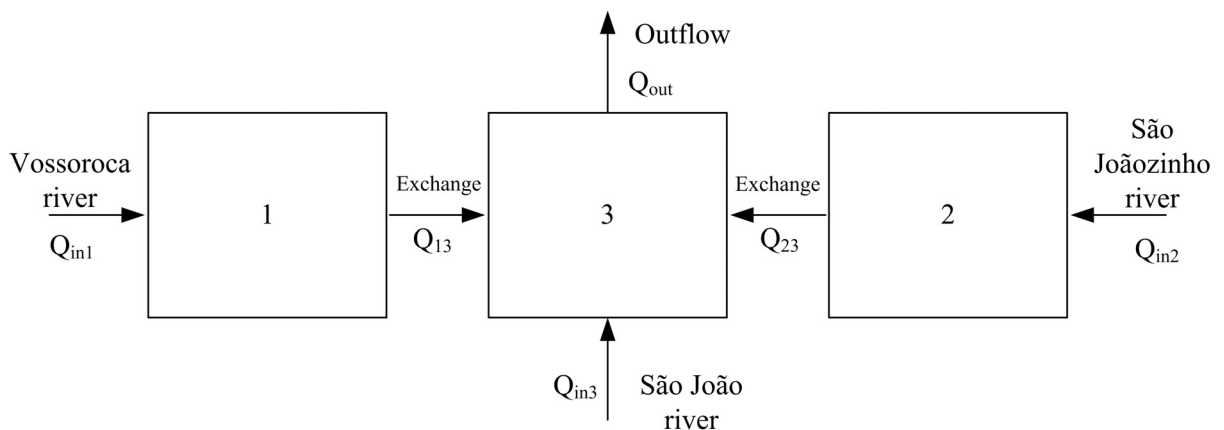


Figure 43 – Scheme of exchange using a system of reactors in the sector model

sector 2 and 3.

The solution for this system of equations is:

$$T_1 = \frac{Q_{in1}\rho_{in1}c_{pin1}T_{in} + \rho_1c_{p1}\frac{V}{\Delta t}T_1^0}{\rho_1c_{p1}\frac{V}{\Delta t} + Q_{13}\rho_1c_{p1}} \quad (22)$$

$$T_2 = \frac{Q_{in2}\rho_{in2}c_{pin2}T_{in} + \rho_2c_{p2}\frac{V}{\Delta t}T_2^0}{\rho_2c_{p2}\frac{V}{\Delta t} + Q_{23}\rho_2c_{p2}} \quad (23)$$

$$T_3 = \frac{Q_{in3}\rho_{in3}c_{pin3}T_{in} + Q_{13}\rho_{13}c_{p13}T_1 + Q_{23}\rho_{23}c_{p23}T_2 + \rho_3c_{p3}\frac{V}{\Delta t}T_3^0}{\rho_3c_{p3}\frac{V}{\Delta t} + Q_{out}\rho_3c_{p3}} \quad (24)$$

where T_1^0 , T_2^0 and T_3^0 is the temperature in a previous time step and Δt is the time step. These equations are applied in the modeling for each layer that is connected by the sectors (each layer is a mixed reactor). Q_{13} and Q_{23} were calculated considering a water balance, since water level variation is known.

Results of the sector model applying a system of reactors to simulated the heat exchange in the horizontal direction is shown in Figure 44. The sector simulation shows lower temperature in deeper layers, as expected from measurements. At sector 3, the mean bottom temperature is 13.49°C and, in the measurements, 13.99°C . MAE for the bottom layer was $0.57 \pm 0.02^\circ\text{C}$. In the surface layer, on the other hand, the mean surface temperature was 16.15°C in the modeling, while in the measurements, 17.68°C , with a MAE of $1.7 \pm 0.01^\circ\text{C}$. The MAE for the simulation was $1.10 \pm 0.99^\circ\text{C}$.

The surface temperature for sectors 1, 2 and 3 is shown in Figure 45. In general, if temperature decreases at the surface, it decreases faster in sectors 1 and 2. The increase of surface temperature also occurs faster in sectors 1 and 2. The mass of water of these two sectors is lower than sector 3 – then, for the same heat flux at the air-water interface, the effect of this heat flux is higher in sectors 1 and 2. The mean surface temperature in sector 1 was 15.72°C while, in sector 3, 16.14°C .

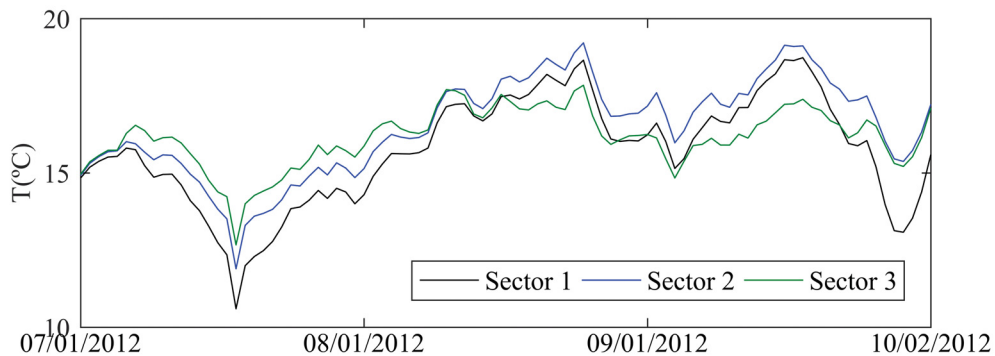


Figure 45 – Surface temperature of Vossoroca reservoir using a system of reactors to calculate heat exchange between the sectors

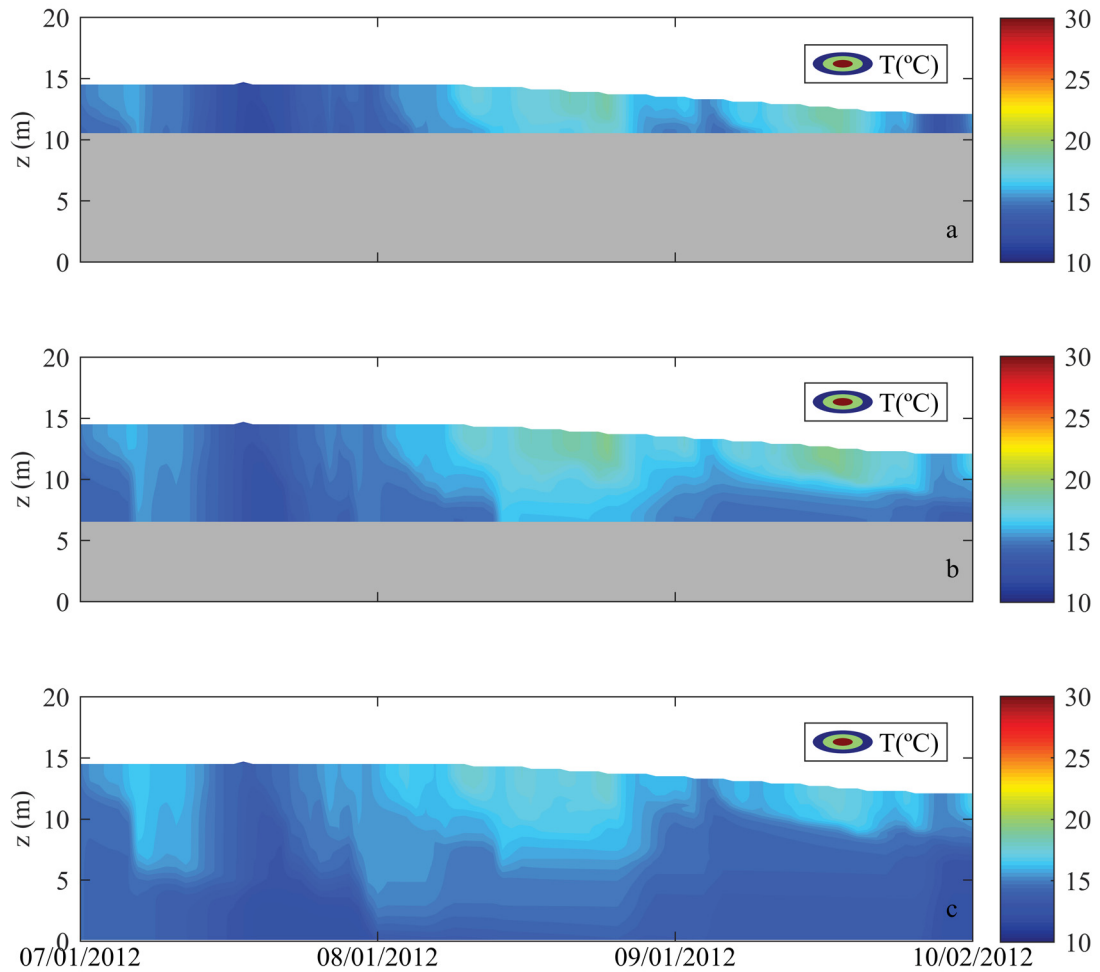


Figure 44 – Sector model of Vossoroca reservoir using a system of reactors to calculate heat exchange between the sectors. a) Sector 1, b) Sector 2 and c) Sector 3

5.2 Summary of the chapter

This chapter showed the application of one-dimensional model MTCR-1 model for Vossoroca reservoir, and the development and application of the sector model. The one-dimensional modeling has the advantage of high processing time and less calibration data, as the sector model proposed. The one-dimensional model may be applied to reservoir classification – the comparison between vertical temperature gradients and physical indices, calculated from model results and measured data, showed that one-dimensional model MTCR-1 can be used for reservoir classification (mixing and stratification periods). The sector model, which development and application is showed in this chapter, may be applied independently (no connection between the reservoir areas) or connecting different regions of the reservoir. The error calculated for the region where temperature is measured in Vossoroca reservoir is even lower than the one-dimensional model – with

the same advantages of one-dimensional models, high time processing and less calibration data. The next chapter shows the three-dimensional modeling for Vossoroca reservoir and comparison between three-dimensional modeling and one-dimensional and sector models.

6 Three-dimensional modeling

A three-dimensional model is an amplification of the sector approach – here the reservoir is divided in a much higher number of sectors that are connected and exchange properties. Usually this fine resolution is also related to a very large time for processing. In this section, the 3D modeling for Vossoroca reservoir and related analysis are presented. The proposed scenarios of this section are:

- Comparison between heat flux models in the three-dimensional model;
- Grid testing: tests of different grid configuration;
- The full 3D modeling of Vossoroca reservoir and data analysis;
- Sector configuration: comparison with the sector model and analysis if it is possible to use a more complex model in a simple configuration.

6.1 Comparison between heat flux models in Delft3D

Delft3D model has five different models to estimate the heat fluxes between the air and water, as showed in Section 2.3.3. In this section, it is shown the results of the Vossoroca reservoir modeling using Murakami and Ocean heat flux models and an analysis of the difference between applying each model. The modeling of Vossoroca reservoir was performed during approximately three months using Delft3D. The model was set up with 14 layers and uniform initial temperature (14.5 °C). Running the model without parallelization the time required is 12 days (with parallelization 7 days).

The two simulations present distinct results – using Murakami model, surface and bottom temperatures increase more than using the Ocean model, as it is shown in Figure 46, different from what was expected according the measurements. Table 20 shows the error calculated in relation to measurements in the simulations using Murakami and Ocean heat flux models. Both absolute and relative errors shows that Murakami model has a higher error in comparison to measured data in Vossoroca reservoir.

Table 20 – Absolute and relative error in the 3D modeling using Murakami and Ocean heat flux models

Error	Murakami	Ocean
Absolute (°C)	1.33 ± 0.93	0.64 ± 0.54
Relative (°C)	1.18 ± 1.11	0.16 ± 0.82

To analyse why this difference in the water column temperature occurs, the heat flux equations of this models were compared using the input data for Delft3D and surface water temperature from Murakami model simulation.

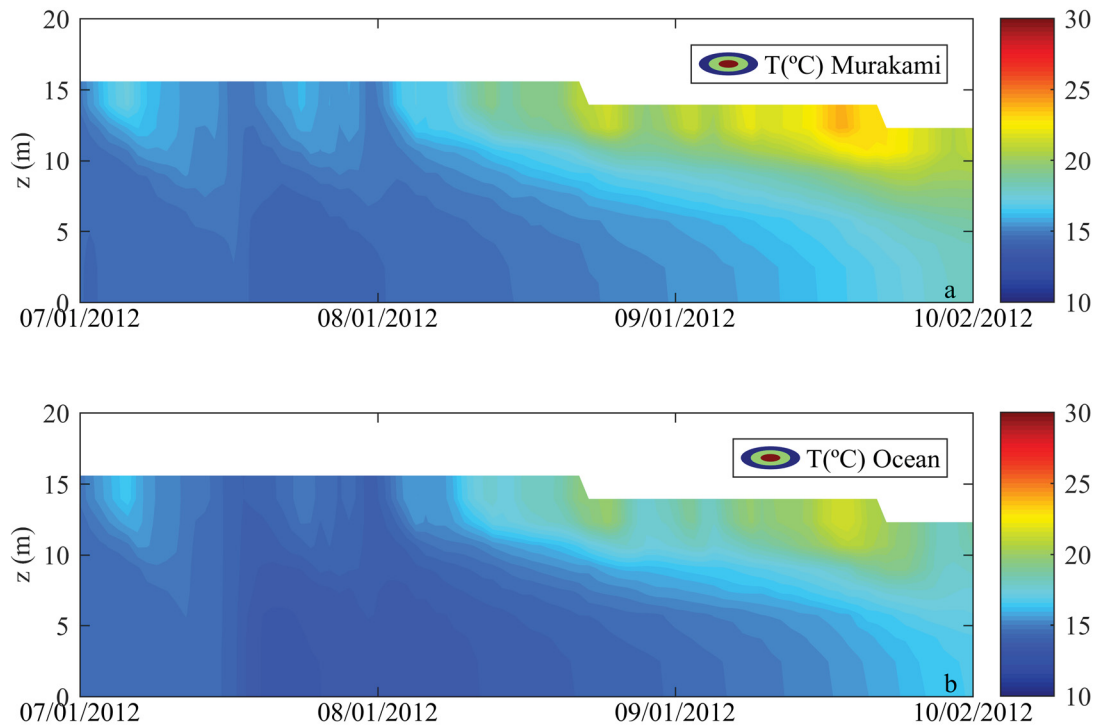


Figure 46 – Temperature results using a) Murakami and b) Ocean heat flux models in Delft3D

Total heat flux (Q_{tot}) is calculated as (Deltares, 2014)

$$Q_{tot} = Q_{sn} + Q_{an} - Q_{br} - Q_{ev} - Q_{co} \quad (25)$$

where Q_{sn} is the net incident solar radiation (short wave) (Wm^{-2}), Q_{an} is the net incident atmospheric radiation (long wave) (Wm^{-2}), Q_{br} is the back radiation (long wave) (Wm^{-2}), Q_{ev} is the evaporative heat flux (latent heat) (Wm^{-2}) and Q_{co} is the convective heat flux (sensible heat) (Wm^{-2}). For Murakami and Ocean heat flux models it is defined the effective back radiation (Q_{eb}) as $Q_{eb} = Q_{br} - Q_{an}$.

Figure 47 shows the total heat flux calculated using Murakami and Ocean models. When the reservoir loses heat, this lost is bigger when applying the Ocean model. The mean energy flux is 102.8 Wm^{-2} and 10.3 Wm^{-2} for Murakami and Ocean model, respectively. Therefore, it is necessary to investigate the terms in the total heat flux equation to identify why this difference occurs.

Figure 48 shows each term of the heat balance. From the figure, the greater differences occur in the terms corresponding to evaporation and convective heat fluxes – in the evaporation term, the mean heat flux is 3.32 Wm^{-2} and 72.3 Wm^{-2} for Murakami and Ocean models, respectively. In the convective heat fluxes, the mean heat flux is 1.25 Wm^{-2} for Murakami model, and 29 Wm^{-2} for Ocean model.

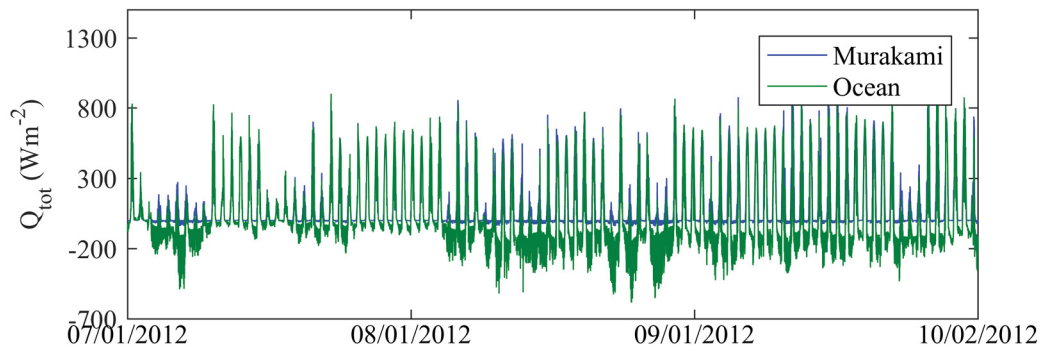


Figure 47 – Heat flux with Murakami and Ocean models

From the equations for the two models, the cause of this difference is a calibration parameter in the evaporation equation. In the wind speed function: $f(U_{10}) = cU_{10}$, $c=1.2 \cdot 10^{-9}$ for Murakami model, while in the Ocean model, this parameter is 0.0015. This parameter in Murakami model was calibrated for one situation, in Japan (Murakami et al., 1985). The term related to convection had the same shape because convective heat flux is calculated as a function of evaporation. From the results of heat fluxes estimated for both models, it was decided to use Ocean model for further simulations.

6.2 Grid influence

After comparing heat flux models, results using different number of layers were tested. The three-dimensional model was tested with 10, 14 and 20 uniform layers, and this helped to identify the best configuration to run Delft3D to Vossoroca reservoir, using Ocean heat flux model. Figure 49 shows the results of the model.

The comparison of the results with measured data is shown on Table 21. In general, the error and standard deviation decreased, with the increase in the number of layers. To perform simulations with the 3D model, the number of layers used is, therefore, 20 layers.

Table 21 – Absolute and relative error in the 3D modeling of Vossoroca reservoir for the grid testing

Error	10 layers	14 layers	20 layers
Absolute (°C)	1.17 ± 1.13	0.64 ± 0.54	0.50 ± 0.31
Relative (°C)	0.70 ± 1.47	0.16 ± 0.82	-0.47 ± 0.36

6.3 Three-dimensional modeling in Vossoroca reservoir

The modeling of Vossoroca reservoir was performed during approximately three months (from July/2012 to October/2012) using Delft3D. The grid is orthogonal and was defined with 342 points in M-direction and 347 in N-direction – the size of the Cartesian grid cells is 15 m x 15 m. In the vertical direction, Z-model was used with 20 layers, since it

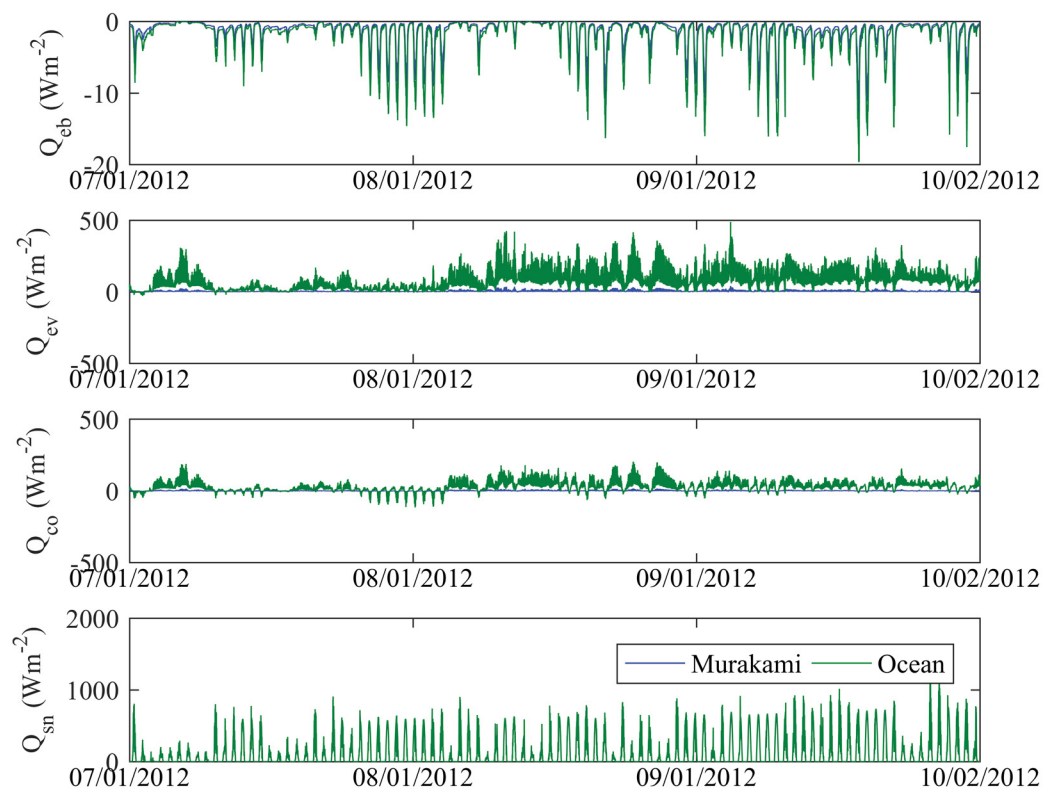


Figure 48 – Components of heat flux in Murakami and Ocean models

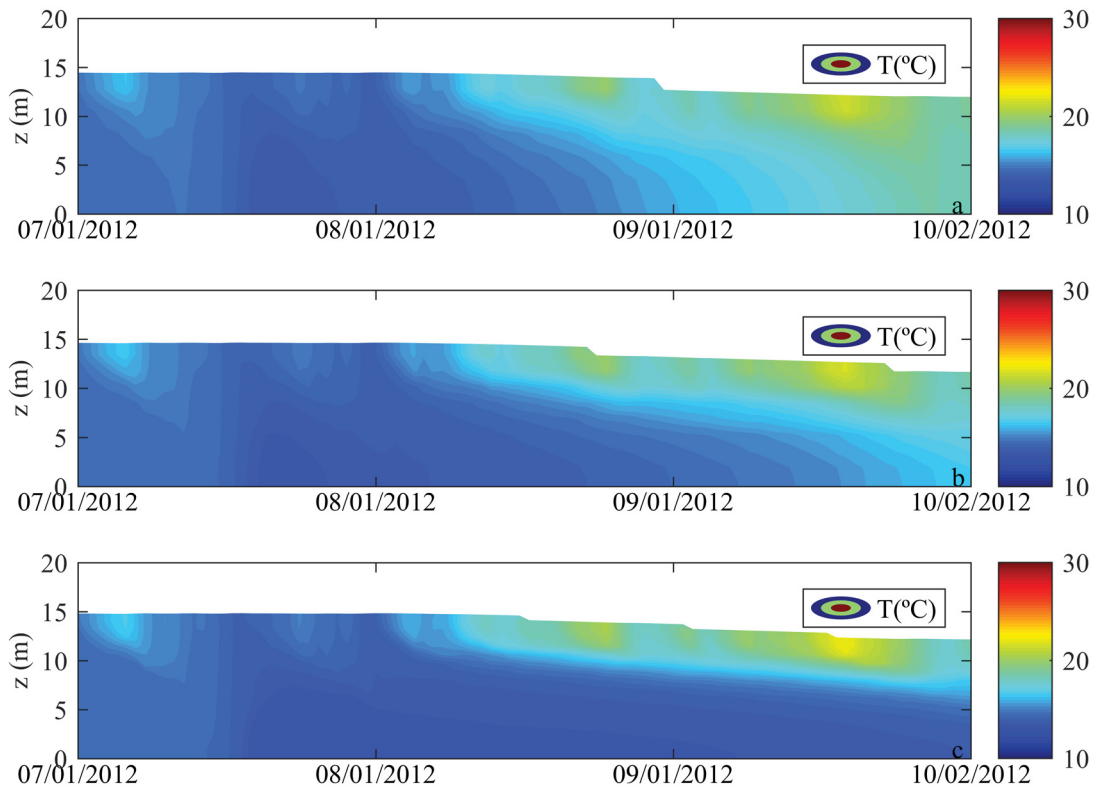


Figure 49 – Temperature in Vossoroca reservoir. Three-dimensional model with a) 10 b) 14 and c) 20 layers.

is a recommendation to represent thermal stratification in lakes and reservoirs – σ model was tested, but increased mixing in the water column. UNESCO equation was used to calculate water density and salinity was set zero in the modeling.

For the turbulence closure scheme, k - ϵ model was used to calculate the vertical eddy viscosity, and vertical eddy diffusivity (m^2s^{-1}). For the background vertical viscosity and diffusivity, the coefficients were considered calibration coefficients, and fixed during the simulation. The background horizontal viscosity and diffusivity are also calibration coefficients and fixed during the simulation. Table 22 shows the parameters related to turbulence calibrated for Vossoroca reservoir modeling.

Delft3D considers there is no heat flux between the bottom of the reservoir and the water. At the surface, five heat flux models are available to estimate air-water fluxes. We compared Murakami and Ocean models to define the model used in Vossoroca reservoir – the results of Section 6.1 show that Ocean model represented better the energy fluxes at the air-water interface and this model was used for Vossoroca modeling. Secchi depth is used as a calibration parameter for solar radiation absorption – in Vossoroca, it was defined as 1.8 m (see Table 22) and constant during the simulation. Dalton number is used for calibration of the evaporative heat flux. Stanton Number for heat convection is a

calibration parameter. Table 22 shows the parameters calibrated for surface heat flux for Vossorooca reservoir modeling. The calibration parameters were defined as the ones that best fitted daily temperature profiles simulated and measured at the floating platform and presented lower errors. The mean absolute error (MAE) was used with this purpose, and standard deviation (SD). It was also calculated the mean relative error of the simulation.

The time step of the simulation was set in 3 s, respecting Courant-Friedrichs-Lewy number (CFL). Initial conditions were defined according the measurements and taken as uniform values in the domain. In July, Vossorooca reservoir is mixed and the initial temperature was 14.5 °C. During the period of interest, water level in Vossorooca reservoir varies around 2 m – the initial condition was set-up in –0.42 m. The time necessary to run the model, in parallel (4 processors), in these conditions was 10 days. Table 23 shows the required data to run Delft3D model.

Table 22 – Delft3D model set-up and calibration parameters for Vossorooca reservoir modeling related to turbulence and surface heat flux

	Description	Delft3D set-up
Δt	Time step of the modeling	3 s
Δz	Vertical grid size	0.88 m (20 layers)
Horizontal grid	Horizontal grid size	15x15 m
T_0	Initial condition of temperature	14.5 °C
Water level	Initial condition of water level	–0.42 m
Period	Period of simulation	94 days
Processing time	–	10 days
v_H^{back} (m^2s^{-1})	background horizontal eddy viscosity	0
D_H^{back} (m^2s^{-1})	background horizontal eddy diffusivity	0.001
v_V^{back} (m^2s^{-1})	vertical eddy viscosity	0
D_V^{back} (m^2s^{-1})	background vertical eddy diffusivity	0
L_{oz} (m)	Ozmidov length scale	0
H_{Secchi} (m)	Secchi depth	1.8
c_e (–)	Dalton number (evaporative flux)	0.0013
c_H (–)	Stanton number (heat convection)	0.0013
β	Solar radiation absorbed at surface	0.45
α	Albedo	0.06

The results of 3D modeling are shown in Figure 50. The initial period of simulation starts in July (Winter in South Hemisphere), therefore the water column is well mixed and cold. After that period, temperature of the water column starts to increase due to meteorological conditions, as occurs in September. This is well simulated by the model. The error in temperature is shown on Table 24. Mean absolute and relative errors were estimated. Using mean absolute error, the modeling error was $0.5 \pm 0.31^\circ C$ and the mean relative error, $-0.47 \pm 0.36^\circ C$.

Figure 51 shows the temperature at the points measured at the floating platform. The error for the layers temperature is measured in Vossorooca reservoir was also estimate (Table 25). For the 3D model, the error is from $0.36^\circ C$ to $0.72^\circ C$ – close to the thermocline.

Table 23 – Delft3D model required data for Vossoroça reservoir modeling

Data	Description
Grid	The horizontal grid in Delft3D was defined with 15x15 m, ortogonal, with 342 points in M-direction and 347 in N-direction. The vertical grid was defined with 20 uniform layers, using Z model
Inflows/outflow	In Vossoroça, three rivers contribute to flow – São João river (56% of the total flow), São Joãozinho (28% of the total flow) and Vossoroça river (16% of the total flow). The inflows were defined as total discharge open boundary conditions. Inflow temperature was also required. Daily measurements were used in the modeling.
Meteorological data	Solar radiation, wind speed and direction, air temperature, relative humidity and cloud coverage were required in the 3D modeling, with 2 min time step. Wind speed was considered uniform in the modeling. Meteorological information was used in the heat flux model (Ocean model) and in the turbulence model ($k - \epsilon$ model)

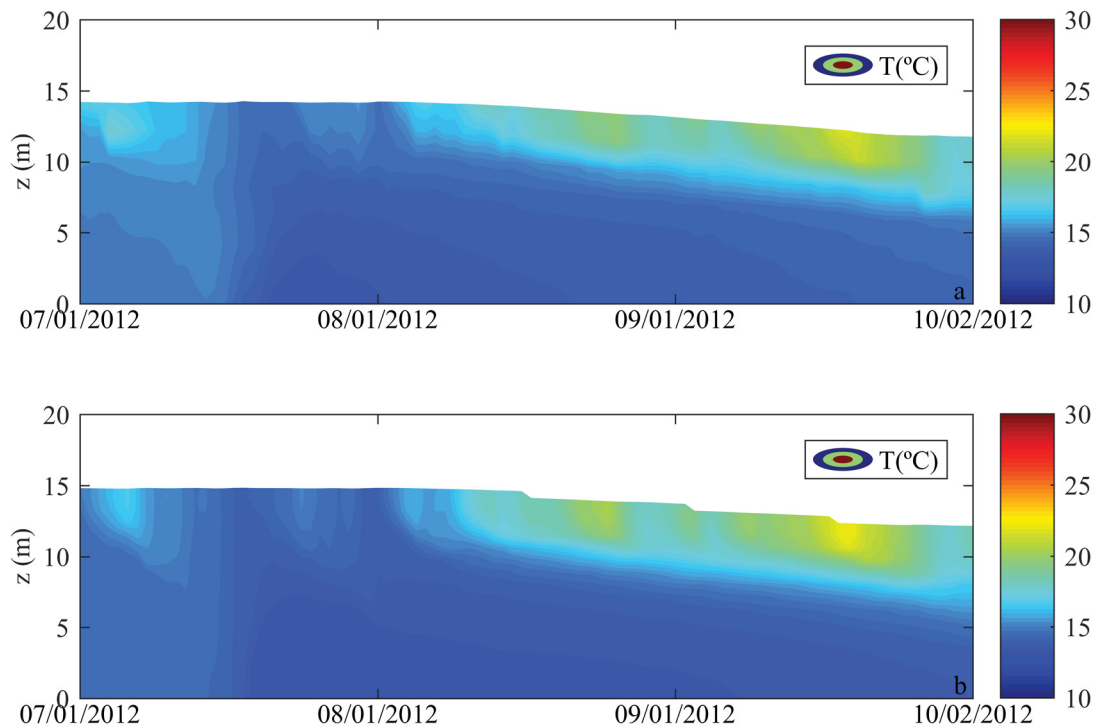


Figure 50 – Temperature results. a) Measurements at the floating platform, b) 3D modeling results

Table 24 – Mean absolute and relative error in the 3D modeling

Mean absolute error (°C)	Mean relative error (°C)
0.50 ± 0.31	-0.47 ± 0.36

Standard deviation is higher close to the surface layer.

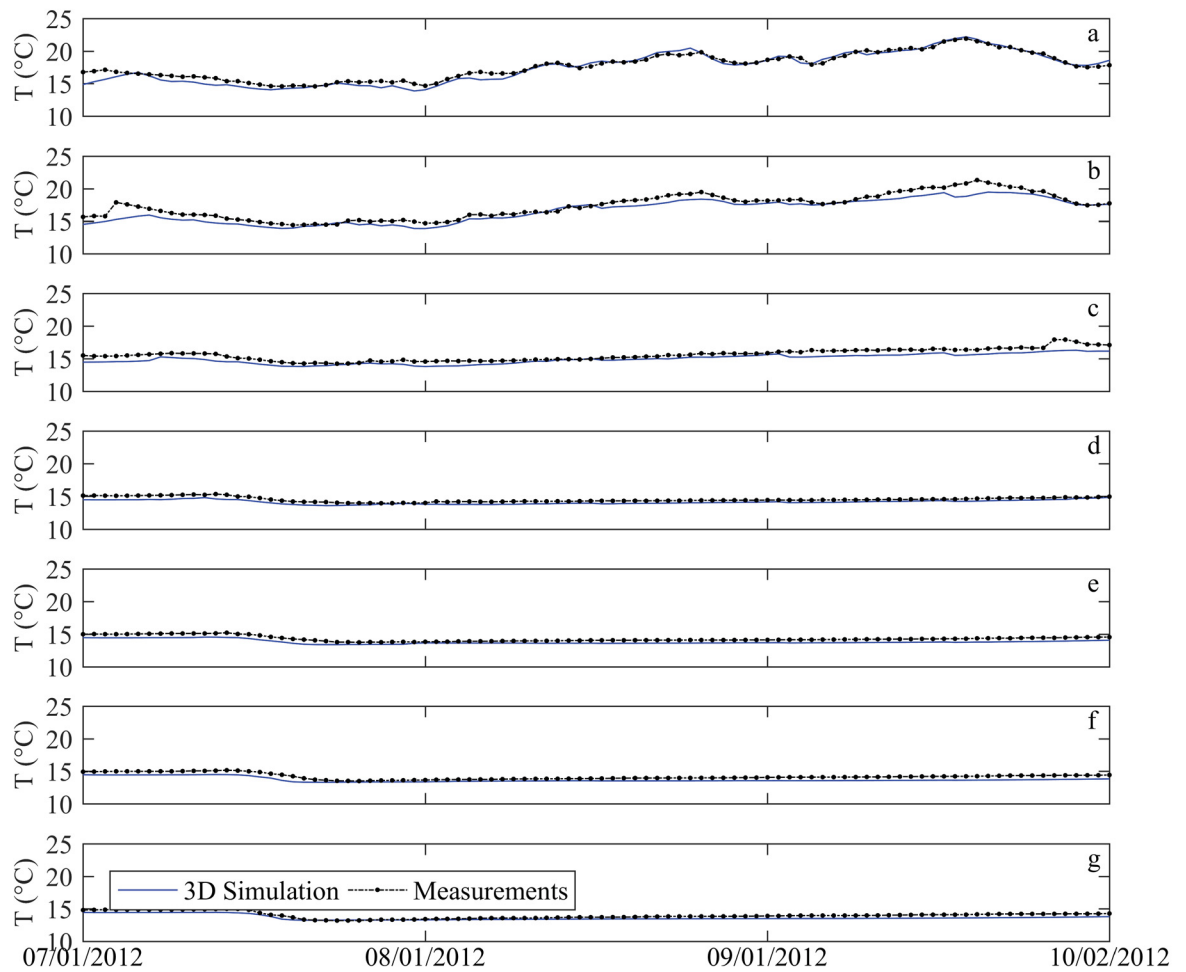


Figure 51 – Comparison between measurements and modeling. Points of comparison, from surface a) 1 m, b) 3 m, c) 5 m, d) 7 m, e) 9 m, f) 11 m and g) bottom

Table 25 – Mean absolute error (MAE) and standard deviation (SD) in the 1D and 3D modeling at the measured points in Vossoroica reservoir

Depth (from surface)	MTCR-1 (°C)	Delft3D (°C)
1 m	1.10 ± 0.11	0.46 ± 0.15
3 m	0.87 ± 0.01	0.72 ± 0.04
5 m	1.30 ± 0.02	0.63 ± 0.04
7 m	1.60 ± 0.02	0.38 ± 0.03
9 m	1.18 ± 0.01	0.48 ± 0.005
11 m	1.04 ± 0.01	0.48 ± 0.002
Bottom	1.20 ± 0.07	0.36 ± 0.001

Figure 52 shows temperature gradients simulated by Delft3D in the area of the reservoir between 09/05/2012 and 09/06/2012 each four hours. Shallow areas show uniform temperature over depth (no gradients). The gradients increase as the depth increases –

may be around 6°C in deeper areas at 16h. The amplitude of this gradients is related to the heat fluxes at surface, so it is expected a decrease in temperature gradients during the night due to loses of energy and mainly, no solar radiation.

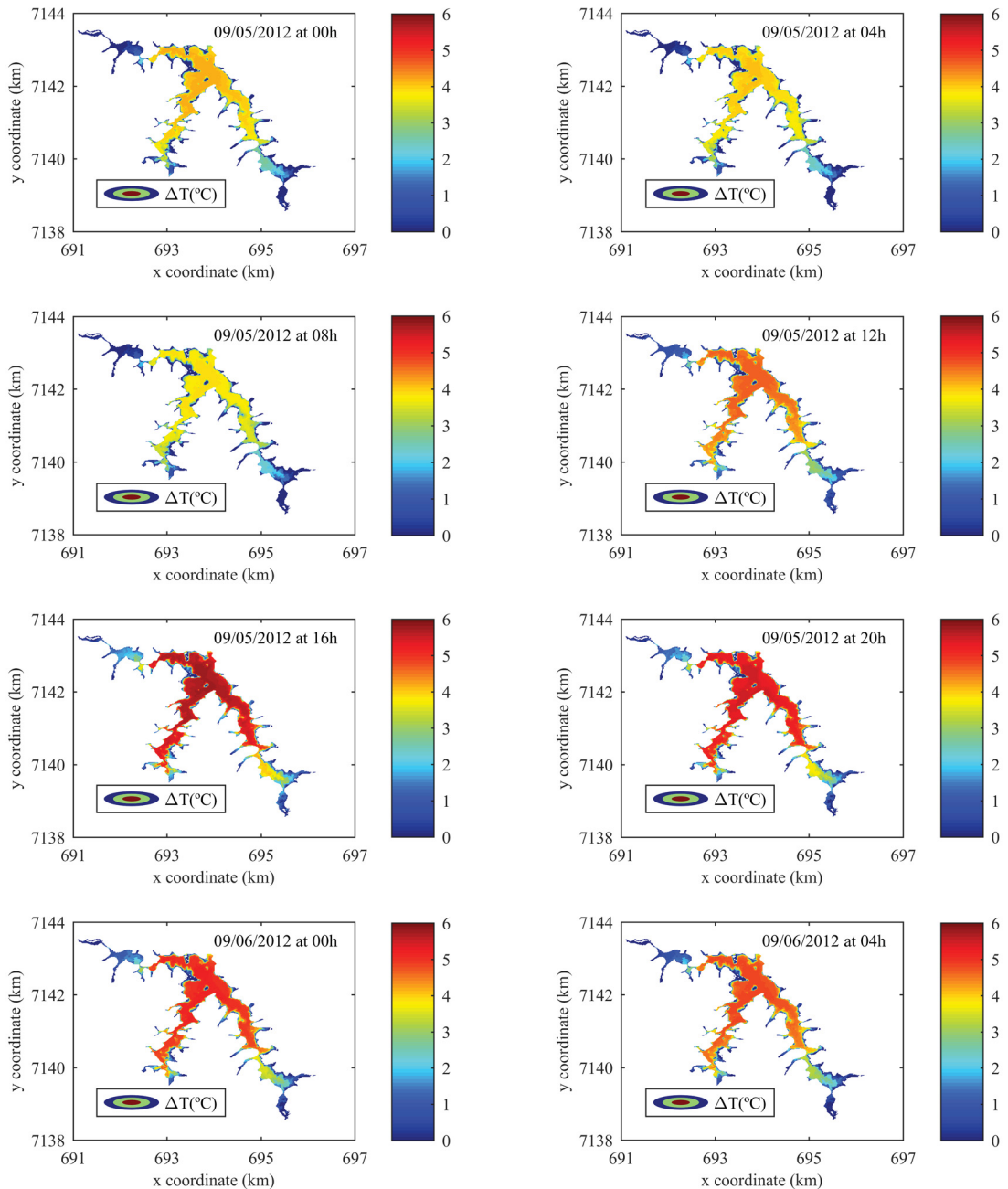


Figure 52 – Temperature gradients (between surface and bottom) in Vossoroca reservoir between September 5th at 00h and September 6th at 04h modelled with Delft3D

Figure 53 shows the period of time (in %) when temperature gradients are expected

in the reservoir area, calculated with results from the 3D modeling. $\Delta T > 1^\circ\text{C}$ occurs in around 80% of the time in most of the reservoir area – the exception is close to São Joãozinho and Vossoroca rivers that are shallow and in the side arms of the reservoir, where this gradient occurs with less frequency. $\Delta T > 2^\circ\text{C}$ occurs around 60% of the time in an area close to the one that $\Delta T > 1^\circ\text{C}$ occurs. $\Delta T > 3^\circ\text{C}$ vary from 0% and 40% of the time near to São Joãozinho river, and the frequency increases moving to deeper regions of the reservoir. The gradients $\Delta T > 4^\circ\text{C}$ occurs with less frequency close to the rivers, since these regions are shallower, as well in the side arms. In the deepest area of the reservoir, $\Delta T > 4^\circ\text{C}$ occurs in around 50% of the time. $\Delta T > 5^\circ\text{C}$ are expected is less than 10% of the time in shallow areas – close to the rivers and also side arms. The frequency increases moving to deeper areas and occurs in around 40% of the time. $\Delta T > 6^\circ\text{C}$ occurs with lower frequency in all the reservoir area – in the deepest area, in less than 20% of the time. The 3D modeling shows that, for the period considered in the modeling, most of the time, the reservoir is stratified with gradients of at least $\Delta T > 1^\circ\text{C}$. The exception are the regions close to the rivers and side arms in Vossoroca reservoir, that present uniform temperatures and do not stratify. The model also give information about the three-dimensionality of processes in Vossoroca reservoir, which has consequences for transport processes, analysed later in this work.

6.3.1 Vossoroca reservoir 3D modeling data analysis

In this section, it is presented post-processed calculations from the results of the three-dimensional modeling – Wedderburn and Lake Number, that help on the definition of critical periods as stratification and mixing of the water column. This numbers were calculated with the software Lake Analyzer (Read et al., 2011). Water temperature used to calculated this numbers was taken from the point corresponding to the floating platform. Figure 54 shows Wedderburn and Lake Number for the 3D modeling. Most of time, the results are higher than the critical number ($W=1$ and $L_N=1$) meaning that the reservoir is stratified. Table 26 shows the number of days that this numbers are higher than the critical number and also temperature gradients – in 78 days, gradients higher than 1°C were verified in the reservoir, according to the modeling.

Table 26 – Number of days that $\Delta T > 1, 2$ and 3°C , $W > 1$ and $L_N > 1$ of Vossoroca reservoir 3D modeling (from 94 days)

$\Delta T > 1^\circ\text{C}$ (days)	78
$\Delta T > 2^\circ\text{C}$ (days)	62
$\Delta T > 3^\circ\text{C}$ (days)	54
$W > 1$ (days)	91
$L_N > 1$ (days)	85

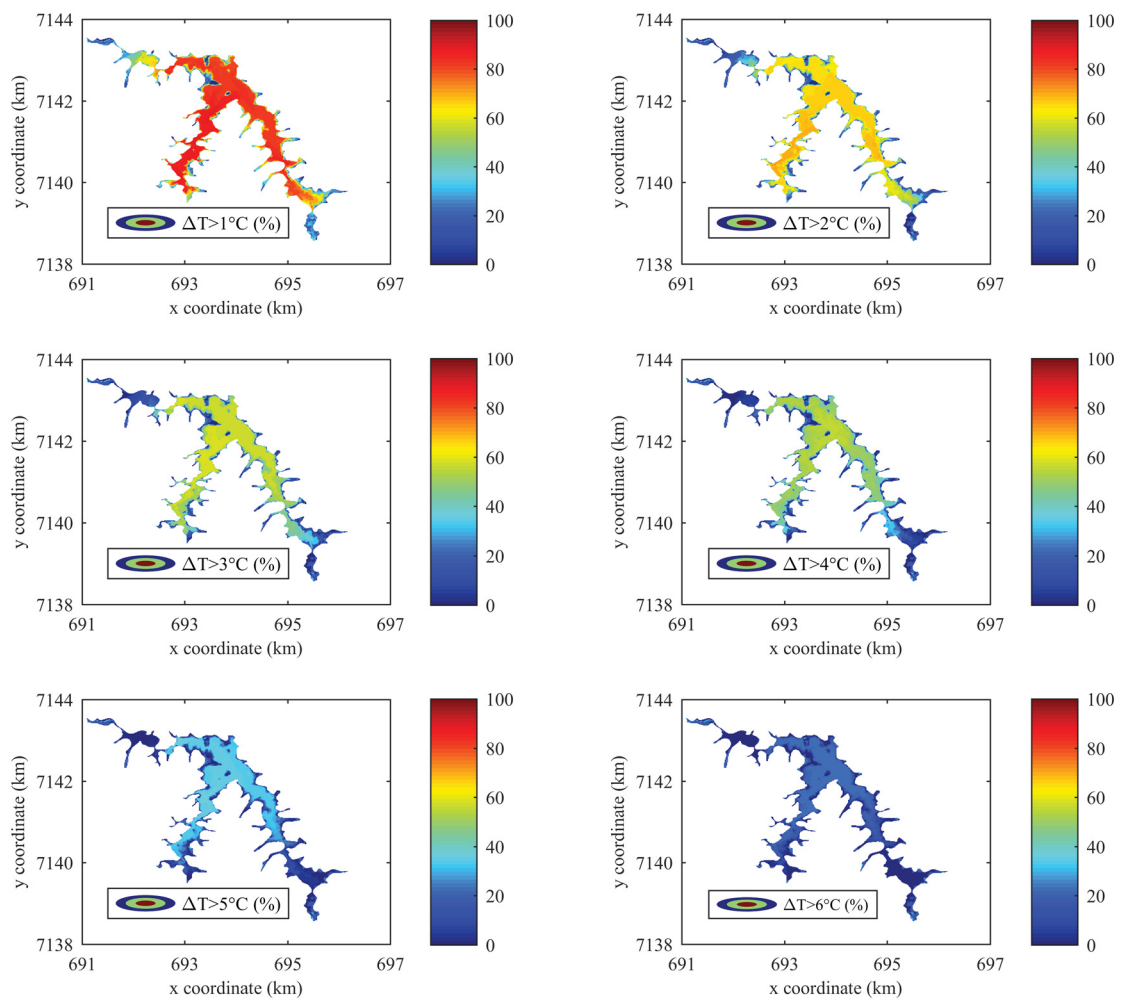


Figure 53 – Period of time (in %) that a certain temperature gradient is expected in Vossoroca reservoir during the period of simulation (94 days)

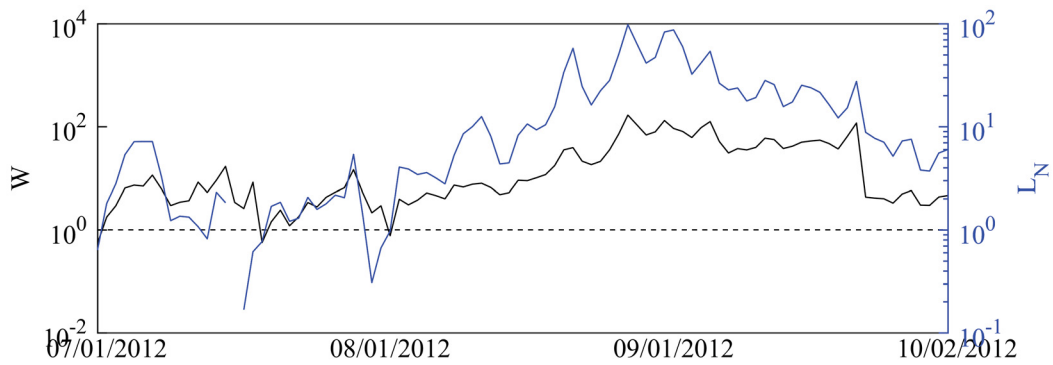


Figure 54 – Wedderburn number and Lake number in Vossoroca reservoir with data of the 3D modeling

6.4 Three-dimensional model as a sector model

In this section, Delft3D was applied in Vossoroca reservoir in sectors. Figure 55 shows the configuration chosen. The reservoir was divided in 4 areas with 4, 8 and 14 m, with 20 layers. The only change in relation to the full 3D modeling presented before was in the model grid. The processing time to run Delft3D model with sectors was lower than 1 min.

Figure 56 shows the results of the modeling. Sector 4 (Figure 56.d) is used for comparison with measured data and the 3D modeling on Section 6.3. The results of the sector model are consistent with the 3D modeling showed before and present the same behavior for the mixed and stratified period. Also, the beginning of stratification is well represented by the model. Table 27 shows the error for Sector 4. The mean absolute error was $0.42 \pm 0.33^{\circ}\text{C}$ and the mean relative error, $-0.18 \pm 0.51^{\circ}\text{C}$. The errors are comparable to the errors of the 3D modeling with the fine grid showed before, but the time of processing is considerable lower.

Table 27 – Mean absolute and relative error in the 3D model as a sector model

Mean absolute error ($^{\circ}\text{C}$)	Mean relative error ($^{\circ}\text{C}$)
0.42 ± 0.33	-0.18 ± 0.51

6.5 Comparison between 1D and 3D modeling

In this section the results of 1D and 3D modeling were compared together, in relation to measurements. For MTCR-1 model, two results are presented – the first considers the distribution of inflows equally in the water column (in the legends of Figures, labelled as MTCR-1) and the second, with the distribution of inflows related to the volume of the layers, presented in Section 5.1 (in the legends of Figures labelled as MTCR-1 modified).

Figure 57 shows the results of measurements, MTCR-1 and Delft3D models. Both models can reproduce the beginning of the heating of the surface waters in August, but in

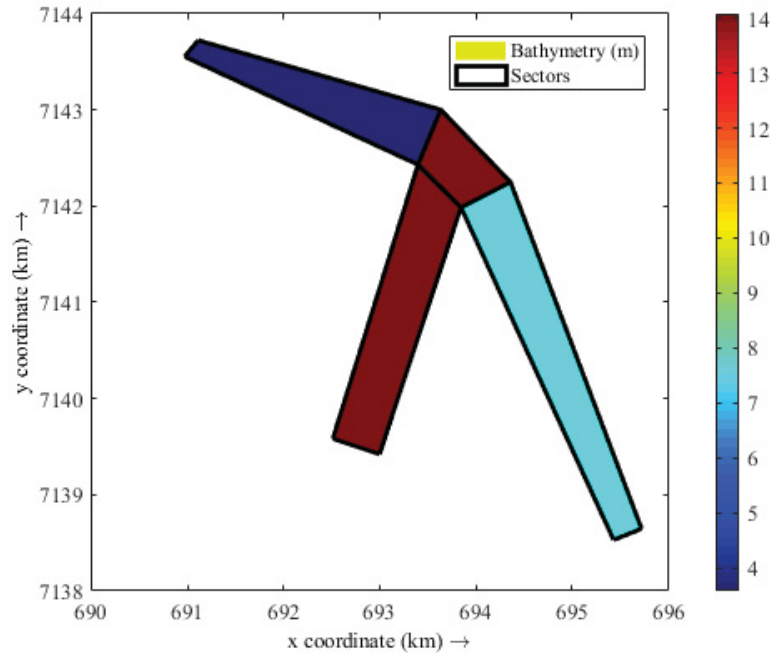


Figure 55 – Sector model configuration in Delft3D

general the 1D modeling increased more temperature in the water column, therefore lower temperature gradients were verified in the modeling distributing equally the inflow. In the case of modified MTCR-1, temperature in deeper layers was also higher, but temperature gradients were better represented. Table 28 summarized the error estimated for MTCR-1 and Delft3D models. MTCR-1 model shows higher error and standard deviation, but can reproduce important periods related to stratification and mixing, and has the advantage in relation to Delft3D of the time required to run the model. Delft3D, on the other hand, can simulate more accurately temperature in the water column.

Table 28 – Mean absolute and relative error in the 1D and 3D modeling of Vossoroca reservoir

Error	MTCR-1	MTCR-1 modified	Delft3D
Absolute ($^{\circ}\text{C}$)	1.18 ± 0.84	1.45 ± 0.97	0.50 ± 0.31
Relative ($^{\circ}\text{C}$)	0.21 ± 1.44	1.18 ± 1.28	-0.47 ± 0.36

In order to compare 1D, 3D modeling and measurements, we calculated the number of days that some gradients are verified in the water column. Figure 58 shows the gradient between surface and bottom. Table 29 shows a comparison of temperature gradients between measured data, 1D and 3D modeling. Gradients higher than 1°C happened in 86 days in the measurements, and 78 were simulated by Delft3D. In the one-dimensional model, on the other hand, this gradient was identified in 49 days. MTCR-1 modified reproduced this gradient in 87 days.

Wedderburn number (W) and Lake number (L_N) were calculated to Vossoroca reservoir, using temperature measurements, meteorological data and modeling results and

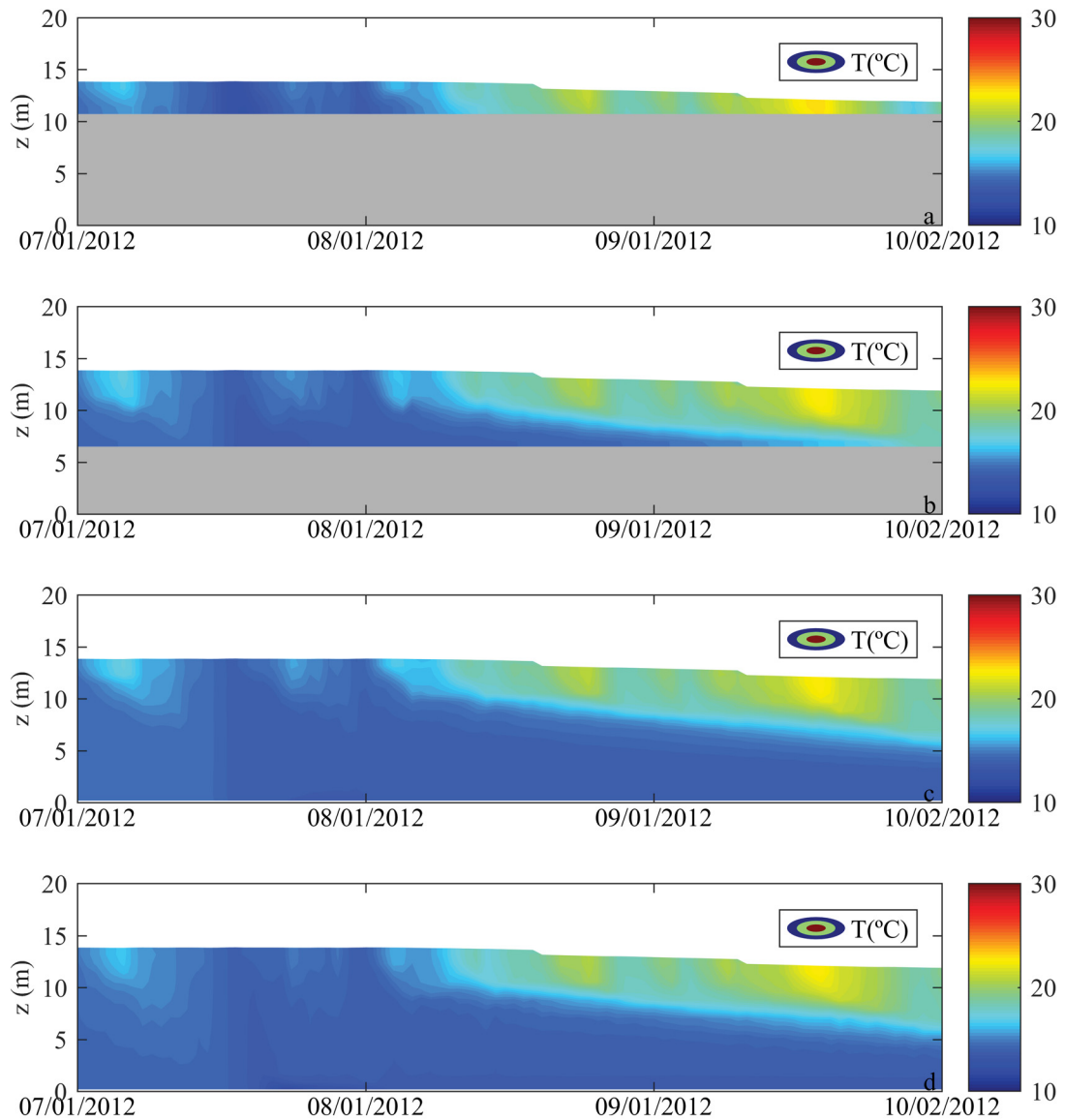


Figure 56 – Delft3D results of temperature as a sector model in Vossoroca reservoir. a) Sector 1 (4 m), b) Sector 2 (8 m), Sector 3 (14 m), Sector 4 (14 m)

compared. These physical indices give information about the potential of mixing ($L_N < 1$ and $W < 1$) or stratification ($L_N > 1$ and $W > 1$) of the water column. Their critical value are $L_N = 1$ and $W = 1$. These indices were calculated using the software Lake Analyzer (Read et al., 2011) and are presented in Figure 59 and Table 29.

For the measurements (Figure 59.a), in general, Wedderburn number is higher than 1, with exception of the beginning of the interested period, where high wind speeds and low differences in the temperature in the water column are verified. In August,

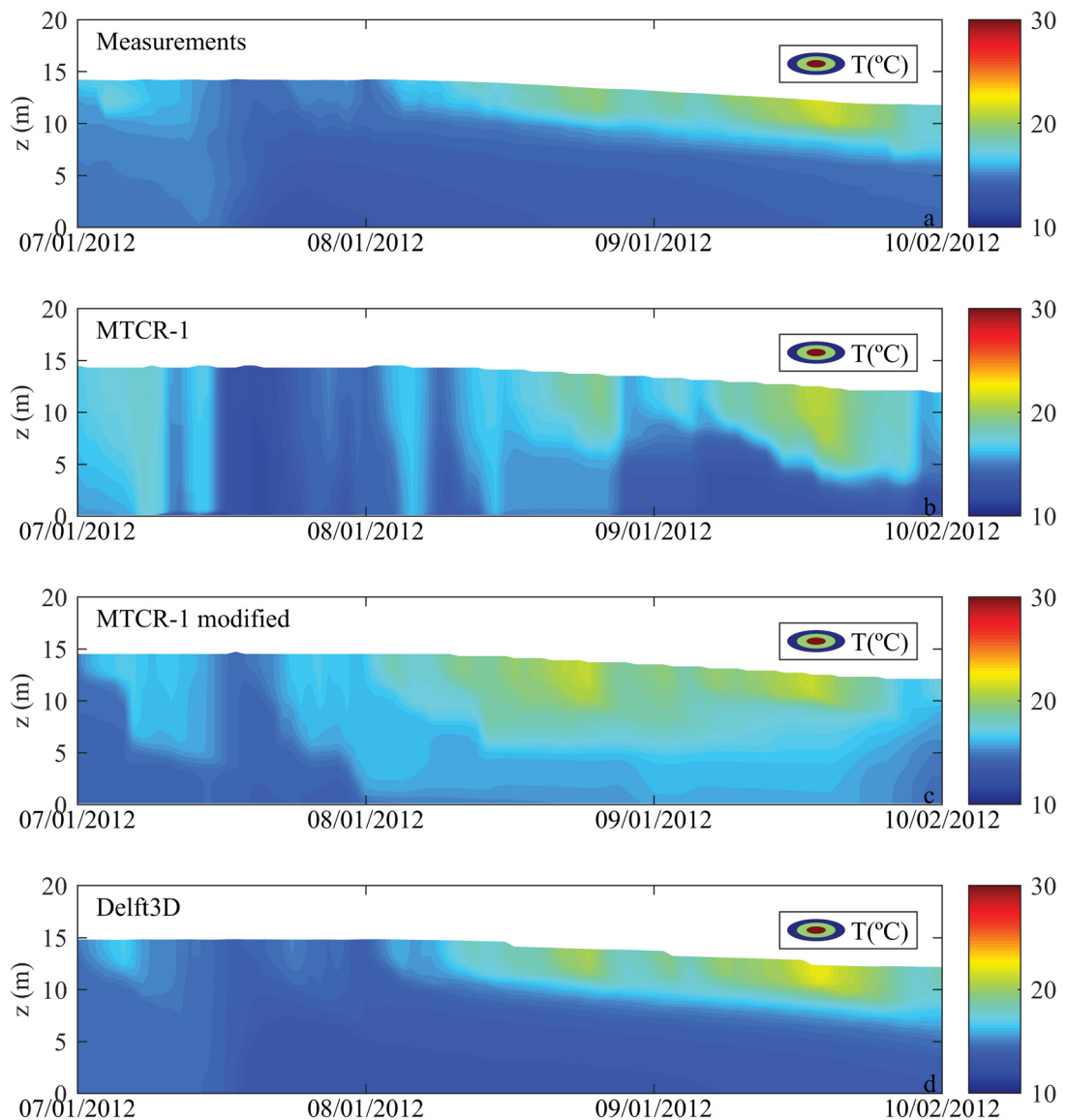


Figure 57 – Temperature in Vossoroca reservoir a) measurements, b) MTCR-1 model, c) MTCR-1 modified and d) Delft3D model

the superficial layer starts to warm, and the increase in temperature gradients combined with low wind speeds result in higher Wedderburn numbers, corresponding to strong stratification. Lake number shows the same behaviour – in the beginning of the period presented, low numbers, indicating weak stratification and allowing mixing in the water column – which is suppressed by the strong stratification after August. Table 29 shows that in 91 days Wedderburn and Lake number are higher than 1, indicating stability of the water column. For the one and three-dimensional model results (Figure 59.b, Figure 59.c

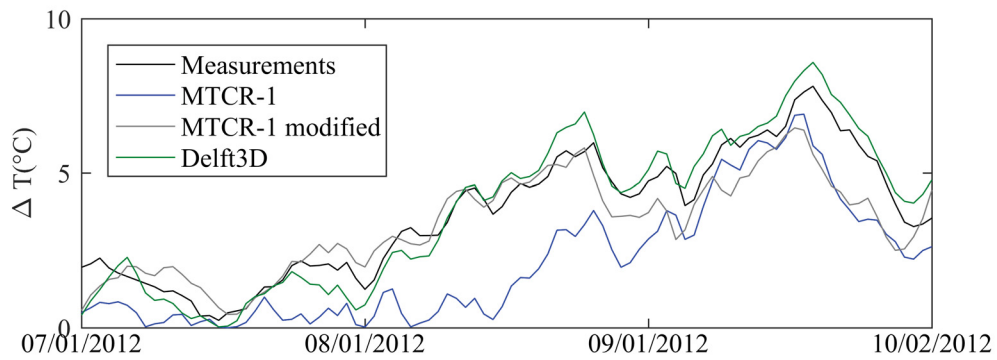


Figure 58 – Temperature gradients of measured data, 1D and 3D modeling

and Figure 59.d), most of time, the results are higher than the critical number ($W=1$ and $L_N=1$), indicating stability of the water column and stratification. The number of days that Wedderburn and Lake number were higher than the critical value was close for the three simulations (see Table 29) – meaning that even the one-dimensional model do not simulate accurately temperature as the three-dimensional model, physical indices show the same behaviour. Also, MTCR-1 modified has the same period of physical indices higher than the critical number as the measurements. Therefore, the one-dimensional modeling may give the same information about stability or tendency of mixing as the three-dimensional model.

Table 29 – Temperature gradients comparison between measured data, 1D and 3D modeling (from 94 days of simulation)

Days	Measurements	MTCR-1	MTCR-1 modified	Delft3D
$\Delta T > 1^\circ\text{C}$	86	49	87	78
$\Delta T > 2^\circ\text{C}$	69	42	71	62
$\Delta T > 3^\circ\text{C}$	56	25	50	54
$W > 1$	91	93	91	91
$L_N > 1$	91	83	91	85

6.6 Sector model analysis

In this section, results of the sector and the three-dimensional models are presented. Figures 60 and 61 show the results of the full 3D modeling (Delft3D), the sector modeling using a 3D model (Delft3D) and the sector model proposed in two points of the reservoir (MTCR-1 modified), with 4 m and 8 m of depth.

In general, the sector model (with and without exchange – Figure 60.c, 60.d, 60.e and 60.f) reproduces the results of the full 3D model in the simulation with depth of 4 m (Figure 60.a), however with underestimated temperatures. The sector modeling using Delft3D model (Figures 60.b) also follows the results of the full 3D model, but different from the sector model, overestimate temperatures (considering the higher temperatures).

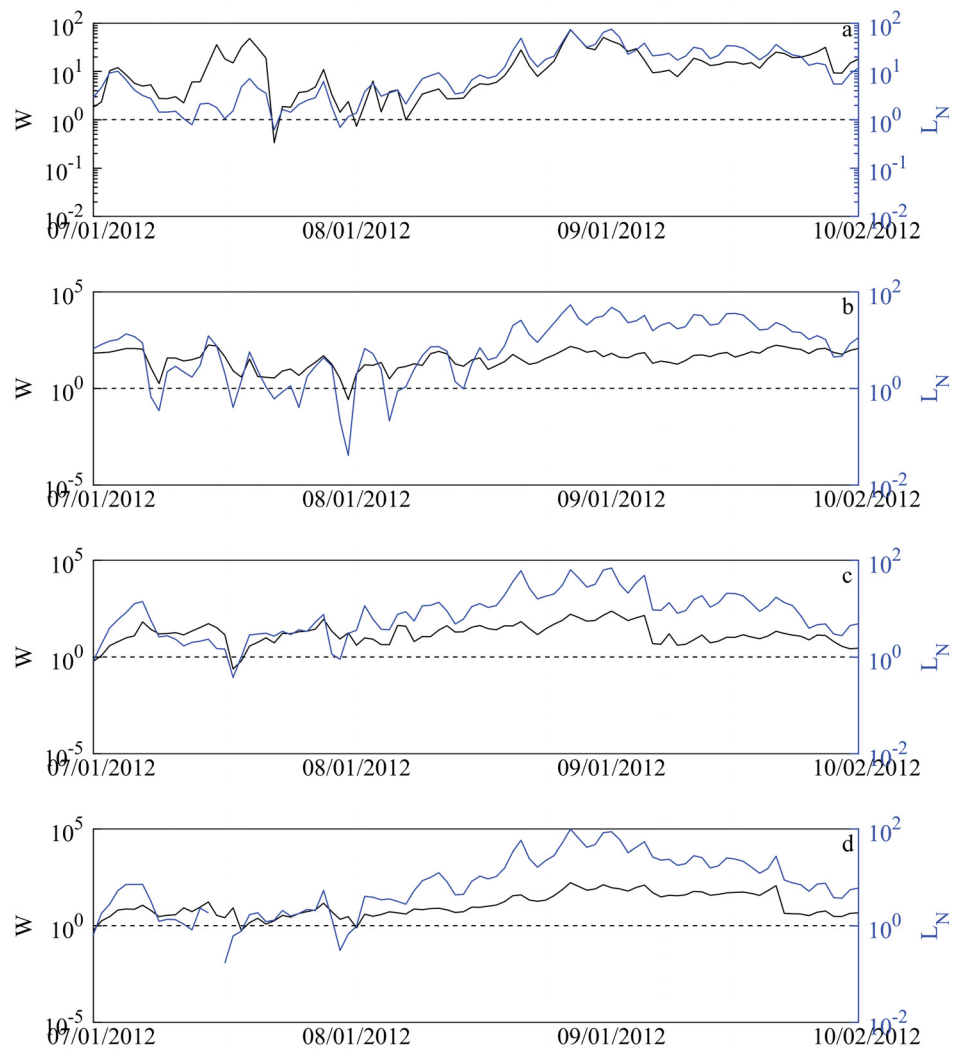


Figure 59 – Wedderburn and Lake Number calculated with a) measured data, b) MTCR-1 results, c) MTCR-1 modified results and d) Delft3D results at the floating platform location

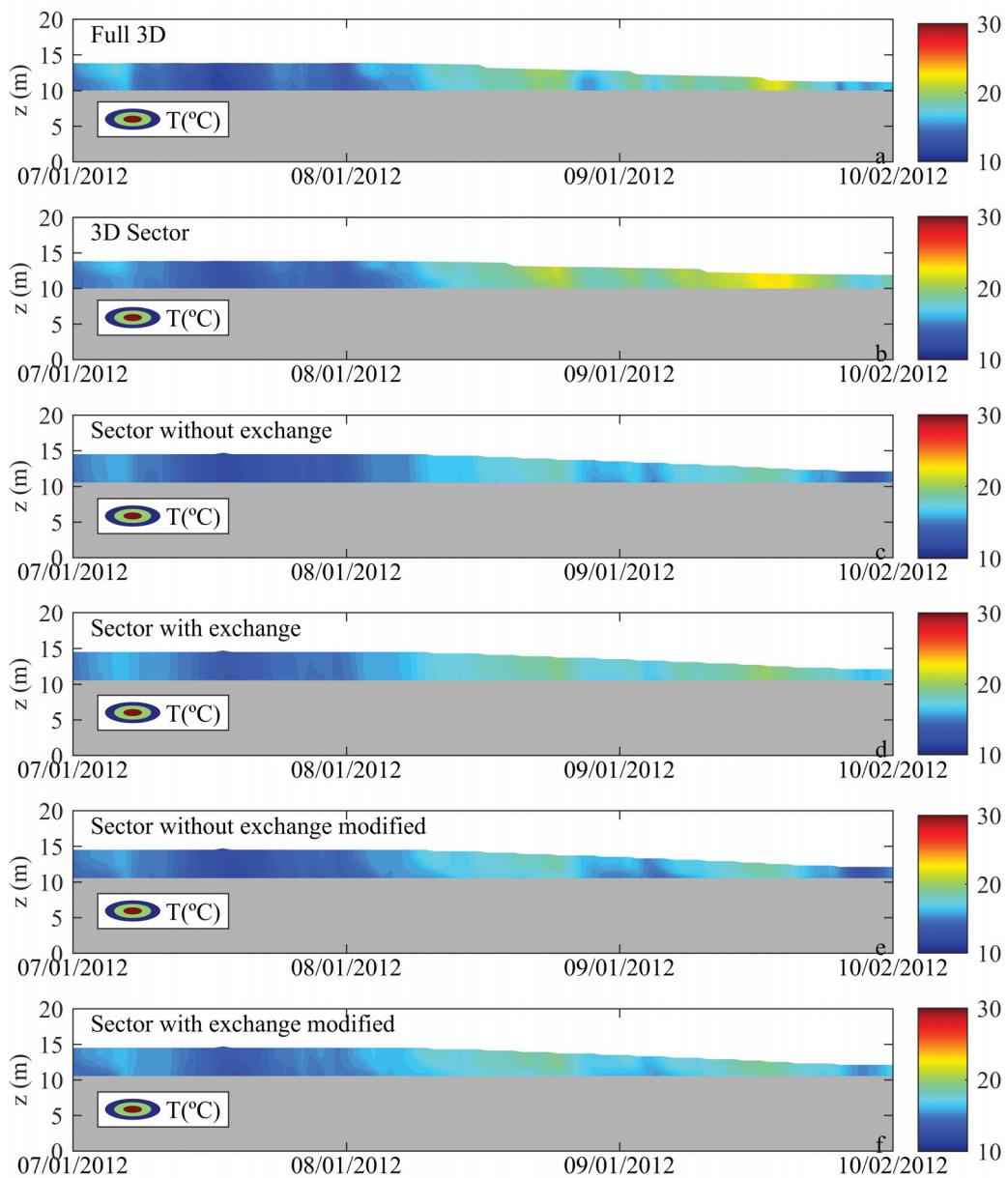


Figure 60 – Water temperature in a point with 4 m depth a) full 3D simulation, b) 3D model as a sector model, c) Sector model without exchange, d) Sector model with exchange, e) Sector model without exchange modified and f) Sector model with exchange modified

Table 30 shows a comparison between surface mean temperature in the models and the difference in relation to the full 3D modeling. All the simulations using the sector model underestimated the mean temperature – the lower difference in relation to the full three-dimensional modeling was in the sector model with exchange (-0.65%) and the higher

difference was in the sector without exchange, with a difference of -7.83% . The 3D sector model, on the other hand, overestimated the results of the full 3D modeling – the difference in the mean surface temperature was 4.45% .

In the case of the simulation with depth of 8 m (Figure 61), the sector model (Figures 61.c, 61.d, 61.e, 61.f) tend to increase faster temperature in deeper layers, but reproduces the general behavior.

The higher temperatures verified on the full 3D modeling (Figure 61.a) near the surface are underestimated by the sector model – the differences between the mean surface temperature of the full 3D modeling and the sector model vary from 3.37% and 6% . In relation to the sector modeling using Delft3D model (Figure 61.b), the model overestimate temperature in relation to full 3D modeling – the difference on mean surface temperature is 1.6% .

Table 30 – Mean surface temperature calculated for sector of 4 m and difference in % between full 3D modeling and the sector approach

Model	Mean surface temperature ($^{\circ}\text{C}$)	Difference from full 3D modeling (%)
Full 3D	16.85	–
3D sector	17.60	4.45
Sector without exchange	15.53	-7.83
Sector with exchange	16.74	-0.65
Sector without exchange modified	15.71	-6.77
Sector with exchange modified	16.54	-1.84

Table 31 – Mean surface temperature calculated for sector of 8 m and difference in % between full 3D modeling and the sector approach

Model	Mean surface temperature ($^{\circ}\text{C}$)	Difference from full 3D modeling (%)
Full 3D	17.50	–
3D sector	17.78	1.6
Sector without exchange	16.45	-6.0
Sector with exchange	16.91	-3.37
Sector without exchange modified	16.50	-5.71
Sector with exchange modified	16.53	-5.54

6.7 Summary of the chapter

In this chapter, the three-dimensional modeling of Vossorooca reservoir is presented. Two heat flux models, Murakami and Ocean models were tested and compared for the definition of which one to use in the modeling. Ocean model represented better the air-water heat fluxes and the temperature in Vossorooca reservoir. Delft3D was applied to Vossorooca reservoir and the results showed good agreement with measurements. Delft3D

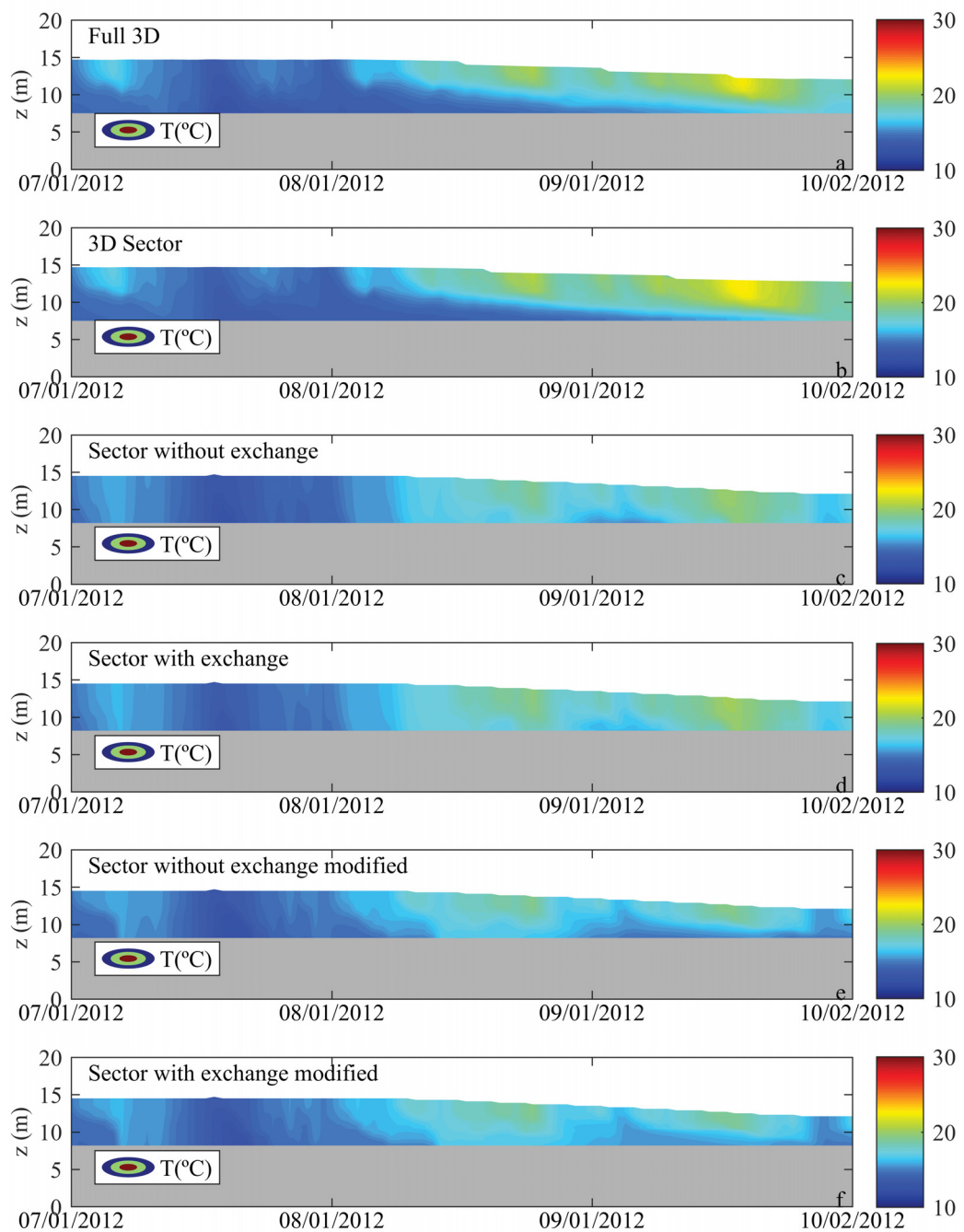


Figure 61 – Water temperature in a point with 8 m depth a) full 3D simulation, b) 3D model as a sector model, c) Sector model without exchange, d) Sector model with exchange, e) Sector model without exchange modified and f) Sector model with exchange modified

was also applied using the sector approach – the horizontal grid was defined with four grid cells, and in the vertical direction, twenty layers. The results also showed good agreement with measurements – therefore, a complex model as Delft3D can be used as a sector model. The results of reservoir classification showed that Delft3D results can be used for this purpose – as the one-dimensional model, that has lower processing time and less data to run and calibrate the models. Comparison of 3D, 1D and sector models showed that a simplified model can be used for reservoir classification and to simulate temperature profiles in different areas of the reservoir.

7 Tracer transport modeling

In this section, it is analysed the path of a conservative tracer in the reservoir, considering river inflows in one hand, that may interfere on thermal stratification and distribution of substances over the water column. On the other hand, the path of a tracer in a side arm of the reservoir, and identify if it is possible that substance transport may occur due changes in temperature.

Two paths were defined and monitored – a longitudinal section starting in São João river until the deepest region of the reservoir and a section in a side arm. Figure 62 shows the paths of interest. The identification if transport may occur due temperature changes was quantified comparing a three-dimensional modeling including temperature and a three-dimensional modeling excluding temperature. Therefore, the effects of temperature on tracer transport were quantified, considering advective and dispersive transport. Figure 63 shows the cross-sections used to quantify advective and dispersive transport.

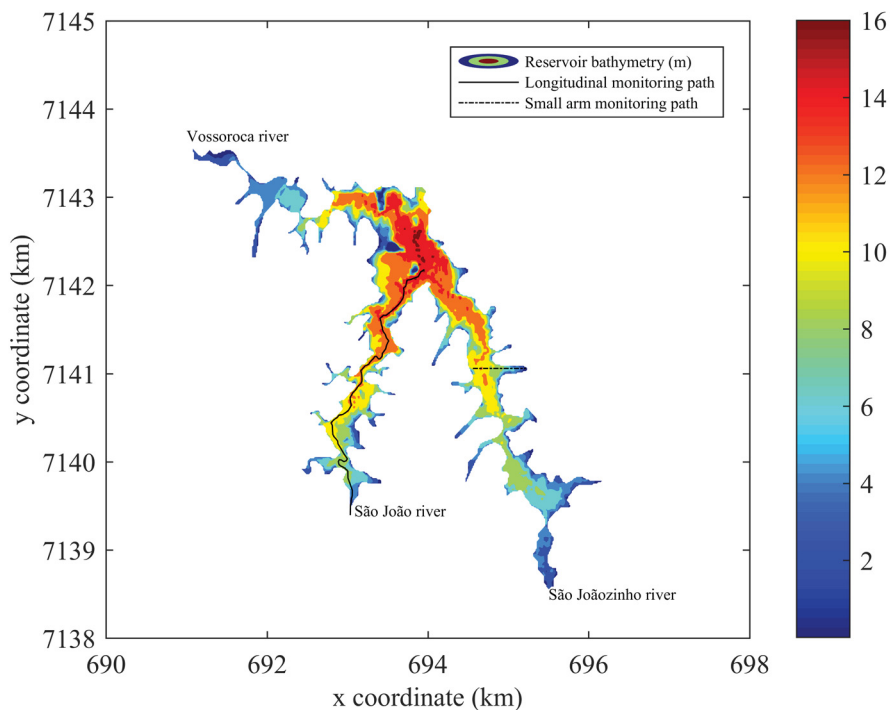


Figure 62 – Monitoring path for tracer modeling

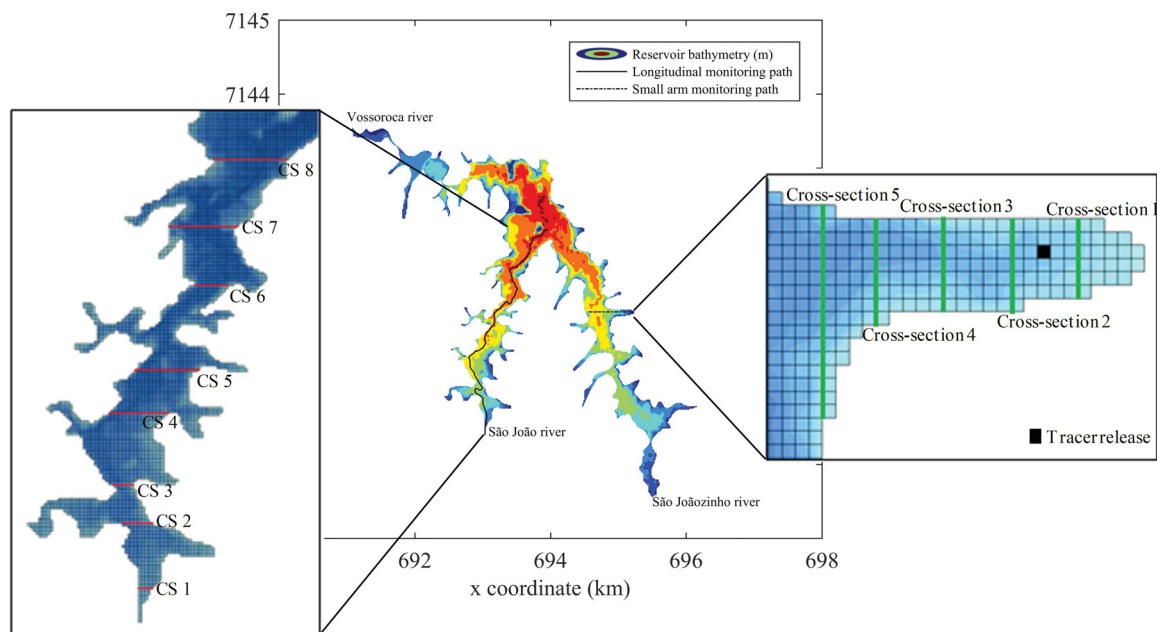


Figure 63 – Cross-sections for river and side arm tracer modeling

7.1 River tracer study

In this section, it is shown the path of a tracer continuously released in São João river. A longitudinal section was defined, following the river over the reservoir, according to Figure 62 and Figure 63. This study aims to show the path of the river in the water column, changing due water density. Figure 64 shows four different time steps in the simulation. As it is shown, depending the river and the water column temperatures, the path the water flows may vary and impact in different ways the dynamic of the reservoir.

On day 07/10/2012, the water flowing to the reservoir has temperature of 15°C , and the concentration of tracer is higher between the surface and bottom of the reservoir, meaning that an intrusion occurs. On the second time step presented, day 07/18/2012, temperature of the inflowing water was 12°C , temperature that is also verified near to the bottom of the reservoir. Therefore, an underflow is identified by the tracer distribution and by the line of 30% of maximum tracer concentration close to the bottom. On day 08/05/2012, temperature of the inflowing water was 17°C , which is higher than surface temperature (mean temperature of 16.3°C). Thus, an overflow occurs, as verified by the tracer distribution on the water column. The last time showed in Figure 64, day 08/28/2012, an intrusion is also verified. The tracer reaches the deepest area of the reservoir in approximately 18 days.

Inflows to the reservoir may act as a source of particulate materials, that may cause water quality variations (adding materials to the more productive zones) (Martin and McCutcheon, 1999), increase turbulence or introducing oxygen in deeper layers. Li et al. showed that storm-rainfall events, which introduce high inflows to the reservoir) reduced

stability as a function of inflow temperature. Huang et al. (2015) analysed the path of turbid density currents in storm-rainfall events, to identify intake location for a drinking water treatment plant. These studies show how inflows may affect thermal structure and water quality in lakes and reservoirs. In Vossorooca reservoir, the modeling showed that the inflow temperature is an important parameter to be monitored, since the path the water flows is a function of water column temperature. Inflows may cause water quality variations and they are relevant for management of these systems. To quantify the effects of mass transport due river inflows, advective and dispersive transport were quantified in a longitudinal section of Vossorooca reservoir.

The transport was quantified using the cumulative advective and dispersive transport of tracer and temperature. Figure 65 shows the cumulative transport in the simulation with temperature. The signs on the graphs are due a convention in Delft3D.

The advective transport of temperature (Figure 65.a) has the same pattern in all the cross-sections, and differences in the cumulative transport are verified in the end of the simulated period, that could be caused by temperature differences – since in the initial period the reservoir is mixed. Dispersive transport of temperature (Figure 65.b) is lower in magnitude when compared with advective transport. Cross-section 7 (CS 7) does not follow the pattern in the other cross-sections. Also, in cross-section CS 1, dispersive transport is close to zero. For the cumulative advective transport of tracer (Figure 65.c), it is necessary time to the tracer released in São João river to reach the cross-sections – therefore, the difference in the cumulative advective transport of the tracer, that is higher in CS 1 and lower in the successive cross-sections. In relation to dispersive transport (Figure 65.d), in magnitude the transport is lower than advective transport. The pattern in dispersive transport follows the dispersive transport of temperature, which is also not relevant is cross-section CS 1.

To analyse the effects of temperature over tracer distribution and path in the reservoir, a 3D simulation without temperature was performed. Figure 66 shows the results of tracer concentration in the water column. Different from what is verified in the modeling with temperature, in this simulation there is no defined path of the tracer – the tracer spreads over the entire water column. The time necessary to the tracer reach the deepest area of the reservoir is approximately 1 month.

The cumulative transport was also calculated for the tracer in the modelling without temperature. The pattern in the transport is the same as showed in Figure 65.c and Figure 65.d, but the magnitude in the transport changed. Table 32 shows the difference in advective and dispersive transport in the simulation, considering temperature and without temperature, in each cross-section monitored. In general, when temperature is considered in the modelling, advective transport increases in all cross-sections, with an exception in CS 1, in which there is a decrease in advective transport. The increase in cross-section CS 8, for example, was approximately 40%. For dispersive transport, on the

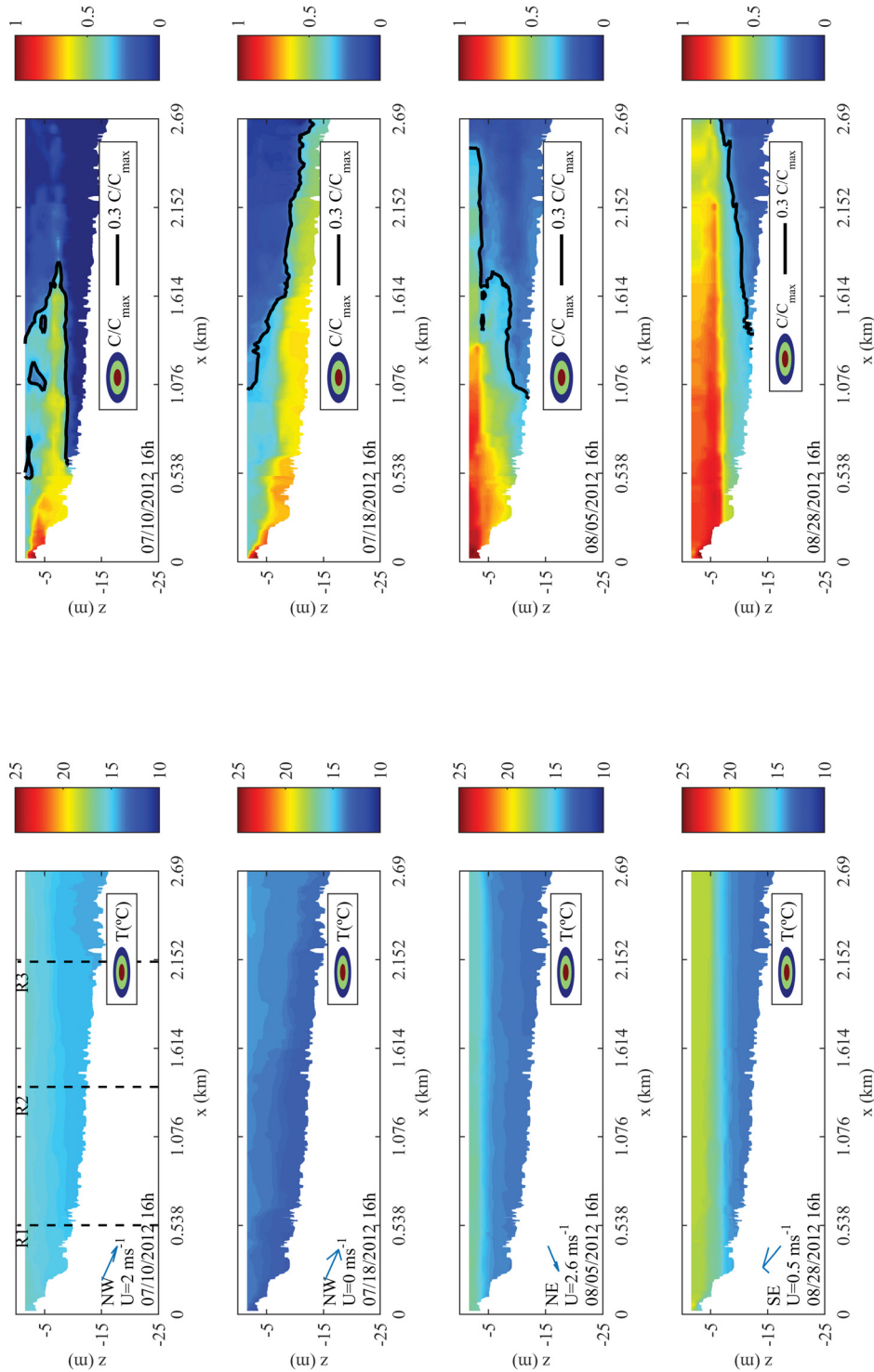


Figure 64 – Water temperature and tracer concentration in a longitudinal section in Vossoroca reservoir

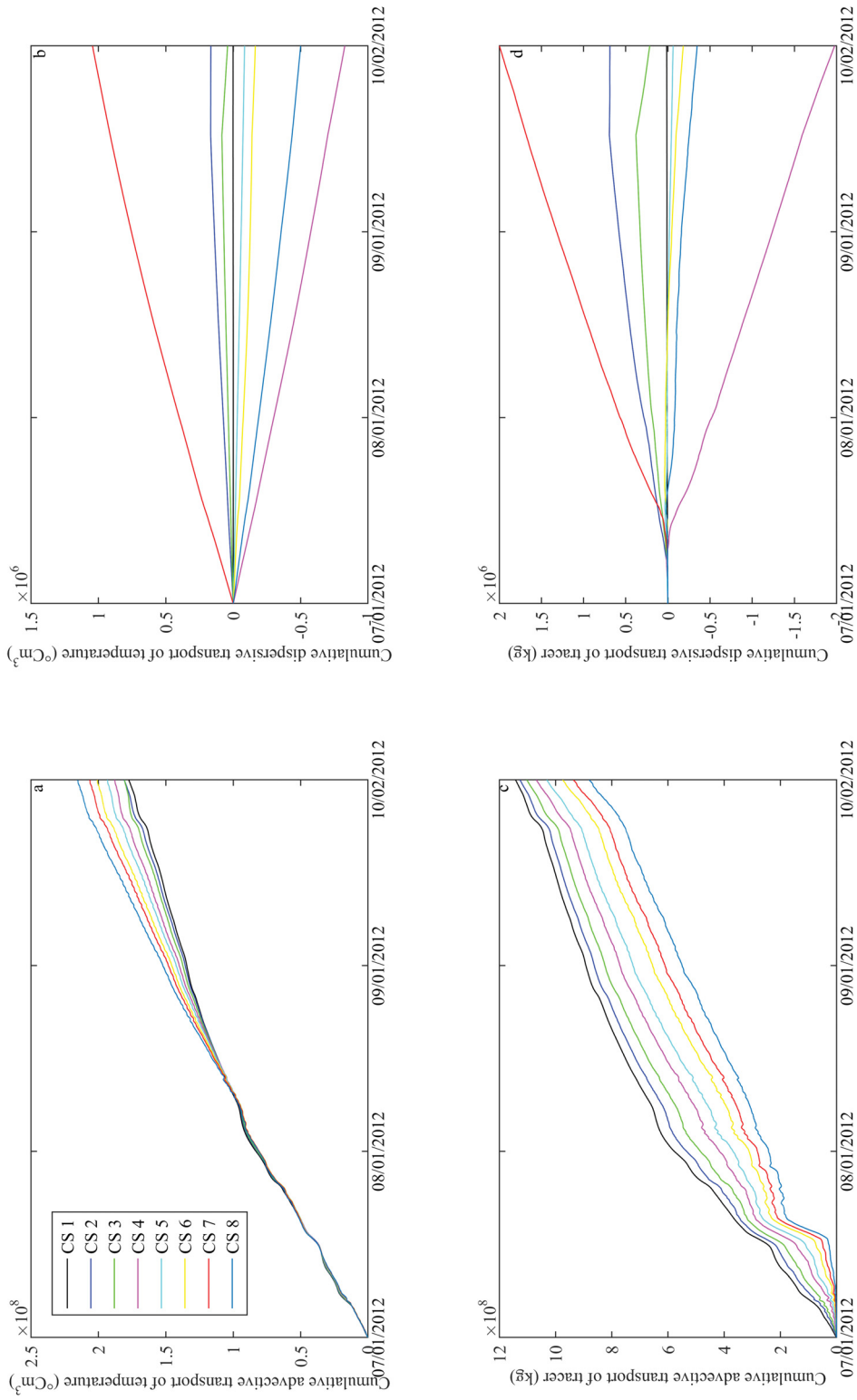


Figure 65 – River tracer modeling. Cumulative a) advective transport of temperature, b) dispersive transport of temperature, c) advective transport of tracer and d) dispersive transport of tracer

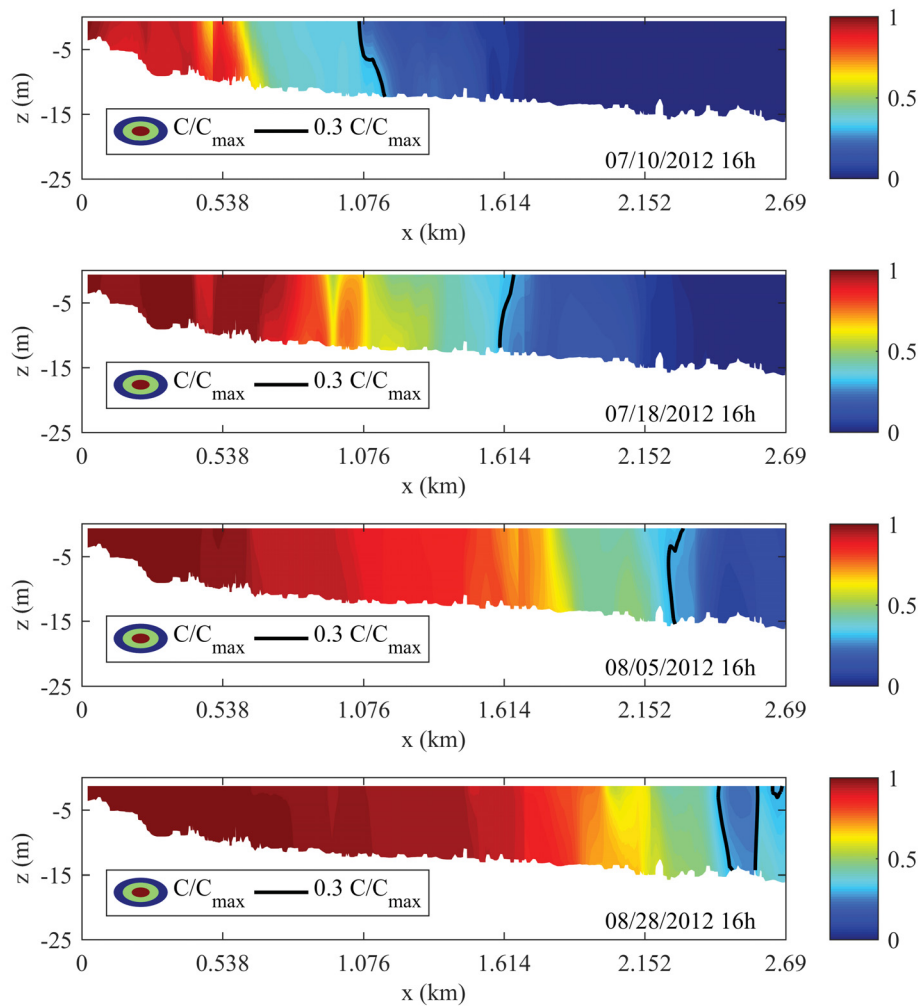


Figure 66 – Tracer concentration in a longitudinal section of Vossoroca reservoir (in this simulation, temperature is not modelled)

other hand, when temperature is included, there is a decrease in dispersive transport – that may reach 421% difference in CS 8.

Due to the differences in tracer distribution, velocity profiles were also analysed (Figure 67) in three points R1, R2 and R3 (see the points in Figure 64) in the time steps already showed. R1 corresponds to the location of cross-section 2 (CS 2), R2 corresponds to the location of cross-section 5 (CS 5) and R3, cross-section 7 (CS 7). When temperature is not considered in the modeling, the velocity profile in the points R1, R2 and R3 is more uniform and no peaks are verified (Figure 67). In the full modeling, with heat transport, on the other hand, some peaks of velocity may be identified and the profile is not uniform. On 07/10/2012, the peak of velocity in R1 corresponds to the location of the intrusion of the tracer. R2 and R3 also present higher velocity near this layer. On day 07/18/2012, the underflow also induces velocities near the bottom layer – R3 has bottom velocities

Table 32 – Difference in percentage between advective and dispersive transport considering temperature and not considering temperature in the river tracer modeling

Cross-section (CS)	Advective transport (%) ⁵	Dispersive transport (%) ⁵
1	−0.24	+71.3
2	+1.9	−110.3
3	+3.2	−129.8
4	+10.7	−109.3
5	+17.3	0.0
6	+27.2	0.0
7	+36.2	−154.9
8	+39.7	−421.2

⁵ Positive sign means that mass transport through the cross-section is higher in the modeling with temperature; Negative sign means that mass transport through the cross-section is higher in the modeling without temperature

between 0.03 and 0.04 ms^{−1}. On day 08/05/2012, the tracer moves in the surface layer – R2 and R3 also have an influence of wind direction (North-east) in the velocity profile. On 08/28/2012, there is a peak in the three points R1, R2 and R3 – which also corresponds to the layer of intrusion, on R3 the velocity may be around 0.04 ms^{−1} in this point. Figure 64 and Figure 67 show that temperature has a direct influence in the dynamics of the system – velocity may increase and substances may be transported according the density effects.

This section showed that the dynamics of the reservoir may vary according to its thermal structure and also the dynamics of river inflowing the reservoir – this can control substances distribution in the water column and have an impact on water quality.

7.2 Side arm tracer study

In this analysis, a small flow was included (less than 1% of the mean flow) coming to the reservoir in the arm (see Figure 62 and Figure 63), in a way that the flow velocity was not influenced by it, and a concentration of a conservative tracer was defined and released continuously. Figure 68 shows a plot of mean velocity in the original situation (without the small flow at the arm) and one including this new flow and the difference between the two simulations (the maximum difference for this time step was 0.006 ms^{−1}). Therefore, it was considered that the flow included in the arm to analyse the tracer distribution does not change the hydrodynamics of this region.

A conservative tracer was continuously released in the side arm during the simulation. The main goal is to identify if temperature may be responsible for substances transport. Figures 69 and 70 show water temperature and tracer concentration each two hours in 09/23/2012 between 00h and 14h. At this day, the side arm is stratified with temperature near to 22°C in the surface layer, and bottom temperature around 14°C. At 00h, the tracer is confined near the shallow area of the side arm, but velocity vectors plotted with

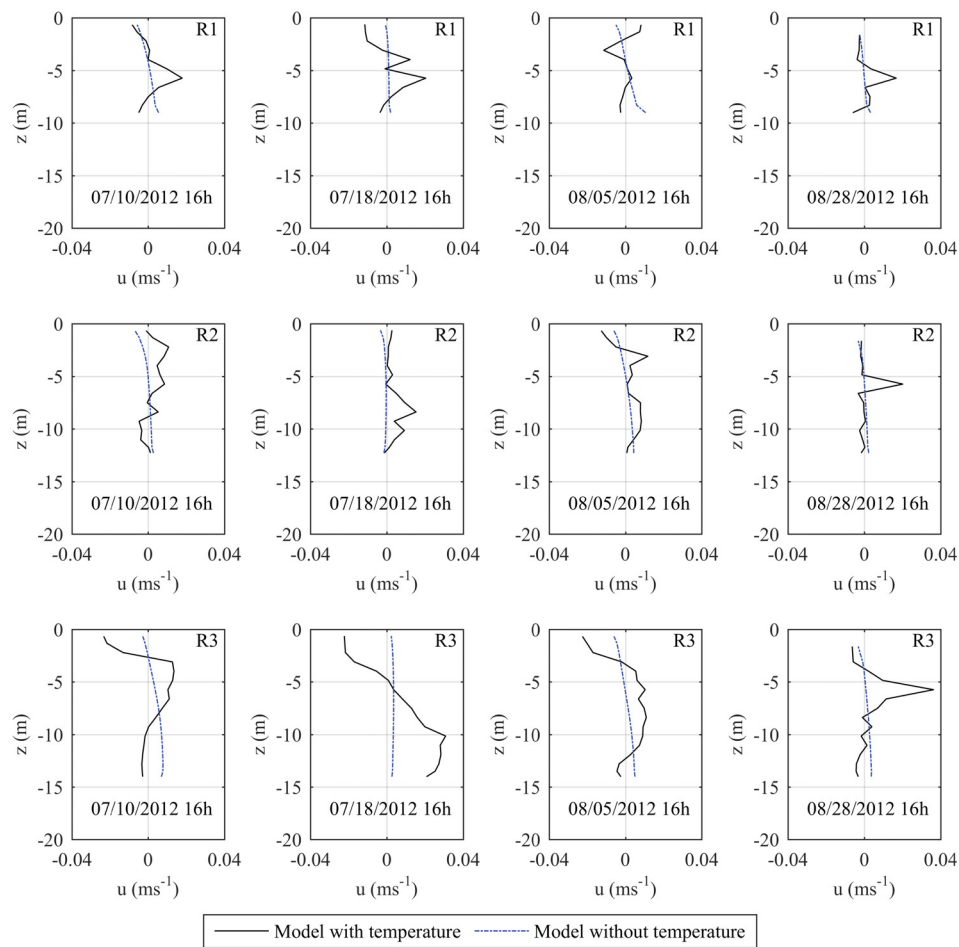


Figure 67 – Velocity profiles in points R1, R2 and R3 (see Figure 64) in the river tracer modeling in Vossoroca reservoir

temperature shows that there is an increase in velocities close to the layer of -6 m, induced by temperature differences between shallow and deeper area. Also, in the surface layer, wind speed act in the North-east direction, but the velocity vector shows the water in the surface moving to East direction. At 02h, the tracer is confined in the shallow region and velocities are still higher in the layer of -6 m. Between 04h and 08h, the tracer spreads and surface temperature decreases – the graph also shows the location of where 30% of the maximum concentration is found in the water column. At 10h, an intrusion of the tracer is identified in the layer of -6 m – velocity vector also shows higher velocities in this region – 30% of the maximum concentration is found around 250 m from the point where the tracer is released. At 12h, no intrusion is verified, the tracer is confined in the shallow region – temperature in the surface layer increased, therefore, temperature does not induce the tracer movement. At 14h, higher velocities are identified near the surface layer, changing the direction of the water movement – the tracer is confined in the shallow region. These effects caused by differential cooling or heating were studied by Monismith

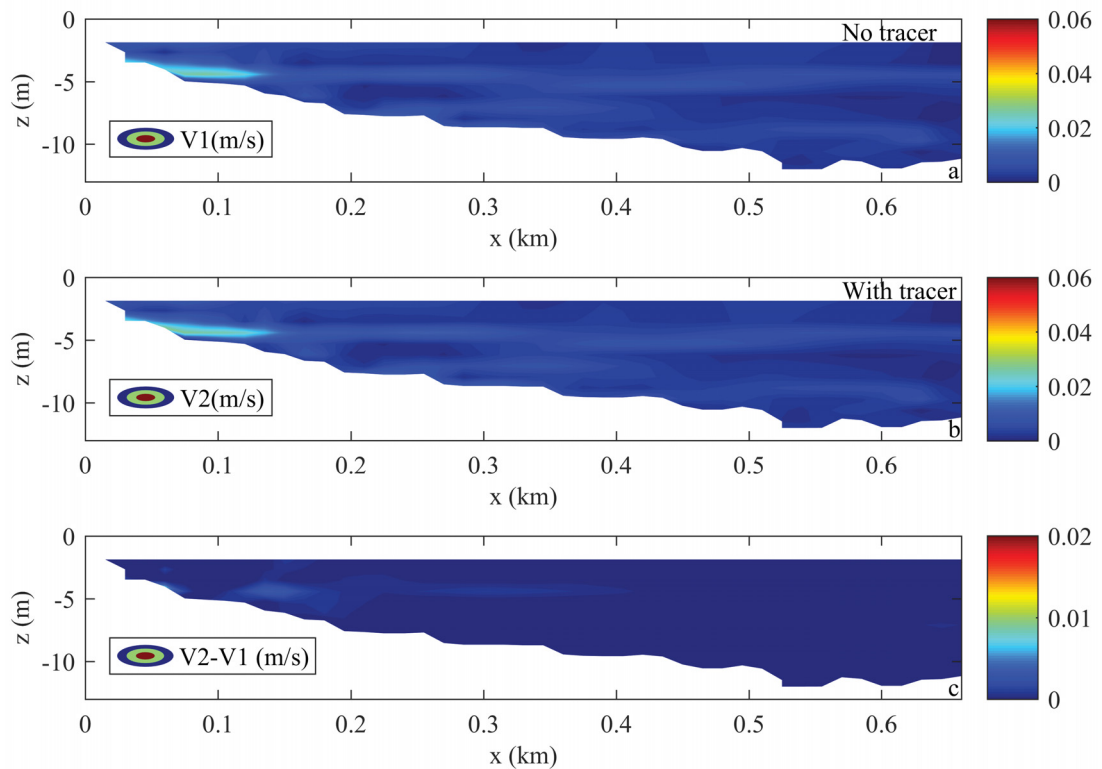


Figure 68 – Velocity in a section of a side arm in Vossoroca reservoir a) No tracer, b) With tracer and c) Difference in velocity in the simulation considering and not considering tracer

et al. (1990), that measured temperature profiles in Wellington reservoir and identified the non-one-dimensional response of the reservoir to heating and cooling, in shallow to deep areas. James and Barko (1991) also measured temperature transects and used a tracer to analyse horizontal transport due differential cooling. Jamos and Barko (1991) identified and quantified the effects of horizontal temperature gradients on mass transport. The modeling of the side arm showed the same behavior as the measurements by Monismith et al. (1990) and Jamos and Barko (1991). Vossoroca reservoir presented horizontal temperature gradients from shallow to deep water, and this induced mass transport in the reservoir. To quantified the transport due temperature differences, advective and dispersive transport were calculated for the modeling.

The transport was quantified using the cumulative advective and dispersive transport of tracer and temperature. Figure 71 shows the cumulative transport in the simulation with temperature. The signs on the graphs are due a convention in Delft3D.

In the case of the advective transport of temperature (Figure 71.a), small differences occur in the initial period of simulation, that could be a result of small temperature gradients between cross-sections and velocities. The transport tend to increase and it is higher in cross-section 5, near the open water in the reservoir. Dispersive transport of temperature (Figure 71.b) also increases in the cross-sections near the open water.

In relation to tracer transport, the advective transport (Figure 71.c) is smaller in cross-section 1, but in all the other cross-sections, the advective transport quantified was close. Dispersive transport of tracer (Figure 71.d), on the other hand, was higher in cross-section 1 and tend to decrease in the other cross-sections.

To analyse the effects of temperature over tracer distribution in the side arm, a 3D simulation without temperature was performed. Figure 72 shows the results of tracer concentration in the water column on 09/23/2012 between 00h and 14h. Different from what is verified in the modeling with temperature, in this simulation the tracer is confined in the shallow region of the arm and no intrusion is verified. At 10h, 30% of the maximum concentration is found around 100 m from the point where the tracer is released.

The cumulative transport was also calculated for the tracer in the modelling without temperature. The pattern in the transport is the same as showed in Figure 71.c and Figure 71.d, but the magnitude in the transport changed. Table 33 shows the difference in advective and dispersive transport in the simulation, considering temperature and without temperature, in each cross-section monitored. In general, when temperature is considered in the modeling, advective transport increases in all cross-sections, with a maximum increase of 9.1% in cross-section 1. For dispersive transport, on the other hand, no defined pattern may be defined – in some cross-sections there is an increase in transport when temperature is considered in the simulation (cross-sections 2 and 3). On the other hand, there is a decrease in dispersive transport when temperature is considered (sections 1 and 5).

To investigate the effects of temperature on mass transport, velocity profiles in two points (P1 and P2) were compared in the side arm showed in Figure 69. Figure 73 shows the velocity profiles at points P1 and P2 in the modeling with and without temperature. In P1, the deeper point, when temperature is not simulated, the velocity profile is more uniform. In the modeling with temperature, on the other hand, the profile is not uniform, and changes in the direction of the flow are identified. In P2, the velocity profile in the modeling without temperature is also more uniform – no flow is induced. In the modeling with temperature, on the other hand, some peaks may be identified in the modeling and they agree with the layer of intrusion (around -6 m), identified in Figures 69 and 70. The higher velocities are around 0.02 ms^{-1} . Therefore, temperature may induce mass transport in side arms of dendritic reservoirs and also be a source for deeper waters.

This section showed clearly the importance of modeling vertical variations when working on reservoir modeling, and the need to link to temperature modeling. Consequences on mass flow are also verified in 2D lake/reservoir models. To highlight those differences, it was performed a 2D simulation with Delft3D (1 layer in the vertical direction), and it was analysed the path and distribution of the tracer concentration, and impacts of this approach on mass transport for the tracer released at the side arm, in comparison with 3D modeling.

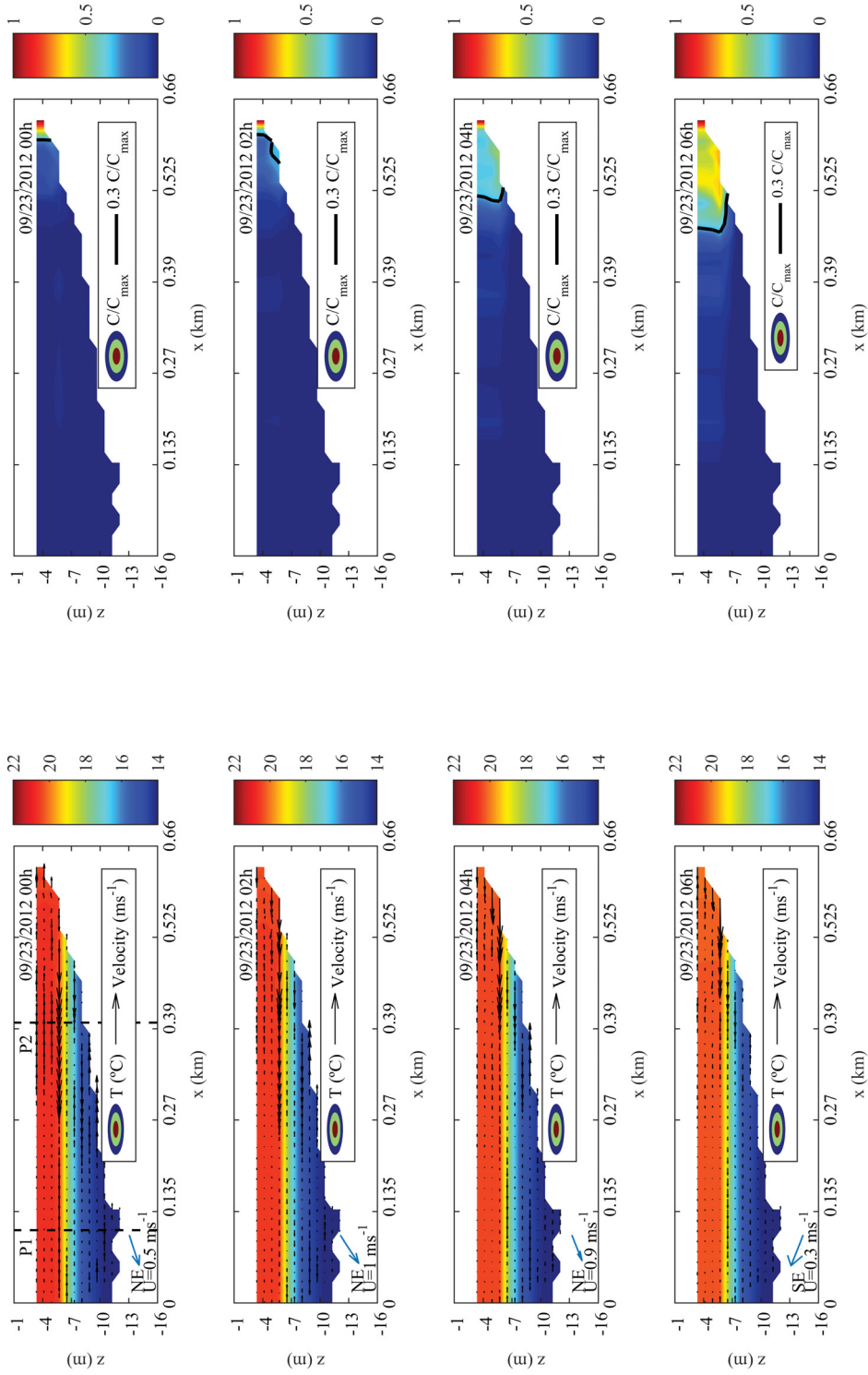


Figure 69 – Water temperature and tracer concentration in a side arm in 09/23/2012 between 00h and 06h

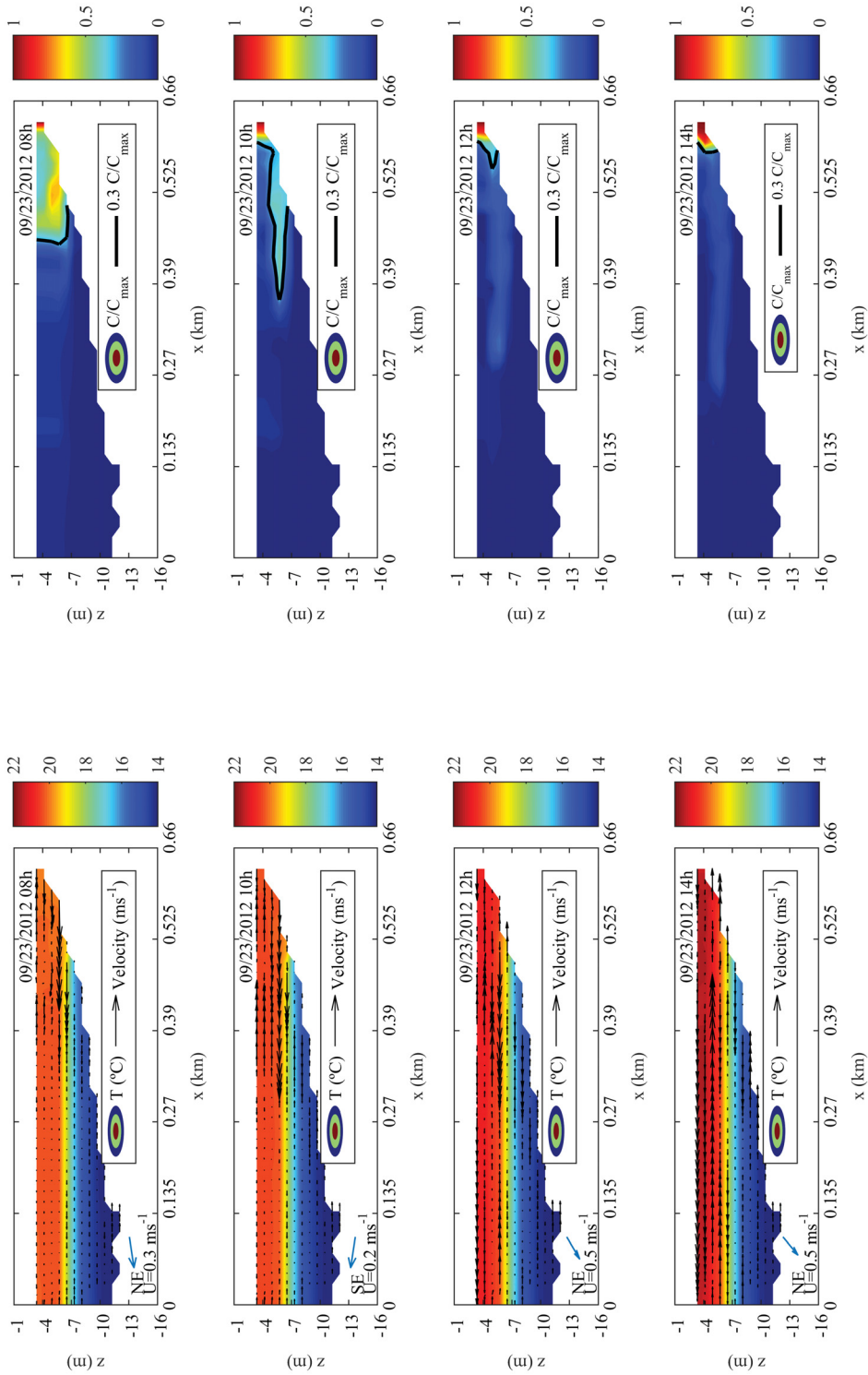


Figure 70 – Water temperature and tracer concentration in a side arm in 09/23/2012 between 08h and 14h

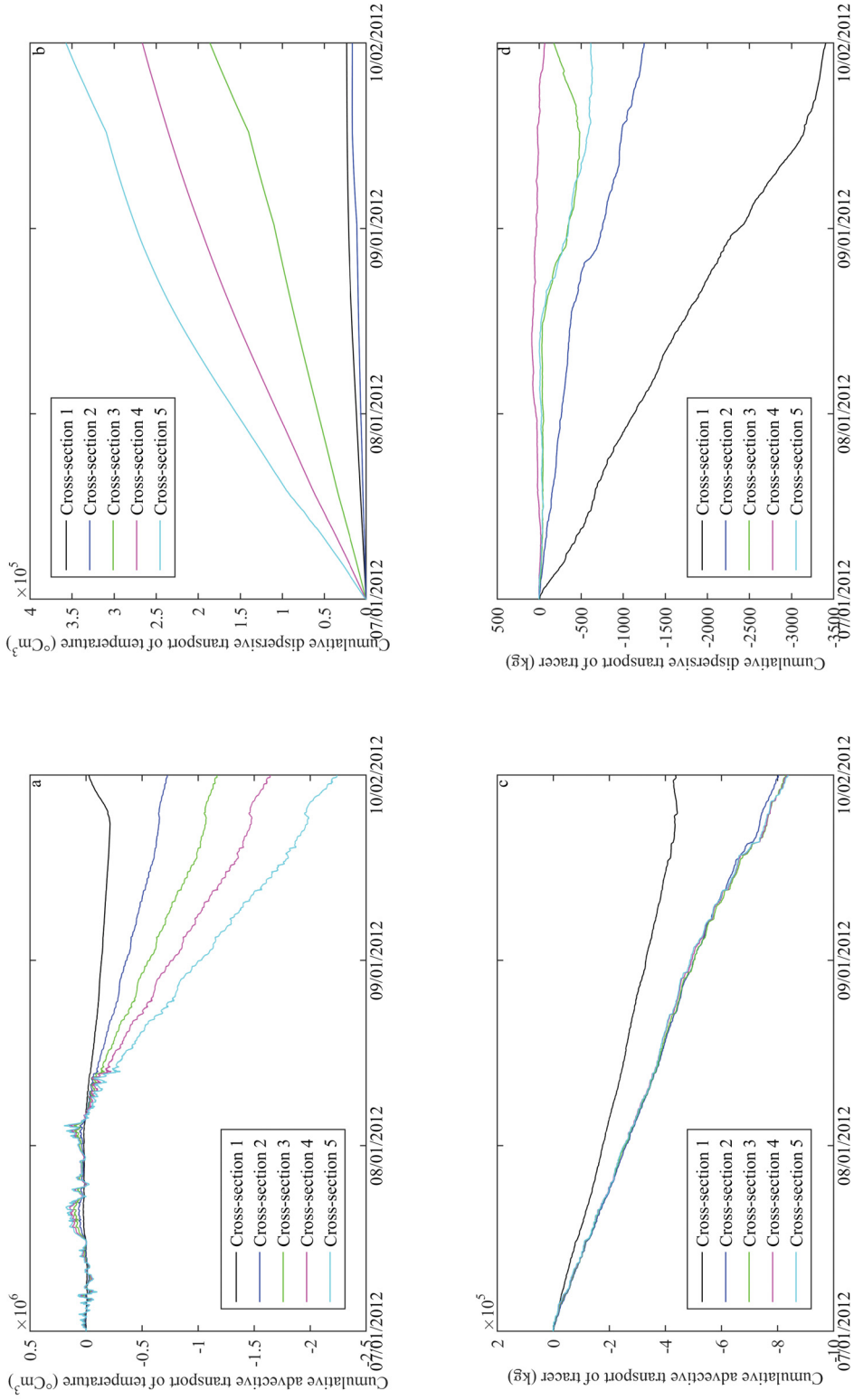


Figure 71 – Side arm simulation. Cumulative a) advective transport of temperature, b) dispersive transport of temperature, c) advective transport of tracer and d) dispersive transport of tracer

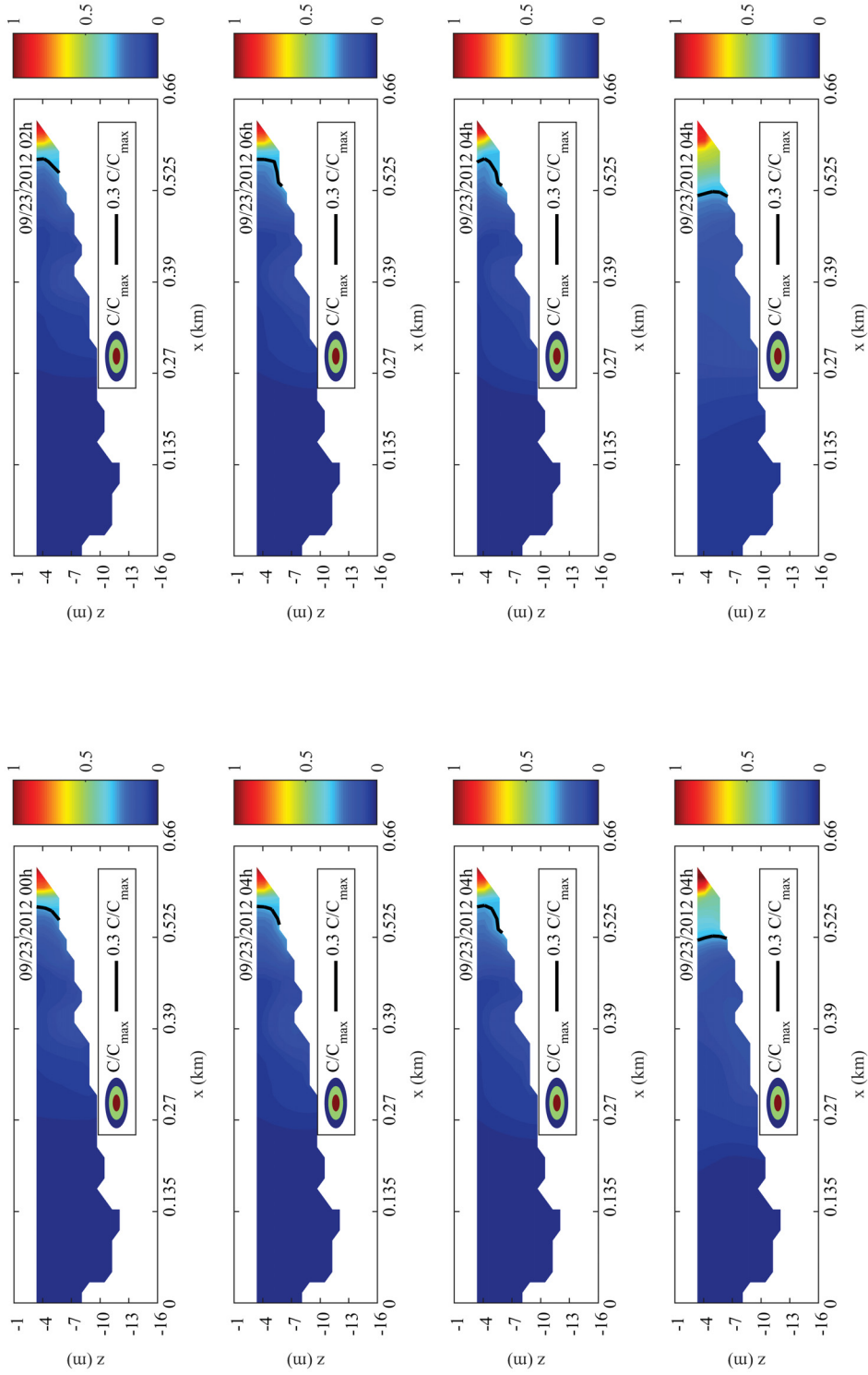


Figure 72 – Tracer concentration in a side arm in 09/23/2012 between 00h and 14h (in this simulation, temperature is not modelled)

Table 33 – Difference in percentage between advective and dispersive transport considering temperature and not considering temperature in the side arm tracer modeling

Cross-section	Advective transport (%) ⁶	Dispersive transport (%) ⁶
1	+9.1	-96.3
2	+2.0	+1.9
3	+4.5	+62.1
4	+4.5	0.0
5	+5.7	-30.8

⁶ Positive sign means that mass transport through the cross-section is higher in the modeling with temperature; Negative sign means that mass transport through the cross-section is higher in the modeling without temperature

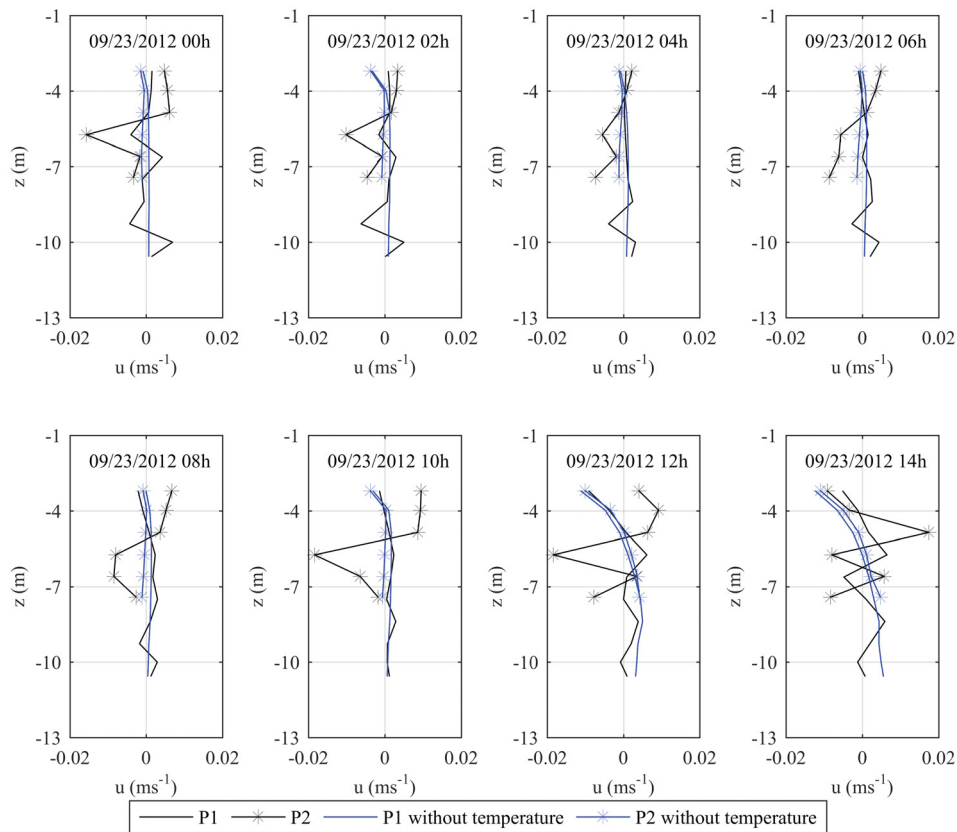


Figure 73 – Velocity profiles in points P1 and P2 (see Figure 69) in the side arm tracer modeling in Vossoroca reservoir

Figure 74 shows the normalised tracer concentrations for P1 and P2 points (see Figure 69). In the 2D modeling, the tracer concentration is uniform in the water column and no stratification effects can be modelled. The intrusion modelled by the 3D model (increase in velocity and tracer concentration) is not simulated by the 2D model. In the deeper point (P1), the highest difference in the mean tracer concentration was on 09/23/2012 14h – the concentration in the 2D modeling was 30% higher than the mean concentration

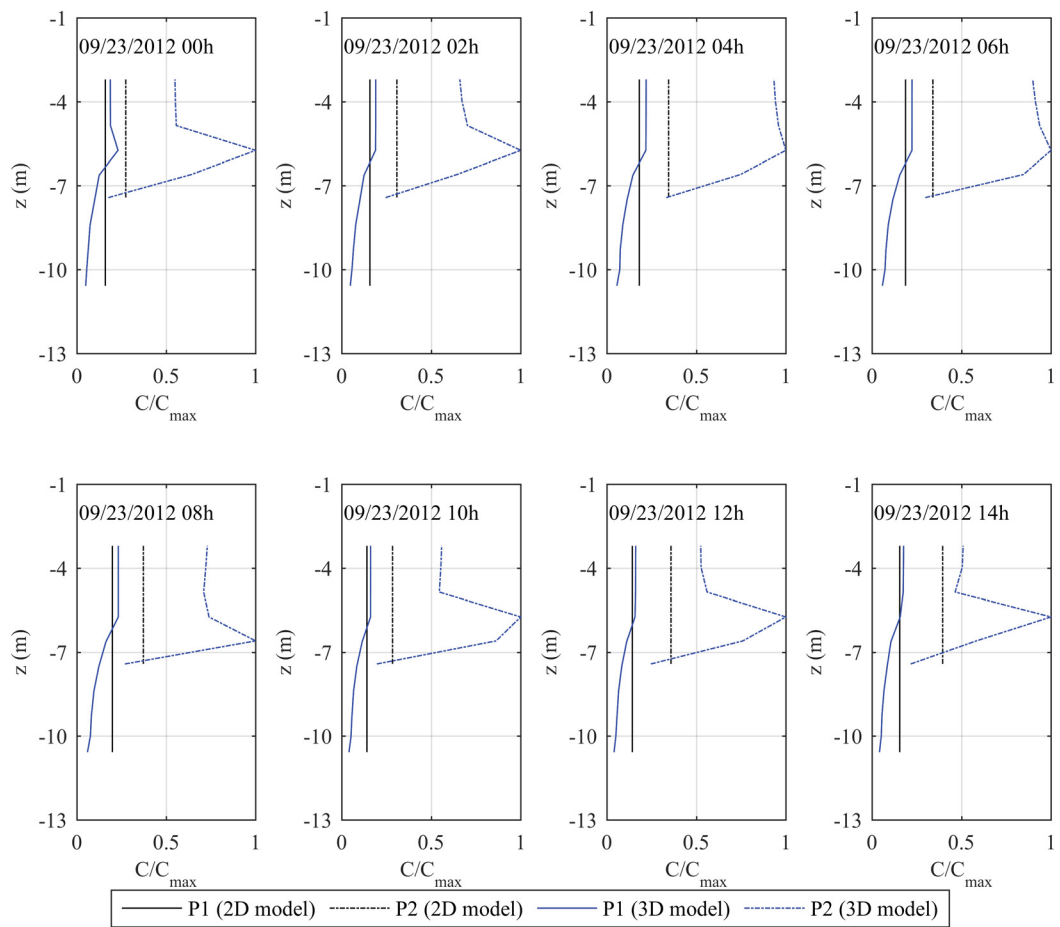


Figure 74 – Normalised tracer concentration in points P1 and P2 (see Figure 69) in the 2D and 3D side arm tracer modeling in Vossoroca reservoir

in the 3D modeling. At point P2, the mean tracer concentration of the 3D model is not reproduced by the 2D model – on 09/23/2012 06h, for example, the mean tracer concentration simulated by the 3D model is 140% higher than the concentration calculated by the 2D model. Therefore, the 2D modeling does not reproduce the mean concentrations that are expected to occur in the side arm modeling. No vertical variations are possible to simulate when a model with one layer in the vertical direction (2D model) is used or when the model does not considers temperature variations, and this affects directly mass transport in lakes ad reservoirs.

7.3 Summary of the chapter

The tracer transport modeling in this section had the objective of studying mass transport due temperature effects. A tracer was continuously released in a river and in a side arm, and to analyse the effects of temperature in mass transport, the 3D model was applied considering the full modeling and applied do not considering heat transport and then, the temperature effects were analysed. For the river tracer modeling, the tracer was continuously released in São João river, and the comparison between the two modeling showed that advective transport is increased due temperature effects and dispersive transport decreased (in magnitude advective transport is more important than dispersive transport). For the side arm tracer modeling, a tracer was continuously released in the shallow area of the arm. The comparison of the modeling showed that temperature also increases advective transport (the most significant transport) and, for dispersive transport, no pattern was possible to define. This section showed the importance of temperature for mass transport, and how temperature can affect water quality, for example, and that temperature has to be considered in studies related to reservoirs – due effects as differential cooling/heating or inflow dynamics.

8 Conclusions

Lakes and reservoirs are usually used for multiple purposes – energy generation, water supply, irrigation and recreation, for example. Reservoirs impact physical and chemical characteristics of a water body – temperature is a key parameter in studies in lakes and reservoirs, since stratification can control substances distribution and have a direct influence on other processes in the water body. The pattern of substances distribution may be related to temperature, which is simpler to measure and model, in relation to other water quality parameters (more processes to be modelled and calibrated). Vertical temperature variations are well known for driving or preventing processes in the water column. Currently, horizontal temperature variations are being studied, and its implications for hydrodynamics and water quality.

Even temperature modeling being simpler than modeling other processes, calibrate a three-dimensional model is complex – due the amount of data, parameters and time spend to run these models. One-dimensional models, on the other hand, are fast and efficient, and need less data to run and calibrate the model. The disadvantage of these models is that they do not allow horizontal temperature variations simulation. Therefore, a Sector model was developed – the reservoir is divided in regions and the one-dimensional model MTCR-1 is applied for each of these sectors. The model may or may not allow heat exchange between the sectors. The model configuration and system representation is kept simple, simulating vertical and horizontal variations, with fast response of the system.

Temperature measurements in Vossoroca and Passaúna reservoirs, with high spatial resolution, showed that vertical and horizontal temperature gradients are verified in both reservoirs. In Vossoroca reservoir, close to São Joãozinho river, the bottom of the reservoir was colder than the deepest region of the reservoir (at the same depth) – this is an indication that the river enters the reservoir as an underflow, with colder temperatures. Close to the surface, horizontal temperature gradients were also verified – a section from a shallow to a deeper region showed differences in surface temperatures. Besides these gradients, no differences in thermocline depth were identified in Vossoroca reservoir.

In Passaúna reservoir, on the other hand, horizontal temperature gradients were more pronounced than the ones measured in Vossoroca reservoir. As in Vossoroca reservoir, the water coming in the reservoir was colder than the reservoir. Surface temperature gradients were also verified, but the main differences occurred in depth, with gradients from shallower water to the deepest point. Also, thermocline depth varied from shallower to deeper water.

Temperature measurements in Vossoroca and Passaúna reservoirs showed evidences that horizontal processes may be important in both reservoirs – the first hypothesis of this Thesis. These horizontal temperature variations are not represented by one-dimensional

models – then, the reservoir was divided in several sectors and the one-dimensional model (MTCR-1) was applied to each of them, allowing an exchange between the sectors and running the model independently. To compare the modeling results, a three-dimensional model (Delft3D) was calibrated for Vossorooca reservoir, and a comparison was performed with measurements of temperature from a floating platform in the deepest point of the reservoir.

Comparison with measured data, one and three-dimensional model results showed that temperature is more accurately simulated by the three-dimensional modeling. MAE for 1D model was 1.18 ± 0.84 °C, while for 3D modeling, 0.50 ± 0.31 °C. Physical indices calculated from 1D model results, on the other hand, showed very similar results comparing the physical indices calculated from measurements. Therefore, a result of this Thesis is that it is possible to identify periods of mixing and stratification with simple models and low time processing – one-dimensional models are recommended to use to identify if the reservoir stratifies and for how long, as a first approach, and complementing three-dimensional modeling.

In this thesis it was shown that it is possible to simulate heat transport in a reservoir using a simple configuration (the third hypothesis of this Thesis) – a sector model, or a complex model as Delft3D in sectors, using high resolution in the vertical direction and possibility to simulate horizontal variations. Some advantages of this approach are related to the time consuming to run the model – one-dimensional models are fast and efficient, and they allow long period simulation. The same is valid for the sector model developed. In the case of three-dimensional models, with the configuration used to Vossorooca reservoir, the time necessary to run 94 days is around 10 days of processing. However, if Delft3D is used in a sector configuration, the time to run the model is around 1 min processing (model with 20 layers and four sectors) and no instabilities were verified. Therefore, these models also allow the analysis of seasonal variations and periods of stratification, necessary to the management of reservoirs, with low time processing and simple configuration.

Another hypothesis tested (the second hypothesis of this Thesis) was related to the horizontal temperature gradients driving mass transport. To verify this, a tracer modeling was performed – the tracer was released in a river and in a side arm of Vossorooca reservoir, and the temperature effects were quantified. The results showed that temperature has an influence over substances distribution in the water column.

For the river tracer modeling, water density determines the path of the river in the water column – as an intrusion, an overflow or underflow. Two simulations were performed – a full three-dimensional modeling and a three-dimensional modeling do not including heat transport, then the differences were analysed for the main river entrance in Vossorooca reservoir (longitudinal section of the reservoir to the deepest point). If temperature is not take into account, the tracer spreads in the entire water column, and do not has a

preferential path, as when water density varies. Therefore, temperature affects advective and dispersive transport of mass in the reservoir. The same behaviour is identified in the side arm tracer modeling – temperature also affects mass transport – when temperature is considered, tracer intrusions from shallow to deeper areas may be identified with modeling, and both advective and dispersive transport are influenced by temperature. Velocity profiles also show differences due density effects. In the modeling without heat transport, the velocity profiles were more uniform, while when temperature was considered, there was a increase in velocity and some peaks of velocity were identified. Therefore, temperature (vertical and horizontal variations) may interfere in mass transport and the path of a substance in the reservoir – and it may affect water quality.

From the simulations and quantification of transport, it was identified that advective transport was enhanced by temperature (which is the most significant transport calculated) – 40% maximum increase in a cross-section in the river tracer modeling, and 9% maximum increase in a cross-section in the side arm tracer modeling. In the river tracer modeling, there was a decrease in dispersive transport considering temperature in the modeling. In the case of the side arm tracer modeling, no pattern was possible to define in the dispersive transport.

A 2D simulation was also performed in Vossoroca reservoir, and the model was not able to reproduce the mean tracer concentration in the water column, and this also highlight the importance of temperature and vertical and horizontal variations on mass transport in lakes and reservoirs.

8.1 Recommendations and future studies

With the analysis presented in this thesis, some recommendations related to measurements and modeling are proposed. In relation to measurements:

1. Measurements with high temporal and spatial resolution – this allows identification of seasonal variations in vertical and horizontal directions in the reservoir. The deployment of a second floating platform to system analysis, as: temperature gradients, internal waves identification and transport processes, and considering models, for calibration. In this thesis, we considered the 3D model calibrated using data from one floating platform installed at the deepest point of the reservoir, with high temporal and vertical resolution.
2. Inflows temperature should be measured at least in a daily scale – tracer modeling showed that inflow temperature in relation to water column temperature determines the path of water in the reservoir and also, mass transport in the reservoir.
3. Meteorological data is the most important set of data in heat transport modeling. Therefore, care must be taken in the data used in models, since as it was showed

in section 4.3 (Heat flux in reservoirs), two stations with 1 km distance presented significant differences in calculated heat fluxes – thus, the location of these measurements is important when working with heat transport.

In relation to modeling of heat transport, this thesis showed that there is potential to use a simple configuration in models to obtain the general behavior of the reservoir, and identification of stratified periods. The recommendations for the heat transport modeling are:

1. Apply a one-dimensional model – this allows the identification if the reservoir stratifies or not and for how long.
2. If variations in horizontal direction and in depth are required, the use of a sector model is recommended, since it is a simple model to set up and fast in time processing. It is possible to use the sector model developed in this thesis or even a more complex model in simple configuration.
3. If mass transport is required in the modeling, the recommendation is to apply a three-dimensional model, due the influence of temperature on the path of a substance in the reservoir, which is not possible to simulate in a simple model.

For future studies, it is recommended the analysis of internal waves in the reservoir – they may have an influence on heat transport and other processes in lakes and reservoirs.

The sector model showed reliable results in comparison with three-dimensional modeling and measurements, therefore, further analysis and development of the exchange between sectors may be performed, and also verify the impact of using more sectors to represent the system, if they can improve or not the system representation. Also, application in other reservoirs, as Passaúna, that is also dendritic, but has only one arm and several river contributions, comparing with three-dimensional modeling and measurements.

The development of a one-dimensional mass transport model, to verify the results presented in this Thesis and compare the results of mass transport of the three-dimensional model. Verify if, as temperature, the model is capable of solving this problem and give fast response and when it can be used. Then, using the mass transport model in sectors, and analyse if they may be used to simulate mass transport, since this thesis showed that this is a three-dimensional process, on the river and side arm tracer modeling.

Running a three-dimensional water quality model for some water quality parameters (oxygen, nutrients for example) and analyse the impacts of vertical and horizontal temperature variations on water quality and other related processes in the water body: can horizontal temperature gradients transport nutrients or oxygen, for example, from shallow to deep waters, during differential cooling periods? What are the implications for the reservoir management and water quality?

9 References

1. ANA – Agência Nacional das Águas, Conjuntura dos recursos hídricos no Brasil, Brasília, 2013.
2. Antonopoulos, V. Z. and Giannou, S.K., Simulation of Water Temperature and Dissolved Oxygen Distribution in Lake Vegoritis, Greece, *Ecological modeling*, Vol. 160, pp. 39-53, 2003.
3. Babajimopoulos, C., Papadopoulos, F. Mathematical Prediction of Thermal Stratification of Lake Ostrovo (Vegoritis), Greece. *Water Resources Research*. v.22(11), pp. 1590-1596. 1986.
4. Barrete, N.; Laprise, R., A One-Dimensional Model for Simulating the Vertical Transport of Dissolved CO₂ and CH₄ in Hydroelectric Reservoirs. In A. Tremblay, L. Varfalvy, C. Roehm, M. Garneaus [eds]. *Greenhouse gas emissions – fluxes and processes: Hydroelectric reservoirs and natural environments*. Springer, 2005.
5. Bell, V.A., George, D.G., Moore, R.J., Parker, J., Using a 1-D mixing model to simulate the vertical flux of heat and oxygen in a lake subject to episodic mixing, *Ecological modeling*, Vol. 190, pp. 41-54, 2006.
6. Bertone, E.; Stewart, R. A.; Zhang, H.; Bartkow, M. and Hacker, C. An autonomous decision support system for manganese forecasting in subtropical water reservoirs, *Environmental modeling & Software*, 73, 133 - 147, 2015.
7. Bonalumi, M.; Anselmetti, F. S.; Wüest, A. and Schmid, M. Modeling of temperature and turbidity in a natural lake and a reservoir connected by pumped-storage operations *Water Resources Research*, 48, 2012.
8. Chapra, S.C. *Surface Water Quality Modeling*. McGraw-Hill Publisher, New York. 1997.
9. Chung, S.; Hipsey, M. and Imberger, J. modeling the propagation of turbid density inflows into a stratified lake: Daecheong Reservoir, Korea *Environmental modeling & Software*, 24, 1467 - 1482, 2009.
10. Chung, S. and Gu, R. Two-Dimensional Simulations of Contaminant Currents in Stratified Reservoir, *Journal of Hydraulic Engineering*, 124(7): 704-711, 1998.
11. Companhia de Saneamento do Paraná. Plano diretor da SAIC: Sistema de Abastecimento de Água Integrado de Curitiba e Região Metropolitana. Curitiba, Sanepar, 2013.

12. Copel. Usina Hidrelétrica Chaminé. Relatório Ambiental. 1999.
13. Curtarelli, M. P.; Alcântara, E.; Rennó, C. D.; Assireu, A. T.; Bonnet, M. P. and Stech, J. L. modeling the surface circulation and thermal structure of a tropical reservoir using three-dimensional hydrodynamic lake model and remote-sensing data, *Water and Environment Journal*, 28, 516-525, 2014.
14. Curtarelli, M. P.; Alcântara, E. H.; Rennó, C. D. and Stech, J. L. Modeling the effects of cold front passages on the heat fluxes and thermal structure of a tropical hydroelectric reservoir, *Hydrology and Earth System Sciences Discussions*, 10, 8467-8502, 2013.
15. Dake, J. M. K., Halerman, D. R. F., *Thermal Stratification in Lakes: Analytical and Laboratory Studies*, *Water Resources Research*, v.5(2), pp. 484-495, 1969.
16. Deltares. User Manual Delft3D-Flow. Ver 3.14. Deltares, Delft, The Netherlands, 2014.
17. Dias, L. N., *Estudo Integrado da Bacia Hidrográfica do reservatório Passaúna (Araucária – Paraná – Brasil), considerando a interrelação da ocupação dos solos com a qualidade das águas*. Dissertation. São Paulo University. 1997.
18. Doan, P.T.K., Némery, J., Schmid, M., Gratiot, N., *Eutrophication of turbid tropical reservoirs: Scenarios of evolution of the reservoir of Cointzio, Mexico*, *Ecological Informatics*, Vol. 29, pp. 192-205, 2015.
19. Edinger, J.E., Duttweiler, D.W., Geyer, J.C., *The Response of Water Temperatures to Meteorological Conditions*. *Water Resources Research*. v.4 (5). pp. 1137-1143. 1968.
20. Elçi, S. *Effects of thermal stratification and mixing on reservoir water quality* *Limnology*, Springer Japan, 9, 135-142, 2008.
21. Esteves, F. A. *Fundamentos de Limnologia*. Interciência. 2a ed. Rio de Janeiro, 1988.
22. Favoreto, R. Z., Perreira Filho, D. L. B., Burmaster, C. L., Hilu, A., Silva, S. B. and Mine, M. R. M., "Modelagem de eventos de vazão máxima natural no reservatório de Vossoroca utilizado o modelo IPH II", In: XV Simpósio Brasileiro de Recursos Hídricos, Curitiba. CD-ROM, 2003.
23. Fischer, H. B. *Transport Models for Inland and Coastal Waters*. Academic Press. 542 p., 1981.

24. Friedl, G.; Wüest, A. Disrupting biogeochemical cycles: Consequences of damming. *Aquatic Science* v.64, pp.55-65, 2002.
25. Galli, C. S.; Abe, D. S. Disponibilidade, poluição e eutrofização das águas. In: Bicudo, C. E. M.; Tundisi, J. G.; Scheuenstuhl, M. C. B., *Águas do Brasil: Análises Estratégicas*. São Paulo, Instituto de Botânica, 2010.
26. Gianniou, S. K., Antonopoulos, V. Z. Evaporation and energy budget in Lake Vegoritis, Greece. *Journal of Hydrology*, n.345, pp.212-223. 2007.
27. Goudsmit, G. H., Burchard, H., Peeters, F., Wüest, A. Application of $k - \epsilon$ turbulence models to enclosed basins: The role of internal seiches. *Journal of Geophysical Research*, 107, n. C12, 3230. 2002.
28. Grassi, M. T., Machado, K. C., Fernandes, A. N., O abastecimento de água em capitais da região Sul. In: Canela, M. C., Jardim, W. F., Sodré, F. F., Grassi, M. T., *Caféina em águas de abastecimento público no Brasil*. Instituto Nacional de Ciências e Tecnologias Analíticas Avançadas – INCTAA. São Carlos: Editora Cubo, 2014.
29. Henderson-Sellers, B. Calculating the Surface Energy Balance for Lake and Reservoir Modeling: A Review. *Reviews of Geophysics*. v.24(3), pp.625-649. 1986.
30. Henderson-Sellers, B., New Formulation of eddy diffusion thermocline models, *Applied Mathematical modeling*, v.9, pp.441-446, 1985.
31. Hipsey, M.R., Bruce, L.C., Hamilton, D.P. GLM – General Lake Model: Model overview and user information. AED Report 26, The University of Western Australia, Perth, Australia. 42pp, 2014.
32. Hocking, G. C., Patterson, J., Quasi-two dimensional reservoir simulation model. *Journal of Environmental Engineering*, v. 117, pp.595-613. 1991.
33. Hodges, BR, Imberger J, Saggio A, Winters KB. Modeling basin-scale internal waves in a stratified lake. *Limnology and Oceanography*, 45, 1603-1620, 2000.
34. Horne, A. J. and Goldman, C. R., *Limnology*, Mc Graw Hill, United States of America, 1994.
35. Hohmann, R., Kipfer, R., Peeters, F., Piepke, G. and Imboden D. M. Processes of deep-water renewal in Lake Baikal. *Limnology and Oceanography*, 42(5), 841-855, 1997.
36. Horsch, G. M. and Stefan, H. G., Convective circulation in littoral water due to surface cooling. *Limnology and Oceanography*, 35: 1068-1083, 1988.

37. Huang, T., Li, X., Rijnaarts, H., Grotenhuis, T., Ma, W., Sun, X. and Xu, J. Effects of storm runoff on the thermal regime and water quality of a deep, stratified reservoir in a temperate monsoon zone, in Northwest China, *Science of the Total Environment*, 458-486, 820-827, 2014.
38. IAP, Instituto Ambiental do Paraná. Qualidade das águas: reservatórios do estado do Paraná 2005 a 2008. 2008.
39. Imboden, D. M. and Wüest, A. Mixing mechanisms in lakes, in A. Lerman, D. M. Imboden & J. R. Gat, eds, *Physics and Chemistry of Lakes*, Springer Verlag, pp. 83-138, 1995.
40. Imberger J., Patterson J.C., *Physical Limnology. Advances in Applied Mechanics* 27: 303-475, 1989.
41. Imerito, A., *Dynamic Reservoir Simulation Model DYRESM v4. v4.0 Science Manual*. Centre for Water Research, University of Western Australia. 2007.
42. James, W. F. and Barko, J. W. Littoral-pelagic phosphorus dynamics during nighttime convective circulation, *Limnology and Oceanography*, 36(S), 949-960, 1991.
43. Jassby, A., Powell, T., Vertical patterns of eddy diffusion during stratification in Castle Lake, California. *Limnology and Oceanography*, vol. 20. 1975.
44. Keupers, I., Willems, P. Development and testing of a fast conceptual river water quality model. *Water Research*, 113, 62-71. 2017.
45. Kim Y. and Kim, B. Application of a 2-Dimensional Water Quality Model (CEQUAL-W2) to the Turbidity Interflow in a Deep Reservoir (Lake Soyang, Korea), *Lake and Reservoir Management*, 22:3, 213-222, 2006.
46. Laval, B.; Imberger, J.; Hodges, B. and Stocker, R. Modeling circulation in lakes: Spatial and temporal variations, *Limnology and Oceanography*, 48, 983-994, 2003.
47. Lee, H.; Chung, S.; Ryu, I. and Choi, J. Three-dimensional modeling of thermal stratification of a deep and dendritic reservoir using ELCOM model *Journal of Hydro-environment Research*, 7, 124 - 133, 2013.
48. León, L.; Lam, D.; Schertzer, W.; Swayne, D. and Imberger, J. Towards coupling a 3D hydrodynamic lake model with the Canadian Regional Climate Model: Simulation on Great Slave Lake *Environmental modeling & Software*, 22, 787 - 796, 2007.

49. Li, X., Huang, T., Ma, W., Sun, X. and Zhang, H. Effects of rainfall patterns on water quality in a stratified reservoir subject to eutrophication: Implications for management, *Science of the Total Environment*, 521-522, 27-36, 2015.
50. Liu, W.C., Chen, W. B. and Kimura, N. Impact of phosphorus load reduction on water quality in a stratified reservoir-eutrophication modeling study. *Environmental Monitoring and Assessment*, 159:393-406, 2009.
51. Männich, M. Estimativa de emissões de gases de efeito estufa em reservatórios e lagos – Contribuições para o monitoramento e modelagem 1D – vertical. Thesis. Federal University of Paraná. 2013.
52. Marti, C. L.; Mills, R. and Imberger, J. Pathways of multiple inflows into a stratified reservoir: Thomson Reservoir, Australia, *Advances in Water Resources*, 34, 551 - 561, 2011.
53. Martin, J.L., McCutcheon, S.C. *Hydrodynamics and Transport for Water Quality Modeling*. CRC Press, Inc, 1999.
54. Ministério de Minas e Energia. *Balanco Energético Nacional 2013 (ano base 2012)*. Relatório Final. 283 p., 2013.
55. Mirinov, D., Kirillin, G., Heise, E., Golosov, S., Terzhevik, A., Zverev, I., Parameterization of Lakes in Numerical Models for Environmental Applications. Proc. of the 7th Workshop on Physical Processes in Natural Waters, A. Yu. Terzhevik, Ed., Northern Water Problems Institute of the Russian Academy of Sciences, Petrozavodsk, Karelia, Russia. pp. 135-143. 2003.
56. Modiri-Gharehveran, M.; Etemad-Shahidi, A. and Jabbari, E. Effects of climate change on the thermal regime of a reservoir *Proceedings of the ICE – Water Management*, 167, 601-611(10), 2014.
57. Monismith, S. G.; Imberger, J. and Morison, M. L. Convective motions in the sidearm of a small reservoir *Limnology and Oceanography*, 35, 1676-1702, 1990.
58. Morillo, S.; Imberger, J.; Antenucci, J. P. and Woods, P. F. Influence of Wind and Lake Morphometry on the Interaction between Two Rivers Entering a Stratified Lake, *Journal of Hydraulic Engineering*, 134, 1579-1589, 2008.
59. Murakami, M., Y. Oonishi and H. Kunishi, A numerical simulation of the distribution of water temperature and salinity in the Seto Inland Sea. *Journal of the Oceanographical Society of Japan* 41: 221-224. 243, 250, 254, 1985.

60. Peeters, F., Livinstone, D. M., Goudsmit, G. H., Kipfer, R., Forster, R. Modeling 50 years of historical temperature profiles in a large central European lake. *Limnology and Oceanography*. v.47(1), pp. 186-197. 2002.
61. Polli, B. A. Modelagem 1D do fluxo vertical de calor em corpos de água horizontalmente homogêneos. Masters dissertation. Federal University of Paraná. 2014.
62. Prestigiacomo, A. R.; Effler, S. W. and Matthews, D. A. Resolution and Analysis of Spatial Variations and Patterns in an Urban Lake with Rapid Profiling Instrumentation, *JAWRA Journal of the American Water Resources Association*, 51, 200-213, 2015.
63. Read, J. S., Hamilton, D. P., Jones, I. D., Muraoka, K., Winslow, L. A., Kroiss, R., Wu, C. H., Gaiser, E. Derivation of lake mixing and stratification indices from high-resolution lake buoy data. *Environmental modeling & Software*, v; 26, pp.1325-1336, 2011.
64. Roget, E. Hydrophysical Measurements in Natural Waters. In: J. Fernando (ed), *Handbook of Environmental Fluid Dynamics*. Volume 2, Oxford: Taylor & Francis Group, 2013.
65. Roget, E., Colomer, J., Casamitjana, X. and Llebotand, J. E. Bottom currents induced by baroclinic forcing in Lake Banyoles (Spain), *Aquatic Sciences* 55/3, 1993.
66. Schladow, S. G., Hamilton, D. P., Prediction of water quality in lakes and reservoirs: Part II - Model calibration, sensitivity analysis and application, *Ecological modeling*, Vol. 96, pp. 111-123, 1997.
67. Smits, J., Boderie, P. and van Beek, J., modeling of the Nam Theun 2 Reservoir: Water quality and greenhouse gases emissions. *Deltares*, 2009.
68. Soares, M. C. S.; Marinho, M. M.; Huszar, V. L. M.; Branco, C. W. C. and Azevedo, S. M. F. O. The effects of water retention time and watershed features on the limnology of two tropical reservoirs in Brazil *Lakes & Reservoirs: Research & Management*, Blackwell Publishing Asia, 13, 257-269, 2008.
69. Soullignac, F., Vinon-Leite B., Lemaire B. J., Martins J.R., Bonhomme C., Dubois, P., Mezemate, Y., Tchiguirinskaia I., Schertzer D., Tassin, B. Performance assessment of a 3D hydrodynamic model using high temporal resolution measurements in a shallow urban lake. *Environmental Modeling and Assessment*, Volume 22, 4, pp 309-322, 2017.
70. Soullignac, F., Lemaire B. J., Martins J.R. , Bonhomme C. , Tchiguirinskaia I., Schertzer D. and Vinçon-Leite B., Mixing regime of a shallow urban lake, *Lake*

- Créteil, France: measurements and simulations, In: 18th International Workshop on Physical Processes in Natural Waters, Germany, 2015.
71. Stepanenko, V., Jöhnk, K. D., Machulskaya, E., Perroud, M., Subin, Z., Nordbo, A., Mammarella, I. and Mironov, D. Simulation of surface energy fluxes and stratification of a small boreal lake by a set of one-dimensional models, *Tellus A: Dynamic Meteorology and Oceanography*, 66:1, 21389, 2014.
 72. Sundaram, T. R., Rehm, R. G. Formation and Maintenance of Thermoclines in Temperate Lakes. American Institute of Aeronautics and Astronautics. v.9(7), pp. 1322-1329. 1971.
 73. Tuan, N.; Hamagami, K.; Mori, K. and Hirai, Y. Mixing by wind-induced flow and thermal convection in a small, shallow and stratified lake Paddy and Water Environment, Springer-Verlag, 7, 83-93, 2009.
 74. Tundisi J. G., Matsumura-Tundisi T. and Calijuri M. C. Limnology and management of reservoirs in Brazil. In: Comparative Reservoir Limnology and Water Quality Management (eds M. Straskraba, J. G. Tundisi & A. Duncan). Kluwer Academic Publishers, Amsterdam, 1993.
 75. UFPR; Lactec. GHG Apine Project. Project report, 2015.
 76. UNESCO/IHA, The UNESCO/IHA measurement specification guidance for evaluating the GHG status of man-made freshwater reservoirs. 55 p., 2009.
 77. Zouabi-Aloui, B., Adelana S. M. and Gueddari M. Effects of selective withdrawal on hydrodynamics and water quality of a thermally stratified reservoir in the southern side of the Mediterranean Sea: a simulation approach, *Environmental Monitoring and Assessment*, 187: 292, 2015.
 78. Veiga, B. V. and Dziedzic, M., Estimating nutrient loads in the Passaúna reservoir with FLUX, *Water International*, 35, 210-222, 2010.
 79. Zouabi-Aloui, B. and Gueddari, M. Two-dimensional modeling of hydrodynamics and water quality of a stratified dam reservoir in the southern side of the Mediterranean Sea *Environmental Earth Sciences*, Springer Berlin Heidelberg, 72, 3037-3051, 2014.
 80. Yang, Y.-H.; Zhou, F.; Guo, H.C.; Sheng, H.; Liu, H.; Dao, X. and He, C.-J. Analysis of spatial and temporal water pollution patterns in Lake Dianchi using multivariate statistical methods *Environmental Monitoring and Assessment*, Springer Netherlands, 170, 407-416, 2010.

81. Yu, S. J., Lee, J. Y. and Ha, S. R. Effect of seasonal diffuse pollution migration on natural organic matter behavior in a stratified dam reservoir, *Journal of Environmental Sciences*, 22(6) 908-914, 2010.
82. Yu, H.; Tsuno, H.; Hidaka, T. and Jiao, C. Chemical and thermal stratification in lakes *Limnology*, Springer Japan, 11, 251-257, 2010.
83. Wahl, B., and Peeters, F., Effect of climatic changes on stratification and deep-water renewal in Lake Constance assessed by sensitivity studies with a 3D hydrodynamic model, *Limnology and Oceanography*, 59(3), 1035-1052, 2014.
84. Weinberger, S., Vetter, M., Using the hydrodynamic model DYRESM based on results of a regional climate model to estimate water temperature changes at Lake Ammersee. *Ecological modeling*, 244, pp. 38-48, 2012.
85. Wells, M.G. and Sherman, B. Stratification produced by surface cooling in lakes with significant shallow regions, *Limnology and Oceanography*, 46, 1747-1759, 2001.
86. Wetzel, R.G. *Limnology*, Saunders College Publishing. 2a ed. United States of America, 1983.
87. Woolway, R.I., Jones, I.D., Hamilton, D.P., Maberly, S.C., Muraoka, K., Read, J.S., Smyth, R.L., Winslow, L.A. Automated calculation of surface energy fluxes with high-frequency lake buoy data. *Environmental modeling and Software* 70, 191-198, 2015.
88. Wüest, A. and M. Schmid. *Physical Limnology*. In: J. Fernando (ed), *Handbook of Environmental Fluid Dynamics*. Volume 1, Oxford: Taylor & Francis Group, 2013.

A Vossoroca reservoir measurements

This appendix shows data measured in Vossoroca reservoir between 2013-2015 which were not present before. The data includes temperature profiles in the floating platform and meteorological data (outliers and data gaps were not removed).

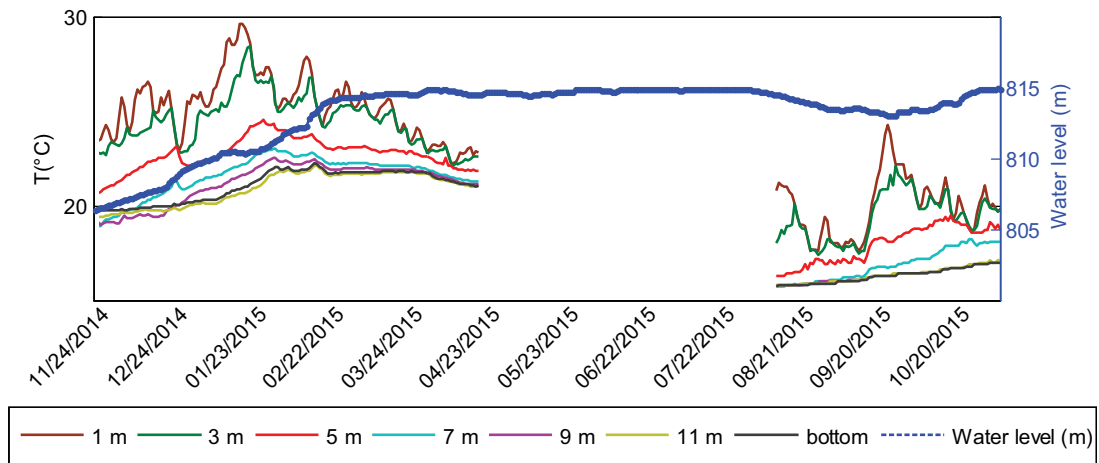


Figure A.1 – Temperature measured in Vossoroca reservoir in the floating platform (measured from surface)

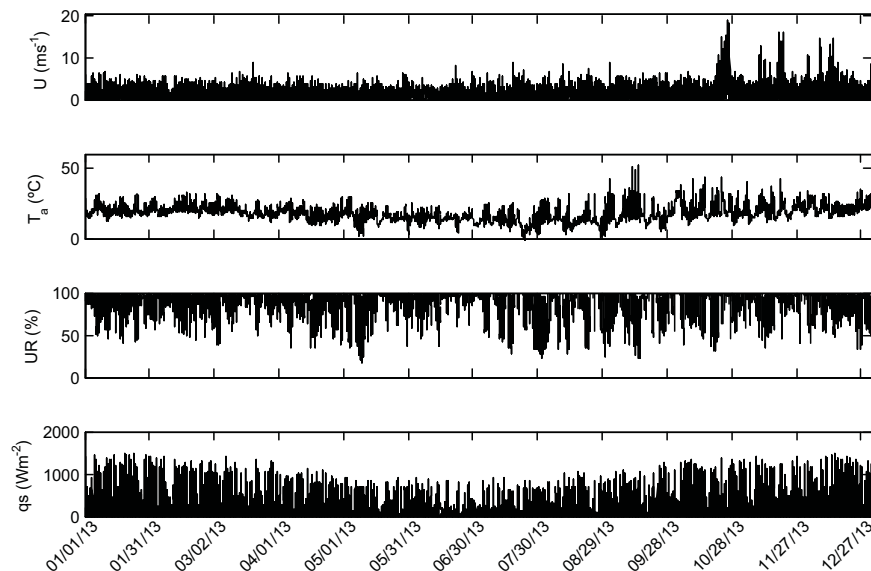


Figure A.2 – Meteorological data near to Vossoroca reservoir (2013). a) Wind speed, b) Air temperature, c) Relative Humidity and d) Shortwave radiation

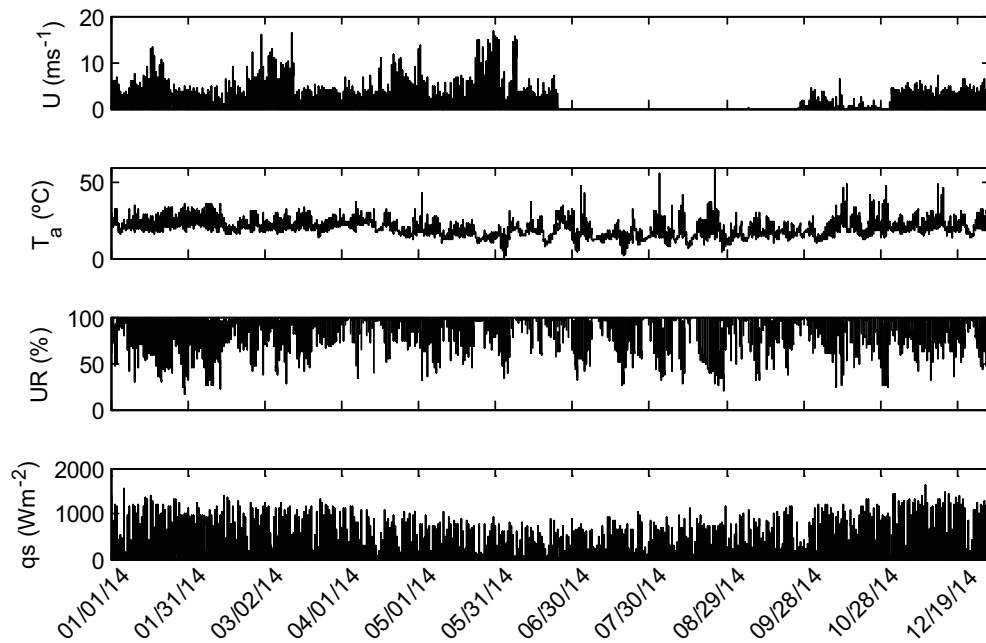


Figure A.3 – Meteorological data near to Vossoroca reservoir (2014). a) Wind speed, b) Air temperature, c) Relative Humidity and d) Shortwave radiation

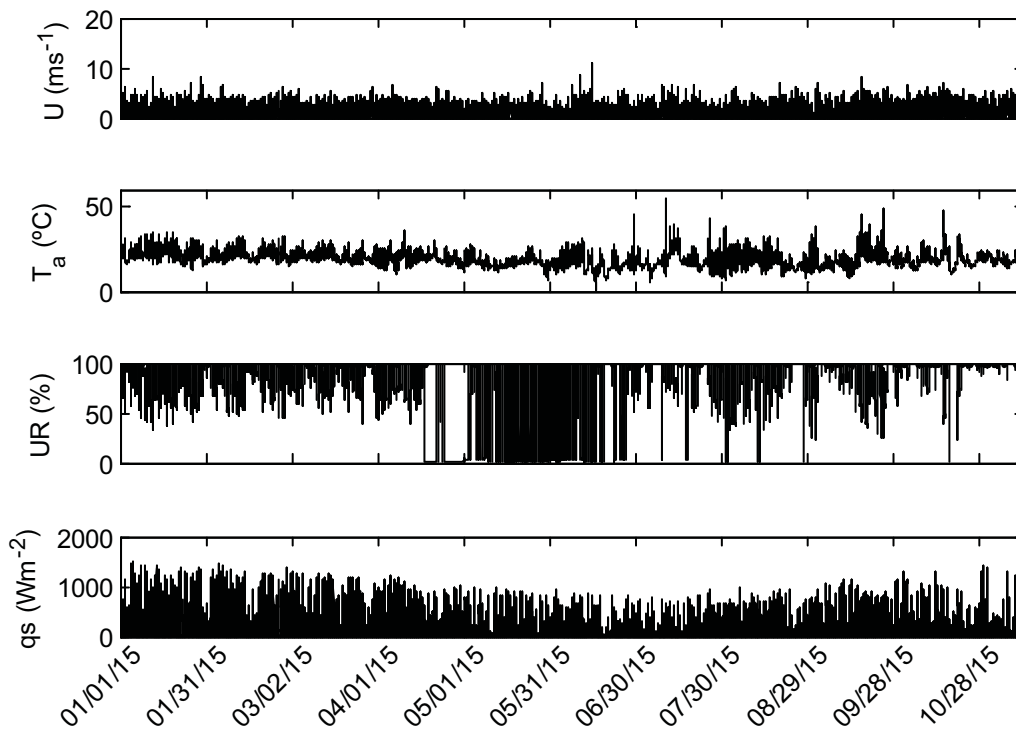


Figure A.4 – Meteorological data near to Vossoroca reservoir (2015). a) Wind speed, b) Air temperature, c) Relative Humidity and d) Shortwave radiation

B MTCR-1 Model

This section describe in more detail the equations in the model MTCR-1 (in Portuguese: "Modelo de Transporte de Calor para Reservatórios"), which is a heat transport model for lakes and reservoirs. The model was implemented in Fortran 95 and the equations were discretized with implicit finite volume method. In addition to the heat transport, the model calculates temperature gradients (between surface and bottom), Wedderburn Number and Lake Number.

The one-dimensional heat transport equation is:

$$A \frac{\partial T}{\partial t} = \frac{\partial}{\partial z} \left[E_z A \frac{\partial T}{\partial z} \right] + \frac{1}{\rho c_p} \frac{\partial A q(z)}{\partial z} + \frac{Q_{in} A T_{in} - Q_{out} A T}{V} \quad (\text{B.1})$$

where z (m) is measured from the fixed bottom, T is the water temperature ($^{\circ}\text{C}$), t is the time (s), A is the horizontal area (m^2), which may depend on depth, E_z is the eddy diffusivity coefficient (m^2s^{-1}), ρ is the water density (kgm^{-3}), c_p is the specific heat of water ($\text{Jkg}^{-1}\text{K}^{-1}$), $q(z)$ is a heat source (Wm^{-2}), represented by solar radiation, Q_{in} is the inflow (m^3s^{-1}), Q_{out} is the outflow (m^3s^{-1}) and T_{in} is the inflowing temperature ($^{\circ}\text{C}$). Both water density and specific heat of water are calculated according to UNESCO's equations (Fofonoff and Millard, 1983).

The heat source term is written as (Dake and Halerman, 1969)

$$q(z) = (1 - \beta) q_{sn} \exp[-\eta(H - z)] \quad (\text{B.2})$$

where β is the portion of downward shortwave radiation absorbed at the surface layer, η is the extinction coefficient (m^{-1}), q_{sn} is the net shortwave radiation reaching the water surface and H is the total depth (m) at a given time.

The wind induced diffusivity coefficient (E) is calculated using the equation (Sundaram and Rehm, 1971):

$$E = E_0 f \quad (\text{B.3})$$

in which E_0 is the neutral eddy diffusivity (non-stratified conditions) coefficient ($\text{m}^2 \text{s}^{-1}$) and f is a function of the Richardson Number Ri (Henderson-Sellers, 1985)

$$f(Ri) = (1 + 37Ri^2)^{-1} \quad (\text{B.4})$$

$$Ri = -\frac{\frac{g}{\rho} \frac{\partial \rho}{\partial z}}{\left(\frac{\partial u}{\partial z} \right)^2} \quad (\text{B.5})$$

where g is the gravity acceleration (m^2s^{-1}) and u is the horizontal component of velocity (ms^{-1}). The Richardson number is a relation between generation or suppression of turbulence by buoyancy forces and turbulence by the wind. If $Ri > 0.25$ stratification is stable, and if $Ri < 0.25$, temperature profile is unstable and turbulent mixing occurs (Wetzel, 1983).

The wind induced value of E is given by (Henderson-Sellers, 1985)

$$E = \frac{\kappa w_s^*(H - z)}{P_0} \exp[-k^*(H - z)] \frac{1}{1 + 37Ri^2} \quad (\text{B.6})$$

where κ is von Karman's constant ($\kappa = 0.4$), w_s^* is the water surface friction velocity (ms^{-1}), P_0 is the neutral Prandtl number ($P = v/\alpha$, which is a relation between momentum diffusivity, v (m^2s^{-1}), and thermal diffusivity, α (m^2s^{-1})) and k^* is a function given by $k^* = 6.6\sqrt{(\sin \phi)U^{-1.84}}$ in which ϕ is latitude and U is the wind speed (ms^{-1}). Prandtl number is a relation between momentum and heat transfer and its neutral value is $P_0=1.0$.

To those known equations an additional source of turbulence, namely from the shear flow from residual currents or inflows is estimated according to the equation of the vertical mixing coefficient for rivers (Fischer, 1981)

$$\bar{\varepsilon}_v = 0.067du^* \quad (\text{B.7})$$

where d is the mean depth of the river or the layer of advective flows and u^* the shear velocity. A percentage (1%) of this mixing was applied to the reservoir due to the distance between the inflows and the measurements in the reservoir. Therefore, the diffusivity coefficient is $E_z = E + \bar{\varepsilon}_v$.

The bottom boundary condition of the heat transport equation given by Giannou and Antonopoulos (2007) assumes no heat exchange with the bed (regarding groundwater inflows),

$$\left. \frac{\partial T}{\partial z} \right|_{z=0} = 0. \quad (\text{B.8})$$

The surface boundary condition is representing a temporally changing heat flux due to meteorological conditions (Babajimopoulos and Papadopoulos, 1986):

$$\rho c_p E_z \left. \frac{\partial T}{\partial z} \right|_{z=H} = -q_n \quad (\text{B.9})$$

where q_n is the heat exchange between the reservoir surface and the atmosphere and is calculated by (Edinger et al., 1968)

$$q_n = K(T_e - T_s) \quad (\text{B.10})$$

where T_e is the equilibrium temperature ($^{\circ}\text{C}$), T_s is the water surface temperature ($^{\circ}\text{C}$) and K is the surface heat exchange coefficient ($\text{Wm}^{-2}\text{ }^{\circ}\text{C}^{-1}$). Equilibrium temperature (T_e) and the coefficient heat exchange (K) are calculated by (Antonopoulos and Gianniou, 2003)

$$T_e = T_d + \frac{q_{ns}}{K} \quad (\text{B.11})$$

$$K = 4.5 + 0.05T_s + \delta f(U_2) + 0.47f(U_2) \quad (\text{B.12})$$

where:

$$f(U) = 9.2 + 0.46U_2^2 \quad (\text{B.13})$$

$$\delta = 0.35 + 0.015T_m + 0.0012T_m^2 \quad (\text{B.14})$$

$$T_m = \frac{T_s + T_d}{2} \quad (\text{B.15})$$

$$T_d = \frac{237.3 \times var}{17.2694 - var} + 273.96 \quad (\text{B.16})$$

$$var = \frac{17.2694(T_a + 273.16)}{(T_a - 35.86)} + \ln RH \quad (\text{B.17})$$

where q_{ns} is the shortwave radiation at the water surface (Wm^{-2}), T_s is the surface temperature ($^{\circ}\text{C}$), U_2 is the wind speed (ms^{-1}) measured at 2 m from the surface, T_d is the dew point temperature ($^{\circ}\text{C}$), RH is the relative humidity (%) and T_a is the air temperature ($^{\circ}\text{C}$).

C Numerical discretization of MTCR-1 Model

This section shows the discretization with implicit finite volume method used to solve the heat transport equation present in Section 2.3.1. Table C.1 shows the discretization of the heat transport equation and boundary conditions. Coefficients of the implicit finite volume method are shown in the form of a tridiagonal equation system ($a_p T_p = a_s T_s + a_n T_n + b_p$), where i is used for space discretization, j for time and m is the total number of cells in space.

Table C.1 – Discretization of the one-dimensional heat transport equation and boundary conditions.

Heat transport equation discretization	Boundary conditions
	Bottom:
	$a_p = 1$
	$a_s = 0$
	$a_n = 1$
	$b_p = 0$
	Surface:
	$a_p = 1$
	$a_s = 1$
	$a_n = 0$
	$b_p = \frac{q_n \Delta z}{\rho_i^j c_{pi}^j E_{zi}^j}$
$a_p = \Delta z + E_{zi+1} \frac{\Delta t}{\Delta z} + E_{zi-1} \frac{\Delta t}{\Delta z} + \frac{Q_{out} A_p \Delta t \Delta z}{V}$ $a_s = E_{zi-1} \frac{\Delta t}{\Delta z}$ $a_n = E_{zi+1} \frac{\Delta t}{\Delta z}$ $b_p = \frac{\Delta t}{\rho c_p} (q_{i+1} - q_{i-1}) + \frac{Q_{in} A_p T_{in} \Delta t \Delta z}{V} + T_p^0 \Delta z$	

D Delft3D Model

In this annex, some relevant equations for the three-dimensional modeling in Delft3D are described. Annex D.1 presents Murakami and Ocean heat flux models equations and, Annex D.2 presents $k - \epsilon$ turbulence model. The full description of the equations may be found in Deltares (2014).

D.1 Heat flux models

Two heat flux models are analysed in this Thesis – Murakami and Ocean heat flux models. The equations for both models are described in this section. Total heat flux (Q_{tot}) is calculated as (Deltares, 2014)

$$Q_{tot} = Q_{sn} + Q_{an} - Q_{br} - Q_{ev} - Q_{co} \quad (D.1)$$

where Q_{sn} is the net incident solar radiation (short wave) (Wm^{-2}), Q_{an} is the net incident atmospheric radiation (long wave) (Wm^{-2}), Q_{br} is the back radiation (long wave) (Wm^{-2}), Q_{ev} is the evaporative heat flux (latent heat) (Wm^{-2}) and Q_{co} is the convective heat flux (sensible heat) (Wm^{-2}). For Murakami and Ocean heat flux models it is defined the effective back radiation (Q_{eb}) as $Q_{eb} = Q_{br} - Q_{an}$.

D.1.1 Murakami model

For the effective back radiation, $Q_{eb} = Q_{br} - Q_{an}$, in Murakami model:

$$Q_{eb} = \epsilon \sigma T_a^4 (0.39 - 0.058 \sqrt{e_a}) (1.0 - 0.65 F_c^2) + 4 \epsilon \sigma T_a^3 (T_s - T_a) \quad (D.2)$$

where ϵ is the an emissivity factor, σ is the Stefan-Boltzmann constant, T_a is the air temperature (K), e_a is the actual air pressure, F_c is the cloud cover and T_s is the water surface temperature (K). The actual air pressure is

$$e_a = r_{hum} 23.38 \exp \left(18.1 - \frac{5303.3}{T_a} \right). \quad (D.3)$$

in which r_{hum} is the relative humidity.

The evaporative heat flux Q_{ev} is calculated according to

$$Q_{ev} = L_v E \quad (D.4)$$

where L_v is latent heat of vaporisation (Jkg^{-1}),

$$L_v = 2.510^6 - 2.310^3 T_s. \quad (\text{D.5})$$

E is the evaporation rate, defined as the mass of water evaporated per unit area per unit time ($\text{kg m}^{-2}\text{s}^{-1}$). E is calculated as a form of Dalton Law of mass transfer

$$E = f(U_{10})(e_s - e_a) \quad (\text{D.6})$$

where $f(U_{10})$ is the wind speed function, which in Murakami model is

$$f(U_{10}) = c_{mur} U_{10} \quad (\text{D.7})$$

in which c_{mur} is a constant, $c_{mur}=1.2 \cdot 10^{-9}$, which corresponds to Dalton number of 0.0016. The saturated vapour pressure e_s is

$$e_s = 23.38 \exp\left(18.1 - \frac{5303.3}{T_s}\right). \quad (\text{D.8})$$

Convective heat flux (Q_{co}) is calculated by the Bowen ratio (R_b), which relates convective heat flux and evaporative mass flux, according to

$$Q_{co} = R_b Q_{ev} \quad (\text{D.9})$$

$$R_b = \gamma \frac{T_s - T_a}{e_s - e_a} \quad (\text{D.10})$$

where γ is Bowen's constant. For Murakami model, $\gamma=0.66$.

Solar radiation (Q_{sn}) may be calculated by the model or specified by the user. The radiation is absorbed at the surface, but also transmitted to deeper water, according to

$$Q_{sn}(z) = \frac{\eta \exp^{-\eta z}}{1 - \exp^{-\eta H}} (1 - \beta) Q_{sn} \quad (\text{D.11})$$

where β is the portion of Q_{sn} absorbed at the water surface, η is the extinction coefficient (m^{-1}) – which is related to Secchi depth ($\eta = 1.7/H_{Secchi}$) and H is total water depth.

D.1.2 Ocean model

For the effective back radiation, $Q_{eb}=Q_{br} - Q_{an}$, in Ocean model:

$$Q_{eb} = \epsilon \sigma T_s^4 (0.39 - 0.05 \sqrt{e_a}) (1.0 - 0.65 F_c^2) \quad (\text{D.12})$$

where ϵ is the an emissivity factor, σ is the Stefan-Boltzmann constant, T_s is the water surface temperature (K), e_a is the actual air pressure and F_c is the cloud cover. The

actual air pressure is

$$e_a = r_{hum} 10^{\frac{0.7859+0.03477T_a}{1.0+0.00412T_a}} \quad (D.13)$$

in which r_{hum} is the relative humidity and T_a is the air temperature (K).

The evaporative heat flux Q_{ev} is calculated according to

$$Q_{ev} = Q_{ev,forced} + Q_{ev,free} \quad (D.14)$$

where $Q_{ev,forced}$ is the forced convection of latent heat and $Q_{ev,free}$ is the free convection of latent heat. $Q_{ev,forced}$ is calculated according to

$$Q_{ev,forced} = L_v \rho_a f(U_{10}) [q_s(T_s) - q_a(T_a)] \quad (D.15)$$

where L_v is latent heat of vaporisation (Jkg^{-1}), ρ_a is the air density (kgm^{-3}), $f(U_{10})$ is a function of the wind speed, q_s and q_a – the specific humidity for saturated air and the air, respectively, calculated according to

$$q_s(T_s) = \frac{0.62e_s}{P_{atm} - 0.38e_s} \quad (D.16)$$

$$q_a(T_a) = \frac{0.62e_a}{P_{atm} - 0.38e_a} \quad (D.17)$$

where e_s and e_a are the saturated and remote vapour pressures. The saturated vapour pressure is calculated according to

$$e_s = 10^{\frac{0.7859+0.03477T_s}{1.0+0.00412T_s}}. \quad (D.18)$$

The wind function $f(U_{10})$ is given by

$$f(U_{10}) = c_e U_{10} \quad (D.19)$$

where c_e is the Dalton number.

The term on evaporative heat flux due free convection is given by

$$Q_{ev,free} = k_s L_v \bar{\rho}_a (q_s - q_a) \quad (D.20)$$

where k_s is the heat transfer coefficient and $\bar{\rho}_a$ is the averaged air density. $\bar{\rho}_a$ is calculated according to

$$\bar{\rho}_a = \frac{\rho_{a0} + \rho_{a10}}{2} \quad (D.21)$$

and

$$\rho_{a0} = \frac{\frac{100P_{atm}-100e_s}{R_{dry}} + \frac{100e_s}{R_{vap}}}{T_s + 273.15} \quad (D.22)$$

$$c = \frac{\frac{100P_{atm}-100e_a}{R_{dry}} + \frac{100e_a}{R_{vap}}}{T_a + 273.15} \quad (D.23)$$

where R_{dry} is the gas constant for dry air ($287.05 \text{ Jkg}^{-1}\text{mol}^{-1}$) and R_{vap} is the gas constant for water vapour ($461495 \text{ Jkg}^{-1}\text{mol}^{-1}$). k_s is zero if $\rho_{a10} - \rho_{a0} \leq 0$, but if $\rho_{a10} - \rho_{a0} > 0$ then

$$k_s = c_{fr,conv} \left(\frac{g\alpha^2}{\nu_{air}\bar{\rho}_a} (\rho_{a10} - \rho_{a0}) \right)^{1/3} \quad (D.24)$$

where $c_{fr,conv}$ is the coefficient of free convection (0.14), ν_{air} is the air viscosity ($16 \cdot 10^{-6} \text{ m}^2\text{s}^{-1}$) and α is the molecular diffusivity of air ($\alpha = \nu_{air}/\sigma$), where $\sigma=0.7$ (for air), the Prandtl number.

The convective heat flux is also split in two parts. The forced convection is

$$Q_{co,forced} = \rho_a c_p g(U_{10})(T_s - T_a) \quad (D.25)$$

where c_p is the specific heat of air and the wind speed function, $g(U_{10})$:

$$g(U_{10}) = c_H U_{10} \quad (D.26)$$

where c_H is the Stanton number.

The free convection is calculated according

$$Q_{co,free} = k_s \bar{\rho}_a c_p (T_s - T_a) \quad (D.27)$$

The total heat flux due convection is then

$$Q_{co} = Q_{co,forced} + Q_{co,free}. \quad (D.28)$$

Solar radiation (Q_{sn}) may be calculated by the model or specified by the user. The radiation is absorbed at the surface, but also transmitted to deeper water, according to

$$Q_{sn}(z) = \frac{\eta \exp^{-\eta z}}{1 - \exp^{-\eta H}} (1 - \beta) Q_{sn} \quad (D.29)$$

where β is the portion of Q_{sn} absorbed at the water surface, η is the extinction coefficient (m^{-1}) – which is related to Secchi depth ($\eta = 1.7/H_{Secchi}$) and H is total water depth.

D.2 $k - \epsilon$ turbulence model

Transport equation for turbulent kinetic energy k (m^2s^{-2}) and energy dissipation ϵ (m^2s^{-3}) are solved in the $k - \epsilon$ model. Two assumptions are considered:

- The production, buoyancy, and dissipation terms are the dominating terms;

- Horizontal length scales are larger than the vertical scales.

The transport equation for turbulent kinetic energy k and energy dissipation ϵ :

$$\frac{\partial k}{\partial t} + u \frac{\partial k}{\partial x} + v \frac{\partial k}{\partial y} + \frac{w}{(d + \zeta)} \frac{\partial k}{\partial \sigma} = \frac{1}{(d + \zeta)^2} \left(D_k \frac{\partial k}{\partial \sigma} \right) + P_k + P_{kw} + B_k - \epsilon \quad (\text{D.30})$$

$$\frac{\partial \epsilon}{\partial t} + u \frac{\partial \epsilon}{\partial x} + v \frac{\partial \epsilon}{\partial y} + \frac{w}{(d + \zeta)} \frac{\partial \epsilon}{\partial \sigma} = \frac{1}{(d + \zeta)^2} \left(D_\epsilon \frac{\partial \epsilon}{\partial \sigma} \right) + P_\epsilon + P_{\epsilon w} + B_\epsilon - c_{2\epsilon} \frac{\epsilon^2}{k} \quad (\text{D.31})$$

in which u , v and w are velocities, t is time, x, y and σ are the coordinates, d is the depth below some horizontal plane of reference (datum), ζ is the water level above some horizontal plane of reference (datum), D_k and D_ϵ are the diffusivity coefficients, P_k and P_ϵ are the production terms, P_{kw} and $P_{\epsilon w}$ are the turbulent energy production terms due to wave action, B_k and B_ϵ are the buoyancy flux terms and $c_{2\epsilon}=1.92$. D_k and D_ϵ are calculated according to:

$$D_k = \frac{\nu_{mol}}{\sigma_{mol}} + \frac{\nu_{3D}}{\sigma_k} \quad (\text{D.32})$$

$$D_\epsilon = \frac{\nu_{3D}}{\sigma_\epsilon} \quad (\text{D.33})$$

where ν_{mol} is the kinematic viscosity (molecular) coefficient, σ_{mol} is the Prandtl-Schmidt number for molecular mixing (6.7 for temperature), ν_{3D} is the part of eddy viscosity due to turbulence model in vertical direction, σ_k and σ_ϵ constants. The production terms, P_k and P_ϵ :

$$P_k = \nu_{3D} \frac{1}{(d + \zeta)^2} + \left[\left(\frac{\partial u}{\partial \sigma} \right)^2 + \left(\frac{\partial v}{\partial \sigma} \right)^2 \right] \quad (\text{D.34})$$

$$P_\epsilon = c_{1\epsilon} \frac{\epsilon}{k} P_k \quad (\text{D.35})$$

where $c_{1\epsilon}=1.44$. The buoyancy flux terms, B_k and B_ϵ :

$$B_k = \frac{\nu_{3D}}{\rho \sigma_{rho}} \frac{g}{H} \frac{\partial \rho}{\partial \sigma} \quad (\text{D.36})$$

$$B_\epsilon = c_{1\epsilon} \frac{\epsilon}{k} (1 - c_{3\epsilon}) B_k \quad (\text{D.37})$$

where ρ is the water density, $\sigma_{rho}=0.7$ for temperature, g is the gravity acceleration, H is the total water depth ($H = d + \zeta$) and $c_{3\epsilon}=0$ to unstable stratification and $c_{3\epsilon}=1.0$ for stable stratification. The energy production and energy dissipation due to waves, P_{kw} and $P_{\epsilon w}$:

$$P_{kw}(z') = \frac{4D_w}{\rho_w H_{rms}} \left(1 - \frac{2z'}{H_{rms}} \right) \quad (\text{D.38})$$

$$P_{\epsilon w}(z') = c_{1\epsilon} \frac{\epsilon}{k} P_{kw}(z') \quad (\text{D.39})$$

where the total depth-averaged contribution of wave breaking is given by D_w (Wm^{-2}), H_{rms} is root-mean-square wave height and z' is the vertical co-ordinate with its origin in the (wave averaged) water level and positive downwards. The boundary conditions to solve the turbulence model are:

$$\epsilon|_{\sigma=-1} = \frac{u_{*b}^3}{\kappa z_0} \quad (\text{D.40})$$

$$\epsilon|_{\sigma=0} = \frac{u_{*s}^3}{\frac{1}{2}\kappa\Delta z_s} \quad (\text{D.41})$$

$$k|_{\sigma=-1} = \frac{u_{*b}^2}{\sqrt{c_\mu}} \quad (\text{D.42})$$

$$k|_{\sigma=0} = \frac{u_{*s}^2}{\sqrt{c_\mu}} \quad (\text{D.43})$$

where u_{*b} is the bed friction velocity, κ is the von Karman constant, z_0 is the bed roughness length, u_{*s} is the friction velocity at the free surface and Δz_s is the thickness of the surface layer.

The eddy viscosity, ν_{3D} , and L , the mixing length, are calculated as:

$$\nu_{3D} = c'_\mu L \sqrt{k} = c_\mu \frac{k^2}{\epsilon} \quad (\text{D.44})$$

$$L = c_D \frac{k \sqrt{k}}{\epsilon} \quad (\text{D.45})$$

where $c_\mu = c_D c'_\mu$, $c_D = c_\mu^{3/4} \approx 0.1925$ and $c_\mu = 0.09$. The eddy diffusivity (D_{3D}) is calculated as:

$$D_{3D} = \frac{\nu_{3D}}{\sigma_c} \quad (\text{D.46})$$

where σ_c is the Prandtl-Schmidt number, calculated as:

$$\sigma_c = \sigma_{c0} F_\sigma(Ri) \quad (\text{D.47})$$

$$Ri = \frac{-g \frac{\partial \rho}{\partial z}}{\rho \left[\left(\frac{\partial u}{\partial z} \right)^2 + \left(\frac{\partial v}{\partial z} \right)^2 \right]} \quad (\text{D.48})$$

where $\sigma_{c0} = 1.3$ for heat transport, $F_\sigma(Ri)$ is a so-called damping function that depends on the density stratification via the gradient Richardson's number (Ri). In the $k - \epsilon$ turbulence model no damping function is used since the influence of stratification on the mixing length is taken into account by the buoyancy terms in the transport equations for k and ϵ . Therefore, $F_\sigma(Ri) = 1$ for all Ri .